Corso di Dottorato in Neuroscienze

Curriculum Neuroscienze e Neurotecnologie

Ciclo XXXII

Coordinatore: Prof. Angelo Schenone

miRNA Dysregulation Drives Neuronal Intracellular Chloride Accumulation in Down Syndrome

Micol Alberti

Supervisors: Dr. Andrea Contestabile

Dr. Laura Cancedda

UNIVERSITÀ DEGLI STUDI
DI GENOVA

Contents

INTRODUCTION 4

1. **Down Syndrome pathophysiology** 4
2. **Pathological mechanisms of Down syndrome** 5
3. **Mouse Models of Down Syndrome** 8
4. **GABAergic transmission** 10
5. **The GABAergic hypothesis for cognitive disabilities in Down syndrome** 13
6. **Biology of microRNAs** 16
7. **microRNAs in development and developmental disorders** 18
8. **Aim of the project** 21

MATERIALS AND METHODS 23

1. **Cloning and plasmid construction** 23
2. **Real-Time Quantitative PCR (RT-qPCR)** 23
3. **Human Brain Samples** 26
4. **Primary cultures and transfection** 27
5. **RNA interference** 29
6. **Viral preparations** 30
7. **Biochemistry** 31
8. **MQAE intracellular chloride imaging** 31
9. **Fluorescent sensor imaging** 32
10. **Luciferase assay** 32
11. **Micro-Electrode Array recordings** 33
12. **Animals** 35
13. **Statistical analysis** 36

RESULTS 37

1. **NKCC1 expression in trisomic neuronal culture** 37
2. **NKCC1 upregulation causes intracellular chloride accumulation in Ts65Dn neurons.** 40
3. **Post-transcriptional regulation of NKCC1 expression in trisomic neurons.** 42
4. **microRNAs play a role in NKCC1 upregulation** 46
5. **Candidate microRNAs target NKCC1-3'UTR** 49
6. **miR497a-5p and miR101-3p regulate chloride levels in primary neurons through the downregulation of NKCC1 expression** 52

7. Overexpression of miR497a-5p and miR101-3p restore inhibitory GABAergic signaling in Ts65Dn neuronal networks 55

8. Long-term overexpression of candidate microRNAs using viral vectors 60

9. The DS-triplicated gene APP regulates NKCC1 *in trans* by competing for miR497a-5p and miR101-3p in Ts65Dn neurons 61

DISCUSSION 63

BIBLIOGRAPHY 71

INTRODUCTION

1. Down Syndrome pathophysiology

Down syndrome (DS) is the most frequent genetic cause of intellectual disability in children and adults. The disorder results from the presence of an extra copy of human chromosome 21 (HSA21) or of a major portion of this chromosome, and hence is also referred as trisomy 21.

The pathology was first described in 1866 by the English physician John Langdon Down [1], but it was only in 1959 that the French geneticist Jerome Lejeune showed that the syndrome was actually due to trisomy of chromosome 21 [2,3].

The onset of DS-related phenotypes occurs during prenatal development, although some of the manifestations of the disorder may become apparent only in adulthood [4].

In DS children, both long and short-term memory are affected. On the other hand, DS children perform worse than healthy children in explicit memory tasks, while learning ability in tasks requiring implicit memory processing is spared. This could be due to the fact that implicit memory typically relies on automatic processes thus requiring low attention levels; on the contrary explicit memory involves intentional learning and retrieval strategies, demanding a high degree of attention [5].

Individuals with DS also display language deficits. Indeed, poor expressive language and impaired reading ability, as well as difficulty in the acquisition of new words probably derive from a disturbance of the verbal short-term memory system [4].

The profile of DS cognitive impairment is accompanied by specific neuroanatomical modifications. First, brains of adults with DS are about 20% smaller than healthy controls. This phenotype is already present during gestation, and it worsens after birth. More specifically, morphological alterations have also been detected in DS people at different ages: children and young adults display decreased volume of the hippocampus and temporal lobe. Later in life, also other regions such as cerebellum, entorhinal and frontal cortex and amygdala appear to be affected [6-9].

These morphological alterations probably derive from the defective generation of neurons during development. Indeed, the hippocampus and neocortex of DS fetuses show reduced number of neurons as well as the cortex of DS children. DS cells display a prolonged G2 phase due to the presence of the extra chromosome 21, possibly leading to reduced proliferation rate during neurogenesis. In addition, increased

apoptosis has also been reported in the hippocampus of DS fetuses. Therefore, brain hypocellularity in DS appears to result from both defective neurogenesis and increased apoptosis [10,11]

In older subjects with DS, age-associated degenerative modifications also take place in the brain. Since the Alzheimer-related gene APP is triplicated in DS, alterations resembling those typical of Alzheimer's disease occur in almost all DS patients showing extensive Aβ pathology and amyloid plaques deposition starting from the age of 30 [5,12].

At the cellular level, neurodevelopmental and degenerative mechanisms contribute to alterations in neuronal compartments such as dendrites. Indeed, dendrites in hippocampus and cortex of the adult DS brain display decreased length and branching, while also spine density is reduced [13-15].

In contrast, fetuses and neonates' brains are characterized by a normal or even increased dendritic branching [15,16], indicating that degenerative mechanisms take place in older children with DS and progress during adulthood with a further reduction of dendritic branching, and length as well as spine density. As for dendritic structures, in many cases neuroanatomical and neurochemical alterations arise during development and gradually progress over aging. Importantly, since dendritic spines play an essential role in network connectivity and brain plasticity, their alterations will probably impact neuronal communication and cognitive performance. Moreover, deficits in many neurotransmitter systems important for brain development such as GABA (which is the main excitatory neurotransmitter during embryonic life), serotonin and dopamine have also been found. Cholinergic system is also affected during aging due to the early-onset Alzheimer's degeneration [5,17].

2. Pathological mechanisms of Down syndrome

Trisomy 21, is one of the three human trisomies viable in the postnatal period (together with 13 and 18), probably due to the small size of chromosome 21 and to the low density of its functional DNA elements.

The full sequencing of chromosome 21 was achieved in 2000, showing that it contains only 173 protein-coding genes [18]. These genes display broad diversity in their functional properties including kinases, genes involved in the ubiquitination pathway, seven ion channels, members of the interferon receptor families and, importantly, 18 transcription factors. Moreover, the chromosome is rich in genes encoding for long non-coding RNAs and it also encodes 29 microRNAs [18-20].

Two main hypotheses have been proposed to explain genotype-phenotype correlation in DS. The first, called "gene-dosage effect", states that DS phenotypes results from the dosage imbalance of some triplicated dosage-sensitive genes. Supporting this hypothesis, the study of individuals bearing partial trisomy 21 allowed the identification of a subset of chromosomes 21 genes whose triplication was

responsible for most of DS manifestations. Those genes are located on a region spanning about 5.4Mb on HSA21q22, called "DS critical region" (DSCR). However, further experiments performed using specific mouse strains trisomic for DSCR gene orthologues, showed that DSCR triplication can only explain some of the symptoms. This evidence suggested that more complex mechanisms are involved in DS pathology [21]. Moreover, when the trisomic Ts65Dn mouse (which carries the triplication of the distal portion of mouse chromosome 16, encompassing genes orthologous to human genes in the DSCR) was crossed with mice carrying a deletion of the critical region (returning DSCR gene dosage to normal levels), DS-related phenotypes were only attenuated compared to Ts65Dn [22,23]. Therefore, at least in animal models, DSCR is partially necessary to cause the phenotype, but it is not sufficient to produce all the symptoms of the syndrome. Probably, the dosage imbalance of DSCR genes directly contributes to some phenotypes, but more complicated mechanisms are needed to explain all DS manifestations [22].

On the other hand, according to the "Amplified Developmental Instability" hypothesis, a secondary effect exerted by the triplicated genes on the whole genome can lead to global gene expression dysregulation. This would contribute to at least some aspects of the pathology. For example, triplicated transcription factors could regulate the expression of genes located on other chromosomes, leading to a genome-wide expression dysregulation [22,24]. Indeed, when analyzing mRNA expression in the dorsolateral prefrontal cortex and the cerebellar cortex of DS people, Olmos-Serrano et al. found many differentially expressed genes localized throughout the genome. Therefore, non-HSA21 genes significantly contribute to DS phenotype. Interestingly, less than 50% of those genes were upregulated while the others were downregulated, showing that triplication of HSA21 can exert both positive and negative regulation of genes located on other chromosomes [25].

Accordingly, a study on fetal fibroblasts derived from monozygotic twins discordant for trisomy 21, identified distinct chromosomal domains composed of adjacent genes sharing the same differential expression profile; meaning that regions of upregulated genes follow areas in which genes are downregulated [26].

Interestingly, Olmos Serrano et al. also found that less than 15% of chromosome 21 genes were upregulated compared to controls in the prefrontal cortex and the cerebellar cortex of DS people. This indicates that regulatory feedback loops may compensate the gene-dosage effect [25].

Besides, a previous study in lymphoblastoid cell lines had shown that 56% of HSA21 genes were expressed at normal levels and that the DS/control ratio was significantly lower than the expected 1.5 for many differentially expressed HSA21 genes. This indicates that compensation is mostly due to functional negative feedback loops [27].

DNA methylation can be one of the mechanisms involved in extensive gene expression alterations as well as in mechanisms of compensation. Whole-genome bisulfite sequencing in the frontal cortex of DS people highlighted that even if there are no differences in the global methylation level, in DS brains there are regions of differential methylation distributed across the entire genome, the majority of these regions appeared to be hypermethylated [28]. Moreover, Mendioroz et al. showed that increased CpG methylation is already present in fetal DS brain and mainly affects developmentally regulated genes. Indeed, differential methylation frequently involves sequences containing binding sites for transcription factors that are critical for brain development [29]. In fact, HSA21 encodes several proteins involved in DNA methylation pathways that could mediate these epigenetic changes such as folate pathway enzymes and DNA methyltransferases DNMT3L and N6AMT1 [28,29].

Chromatin architecture within the nucleus could also be an important factor determining some DS-related phenotypes. The assessment of mating performances in three different mouse models (Ts65Dn, Ts1Cje and Rb2Cje, which will be described in the next chapter) revealed that the presence of the triplicated genes as an extra chromosome in Ts65Dn was impairing normal spermatogenesis and therefore fertility. The other two models seem not to be affected, possibly because they are characterized by the translocation of the trisomic region rather than the presence of an extra chromosome. Additionally, the presence of triplicated genes as an unpaired chromosome lead to global gene expression dysregulation that was not detected in the absence of the extra chromosome [30].

A critical aspect of DS-related mechanisms of gene dysregulation may also involve the spatio-temporal dynamics of gene expression. Since the pattern of differentially expressed genes differs between brain regions and throughout development, distinct biological processes will be likely affected at different stages of brain development and during adulthood [25]. For example, sequencing data from DS-derived neural progenitor cells (NPCs) and differentiated NPCs, revealed that some pathways (such as focal adhesion and extracellular matrix function) are dysregulated at both stages of differentiation while others are dysregulated only at specific stages. Interestingly, NPCs dysregulated clusters of genes are mostly involved in pluripotency, synapse formation and DNA replication. These functions are of paramount importance in the early stages of neurogenesis. Upon differentiation, pathways that were found to be affected by trisomy where mainly related to metabolism (glycolysis and gluconeogenesis), axon guidance and TGF-beta signaling [31]. Moreover, differences were detected in the pattern of dysregulated genes found in trisomic fetal brains compared to the adult dorsolateral prefrontal cortex. The two groups of samples also differed in the degree of HSA21 gene upregulation. While fetal brains largely adhere to the dosage-effect model with a 1.5-fold increase, in adult prefrontal cortex the upregulation was in some

cases higher than the expected 1.5-fold, probably due to the emergence of compensatory effects or to changes occurring later in life [32].

3. Mouse Models of Down Syndrome

Chromosome 21 encodes approximately 552 genes of which 173 are protein-coding genes, 49 are keratin-associated proteins (KRTAP; a large family of structural proteins expressed in hair fibers) and 325 are non-protein-coding genes. Approximately, 158 orthologous non-KRTAP protein-coding genes are present in the mouse genome and are located on three different chromosomes: 102 genes map on the telomeric portion of mouse chromosome 16 (Mmu16) spanning about 28Mb; 19 genes map on an internal segment of mouse chromosome 17 (Mmu7) of about 3Mb; 37 genes are located on an internal portion of mouse chromosome 10 (Mmu10) of about 3Mb [33,34].

Different mouse models, trisomic for different sets of chromosome 21 genes, have been developed, aiming at investigating the many aspects of Down syndrome pathology (Fig.1).

In 1993, Davisson et al. created the Ts65Dn model, which carries the translocation of a segment of Mmu16 on the centromeric region of Mmu17, resulting in a small freely-segregating extra-chromosome. The Ts65Dn mouse is currently the only model bearing a genuine aneuploidy. However, in addition to the triplication of 92 genes orthologous to HSA21, Ts65Dn mice also carry trisomy of 35 Mmu17 protein-coding genes that are non-homologous to HSA21. Despite this latter genetic issues, Ts65Dn mice recapitulate many of the phenotypic features of the human syndrome and it is currently the only mouse model used for preclinical identification of pharmacological interventions targeting DS cognitive impairment [4,35,36].

Additional DS mouse models are trisomic for a subset of genes triplicated in Ts65Dn, but are not characterized by an extra freely segregating chromosome. The Ts1Rhr was the first model created using Cre-lox technique to carry the triplication of the genes orthologous to DSCR. However, this model failed to reproduce all the features of DS phenotype, indicating that in mice the only triplication of this region is not sufficient to explain all aspects of the pathology [21]. Cre-lox techniques were also used to create mouse models bearing tandem duplications of the three complete syntenic regions of HSA21. In particular, the Dp(16)1Yey model is trisomic for the entire Mmu16 region syntenic to HSA21, containing 110 orthologous genes [37], while Dp(17)1Yey and Dp(10)1Yey carry the triplication of Mmu17 and Mmu10 syntenic regions, respectively [38]. Although these models are optimal in terms of genetic triplication, they lack the freely-segregating extra chromosome, which is present in Ts65Dn model as well as in the vast majority of persons affected by DS [30].

In 2005, O'Doherty and colleagues developed the first transchromosomic mouse line (Tc1) which carries a freely-segregating copy of the human chromosome 21. Human sequences are expressed both at the level of mRNA and protein; however, Tc1 mouse displays mosaicism of the extra-chromosome in several tissues, and the trisomy is not complete due to some chromosomal deletions and rearrangement [39].

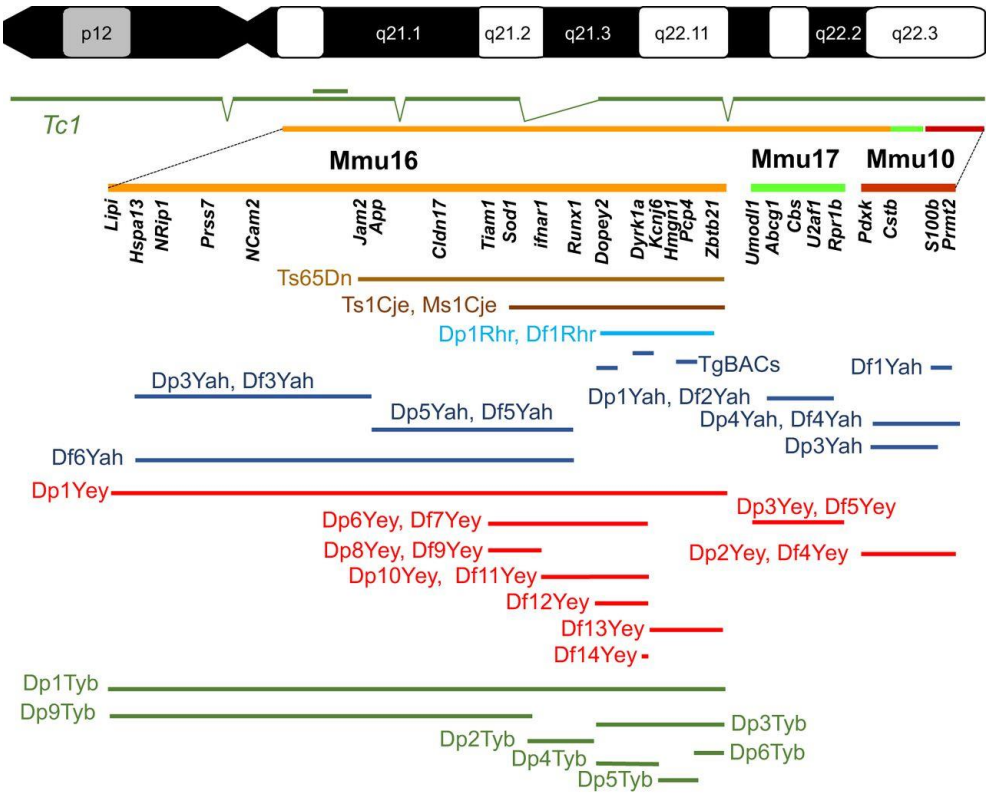

Figure 1: Down Syndrome mouse models. Representation of HSA21 and mouse orthologous regions on mouse chromosomes 16, 17 and 10. The segment of chromosome triplicated in different mouse models of DS are also reported. From: Herault Y., et al., Disease Models and Mechanisms, 2017.

In summary, Ts65Dn remains the best-characterized model of DS and also the most widely used since it reproduces many phenotypic features of the human pathology.

Ts65Dn mice show impaired performances in hippocampal-dependent tasks such as T-maze, contextual fear conditioning and novel object recognition. Spatial memory is also reduced in the Morris water maze test [35,40-42]. In addition, Ts65Dn mice are hyperactive in open field and plus-maze test, in which wild-type animals are usually cautious.

Ts65Dn mice also display neuromorphological alterations typical of DS. For instance, the brain volume of Ts65Dn mice is reduced compared to controls during the embryonic period and cell density is

decreased during prenatal and early postnatal life in the neocortex. Also, the dentate gyrus of these mice has fewer granule cells at all ages [10,43]. These alterations are probably due to reduced neural-precursor proliferation during embryonic and postnatal development. On the other hand, Ts65Dn mice show a larger population of GABAergic neural progenitors in the medial ganglionic eminence, resulting in higher numbers of GABAergic interneurons in both hippocampus and cortex later in life [44].

4. GABAergic transmission

γ-aminobutyric acid (GABA) is the primary inhibitory neurotransmitter in the adult brain through binding to both ionotropic ($GABA_AR$) and metabotropic ($GABA_BR$) receptors.

$GABA_BRs$ are $G_{i/o}$-protein-coupled receptors. They are mostly located extra-synaptically and, they can be activated by neurotransmitter spilled out from the synaptic cleft thanks to their high affinity for the ligand. When coupled with $G\alpha_{i/o}$ subunits, $GABA_BR$ activation leads to adenylate cyclase inhibition and to a consequent reduction of cAMP levels and PKA activity. When coupled to $G\beta\gamma_{i/o}$ subunits, $GABA_BRs$ inhibit voltage-gated calcium channels and activate G protein-coupled inwardly-rectifying potassium channels (GIRK). Through these mechanisms, pre-synaptic $GABA_BRs$ can reduce vesicle release, whereas $GABA_BRs$ located at the spine neck and on the dendrites reduce neuronal excitability [45,46].

$GABA_ARs$ are ligand-gated channels permeable to chloride ions and, to a lesser extent, to bicarbonate ions. They are composed of five subunits. In the central nervous system, the majority of $GABA_ARs$ are formed by two α, two β and one γ subunits. Many isoforms have been identified for each type of subunit. This variability confers different kinetic properties to $GABA_ARs$, depending on their composition. For instance, receptors bearing α1-3, β2-3 and γ2 subunits are characterized by fast kinetics with rapid onset and desensitization, and are frequently located at the synaptic level. On the other hand, the presence of α5 or δ subunits provides the receptor with high GABA affinity and slow desensitization kinetic; these subunits are commonly present outside the synaptic cleft. Notably, extra-synaptic $GABA_AR$ containing α5 and δ subunits are crucial during development when synapses are not entirely formed [47-50]

Upon activation and opening of $GABA_ARs$, the direction of the elicited chloride flux depends on the intracellular chloride concentration ($[Cl^-]_i$) and the related chloride electrochemical gradient. Therefore, regulation of chloride homeostasis is essential to obtain a correct excitatory-inhibitory balance, in the brain. In neurons, $[Cl^-]_i$ is regulated by the opposing action of the chloride imported NKCC1 and the chloride exporter KCC2 [51-53]. In particular, if $[Cl^-]_i$ is low, chloride ions will enter the neuron with a hyperpolarizing effect. On the other hand, if $[Cl^-]_i$ is high, $GABA_AR$ opening will elicit a chloride efflux, causing a depolarization of the membrane potential. In mature neurons, $[Cl^-]_i$ is maintained at around 5-7

mM and the resulting chloride equilibrium potential is more negative than the membrane resting potential. Consequently, chloride currents will have a hyperpolarizing effect (Fig. 2b). In contrast, in developing neurons, $[Cl^-]_i$ is higher (between 15 and 25 mM). Therefore the resulting chloride equilibrium potential is less negative than the membrane resting potential in young neurons. This leads to an outward flow of chloride associated with a depolarizing effect upon $GABA_AR$ opening (Fig. 2a). Importantly, the depolarizing effect of GABAergic transmission is considered essential to the development of neuronal circuits [54-56].

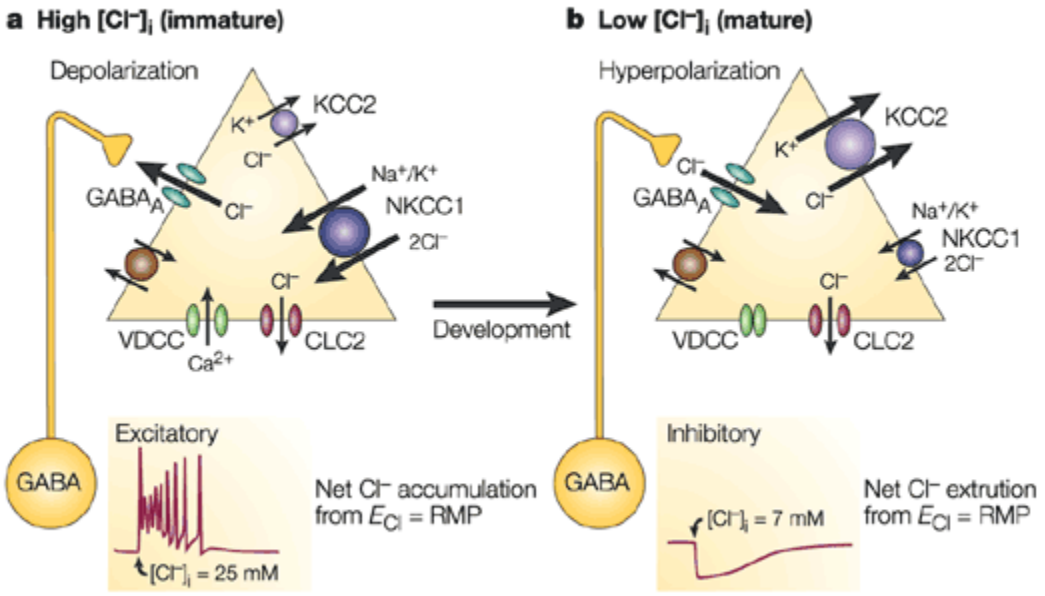

Figure 2: Scheme of NKCC1 and KCC2 cotransporters expression and gradients of chloride ions in immature (a) and mature (b) neurons. From: Ben-Ari Y., Nat Rev Neurosci.,2002

Since, the membrane resting potential (between -60 and -70 mV) and the chloride reversal potential (around -73 mV) are in close proximity, relatively small changes in chloride concentration can trigger a shift in GABAergic transmission polarity from hyperpolarizing to depolarizing [57]. For this reason, in physiological conditions, the action of the two chloride co-transporters KCC2 and NKCC1 tightly regulates $[Cl^-]_i$ to set the reversal potential and the driving force for chloride.

NKCC1 and KCC2 consist of a 12-segment transmembrane domain, essential for ion translocation, and of cytosolic amino- and carboxy-terminal domains required for the regulation of the activity and the trafficking of the protein [58]. NKCC1 is the main chloride importer that shuttles chloride ions inside the

neurons together with K^+ and Na^+, exploiting the inwardly directed electrochemical gradient of sodium, maintained by Na^+-K^+-ATPase pump. KCC2 is a chloride exporter that extrudes chloride against its concentration gradient. This process requires high intracellular potassium levels that are provided by the activity of the ATP-dependent pump Na^+-K^+-ATPase. The two cotransporters are the main responsible for the change in chloride levels occurring during neuronal development and maturation. Indeed, in immature neurons, the expression of NKCC1 is higher than KCC2, whose levels are maintained very low. During neuronal maturation, KCC2 expression increases dramatically in neurons, leading to progressive lowering of $[Cl^-]_i$. This phenomenon is termed "GABA developmental switch" and takes place during the second postnatal week in rodents and between postconceptional week 40 and 50 in humans [54].

The GABA developmental shift, and in particular KCC2 upregulation, is essential to allow mature neurons to recover rapidly after chloride loading. For this reason, KCC2 expression and activity are dynamically regulated in neurons. For instance, Brain-derived Neurotrophic Factor (BDNF) can modulate KCC2 levels with opposite effects in immature and mature neurons. In immature neurons, BDNF signaling is associated with increased KCC2 mRNA and protein levels mediated by ERK1/2 pathway. Moreover, pro-BDNF binding to p75NT receptor inhibits KCC2 expression. Notably, the level of pro-BDNF is high during development, indicating that KCC2 regulation heavily depends on brain development and neuronal maturation [54]. Conversely, in adult neurons, BDNF signaling -through TrkB receptors- results in a reduction in the levels of both KCC2 mRNA and protein together with diminished surface localization.

Apart from expression itself, another important aspect of $[Cl^-]_i$ homeostasis depends on the regulation of KCC2 activity. Protein kinase C (PKC) phosphorylates KCC2 at Ser940, enhancing the transporter activity and its membrane stability [59]. KCC2 activity is also regulated by the activation of glutamate receptors. Kainate receptor subunit GluK2 can form complexes with KCC2 and PKC. PKC- mediated phosphorylation of GluK2 enhances KCC2 activity [60,61]. Moreover, PKC can also directly phosphorylate KCC2 after being activated downstream of metabotropic glutamate receptors [62]. In this framework, an increase in excitatory signaling via glutamate transmission can therefore strengthen inhibitory transmission through the stimulation of KCC2 activity, thus balancing excitation and inhibition.

KCC2 activity is also regulated by changes in ionic composition through the lysine deficient protein kinase (WNK) pathway and its SPAK/OSR1 (SPS-related proline/alanine-rich kinase or the SPAK homolog oxidative stress-responsive kinase 1) effectors. When chloride levels are low, WNK is active and can phosphorylate SPAK/OSR1, which in turn phosphorylates KCC2 on threonine or serine residues, exerting an inhibitory effect. However, high chloride levels block WNK auto-phosphorylation and

activation, thus preventing its inhibitory action on KCC2 activity. Through this mechanism, WNK pathway can regulate chloride extrusion rate depending on chloride loading [54,63]. Interestingly, the HSA21 triplicated gene amyloid precursor protein (APP) can also form complexes with KCC2, preventing the phosphorylation of some tyrosine residues and inhibiting internalization and degradation of the transporter [64].

While the regulation of KCC2 expression has been extensively studied, less is known about the regulation of neuronal NKCC1, except for the observation that seizure induction can upregulate NKCC1 in the brain [65]. However, it is known that WNK-SPAK/OSR1 pathway (that regulates KCC2 activity in response to chloride levels) can also regulate NKCC1 activity, by phosphorylating three threonine residues at the N-terminus of the protein. In this case, WNK activation enhances NKCC1 activity. This mechanism further reinforces the importance of this pathway for the regulation of intracellular chloride concentration so that low chloride levels will trigger KCC2 inhibition together with NKCC1 activation [54,63].

Considering its importance for brain development and neuronal communication, it is not surprising that dysregulation of chloride homeostasis is a major hallmark of many neurological and psychiatric conditions, including chronic pain [66], brain trauma [67-69], autism spectrum disorder [70,71], Down syndrome [72,73],Rett syndrome [74,75], Fragile X syndrome [71,76], Huntington disease [77], Tuberous sclerosis complex [78], 22q11.2 microdeletion syndrome [79], maternal immune activation [80] and some forms of epilepsy [81-83].

5. The GABAergic hypothesis for cognitive disabilities in Down syndrome

According to the GABAergic hypothesis for cognitive disabilities in Down syndrome, alterations in GABAergic signaling play a critical role in determining DS cognitive impairment by altering the physiological excitatory-inhibitory (E/I) balance. Disruption of the optimal E/I balance have been linked to defective synaptic plasticity and memory [72,84,85]. A major alteration leading to E/I imbalance is set in place during ventral neurogenesis, when the progenitor population in the medial ganglionic eminence seems to produce a higher number of interneurons in the Ts65Dn mouse model of DS. This increment is probably due to the overexpression of *Lhx6*, a transcription factor that is essential for neuronal subtype specification. This phenotype has been directly linked to the triplication of HSA21 transcription factors Olig1 and Olig2 that regulate *Lhx6* expression in the medial ganglionic eminence [44]. As a result, the number of parvalbumin and somatostatin-positive interneurons is increased in the cortex and hippocampal CA1 region of Ts65Dn mice [44]. Accordingly, pharmacological inhibition of $GABA_A$Rs rescues both hippocampal synaptic plasticity and memory in Ts65Dn mice [84,86,87].

Although research on the Ts65Dn model showed an increased number of interneurons, studies on human iPSCs-derived neurons have produced conflicting results. Indeed, DS cortical progenitor cells generate a smaller number of GABAergic interneurons compared to euploid controls [88]. Transcriptome analysis of those progenitors highlighted several candidate genes possibly responsible for this phenotype. First of all, DLX homeobox transcription factor (which is essential for interneurons generation) is almost absent in trisomic NPC. Additionally, the triplication of Olig transcription factors can promote progenitor commitment to oligodendrocyte fate at the expense of neuronal fate. In agreement with this hypothesis, trisomic NPCs also display increased expression of the oligodendrocyte myelin glycoprotein (OMG) [88]. Moreover, trisomic GABAergic neurons also show reduced capacity to migrate from MGE while differentiated interneurons show impaired ability to project axons to their target. Migration issues are probably linked to the triplication of a gene related to the actin cytoskeleton pathway, PAK1, whose expression is increased in DS GABAergic interneurons. Accordingly, inhibition of PAK1 partially rescues the migration defects [89].

Hippocampal slices from Ts65Dn mice have been extensively used to assess GABAergic transmission [72]. In line with the observed increase in the number of GABAergic interneurons, also an increase in spontaneous GABAergic postsynaptic events was observed in hippocampal CA1 pyramidal neurons [90]. However, further functional analysis of GABAergic transmission did not find evidence for changes in the frequency of miniature inhibitory postsynaptic currents (mIPSC, which represent activity-independent quantal release of GABA) in the same region [90,91]. Similarly, no difference was found in the density of GABAergic synapses, release probability at GABAergic terminals and evoked $GABA_A$ transmission in the hippocampal CA1 region of adult Ts65Dn mice [91,92]. Therefore, the increased number of GABAergic neurons seems not to be directly associated with increased synaptic contacts in the DS brain, indicating possible compensatory mechanism limiting GABAergic synapse number. Conversely, mIPSC frequency was found decreased (rather than increased) in the hippocampal CA3 region of Ts65Dn mice [93,94]. On the other hand, mIPSC frequency and evoked GABAergic transmission were found increased in the DG of adult Ts65Dn mice, but with this alteration primarily attributed to increased release probability, rather than increased synapse number [95,96]. These apparently conflicting results may simply indicate possible sub-regional differences in the density of GABAergic synapses and its functional consequences. Additionally, increased mIPSC frequency and evoked $GABA_A$ transmission was only found in the hippocampal CA1 of 2 week-old Ts65Dn mice, whereas no difference between trisomic and wild-type mice was found in the first and third post-natal weeks. These results also highlight possible age-related changes that could nevertheless exert a long-lasting effect on hippocampal network properties, contributing to circuit dysfunction later in life [97].

Importantly, HSA21 contains the KCNJ6 gene [98,99] which encodes the subunit 2 of the G-protein coupled inward rectifier potassium channel (GIRK2). Indeed, both mRNA and protein for GIRK2 are increased in the brain of Ts65Dn mice [100,101]. In agreement with the fact that GIRK channels are mainly coupled to $GABA_B$Rs in the adult brain [102], $GABA_B$-activated GIRK currents are increased in Ts65Dn cultured neurons as well as in CA1 pyramidal neurons and in DG granule cells from acute slices of the Ts65Dn hippocampus [92,95,103]. This establishes a direct link between DS genetic triplication and GABA signaling. Increased $GABA_B$/GIRK signaling alters membrane resting potential and contributes to defective long term potentiation (LTP) induction in Ts65Dn mice [95,104].

Since several studies have proven GABAergic signaling imbalance to be involved in cognitive deficits, many studies have assessed the ability of both $GABA_A$ and $GABA_B$ antagonists to improve cognitive performance in DS mouse models. In particular, Fernandez and colleagues tested the efficacy of three diverse non-competitive $GABA_A$ antagonists: pentylenetetrazole, picrotoxin and bilobalide. They found that chronic treatment with these drugs restored LTP and declarative memory in behavioral tasks. Interestingly, the beneficial effect was retained up to two months after the suspension of drug administration [85]. Similar results were found on learning and memory in the Morris water maze after chronic pentylenetetrazole (PTZ) treatment [105]. Accordingly, picrotoxin treatment also rescued LTP in the hippocampal dentate gyrus [96] and CA1 region [84], when administered to slices from Ts65Dn mice. Despite their efficacy, it must be considered that $GABA_A$ antagonists are burdened by possible pro-epileptic and anxiogenic side effects [72,106]. However, a more recent study found that the efficacy of PTZ was maintained even at a dose 10 times lower, therefore possibly defining a safer therapeutic range [107]. Since $GABA_A$ α5-subunit is highly expressed in the hippocampus, but present only at low levels in other brain regions, two different α5-selective antagonists have been tested aiming at reducing the risk of seizure induction while promoting cognition. Both compounds were effective in improving cognitive performance in DS mice [108-111].

Although the vast body of evidence points to excess GABAergic signaling in DS circuits dysfunctions, some studies have provided evidence of defective $GABA_A$-mediated inhibition [97,104,112,113]. In particular, Deidda et al. found that $GABA_AR$ activation is depolarizing rather than hyperpolarizing in the hippocampus and the neocortex of Ts65Dn mice. This action was associated with increased $[Cl^-]_i$ and a more positive value of the chloride reversal potential. Alteration of chloride homeostasis was paralleled by an increased expression of the chloride imported NKCC1 in brain samples from both Ts65Dn mice and DS people, whereas the expression of the chloride exporter KCC2 was unaffected. Moreover, the FDA-approved NKCC1 inhibitor Bumetanide restored chloride reversal potential and rescued memory

impairment in Ts65Dn mice [114] (Fig. 3). In view of these results, the rescue of cognitive deficits in Ts65Dn obtained with $GABA_A$ antagonists could be explained by their ability to reduce aberrant (depolarizing) GABAergic signaling [114]. As Bumetanide modifies intracellular chloride levels rather than acting on $GABA_AR$, its action does not prevent GABA-mediated shunting inhibition[106] and will not likely increase the seizure risk.

.

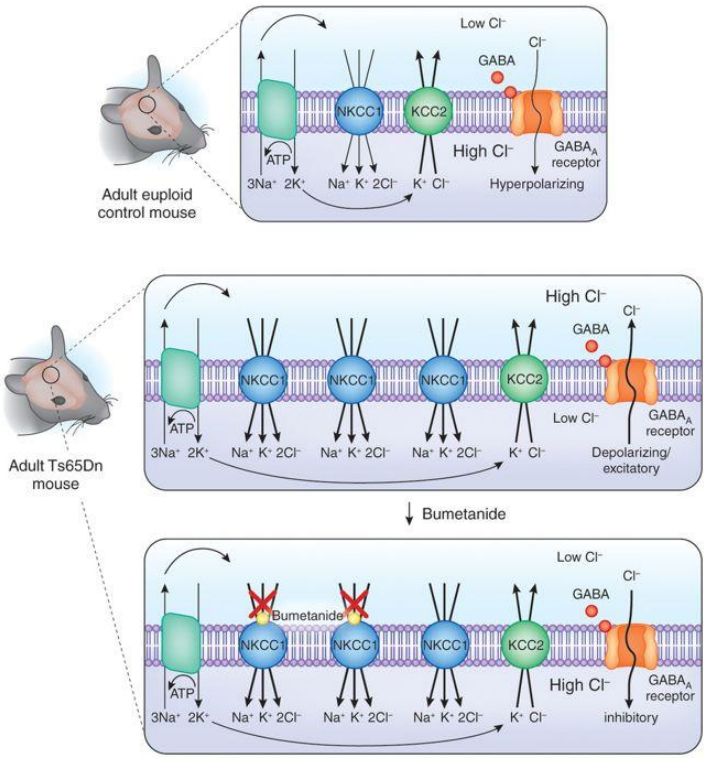

Figure 3: Model of $GABA_AR$-mediated neurotransmission in euploid and Ts65Dn mouse models**.**
From: Costa A.C., Nat Med, 2015.

6. Biology of microRNAs

Over the last decade, microRNAs (miRNAs) have emerged as critical regulators of the expression and function of eukaryotic genomes [115]. miRNAs are 21-22 nucleotides (nt) non-coding RNA molecules that function as negative regulators of gene expression by interacting mainly (although not exclusively) with the 3' untranslated regions (3'UTR) of target mRNAs. The 6-8 nucleotides at the 5' end of the microRNA, called seed sequence, primarily mediate the interaction with targets. After binding, miRNAs can either mediate mRNA degradation or inhibit its translation, depending on their degree of complementarity [116-118].

Complete sequence complementarity usually leads to target cleavage while partial complementarity, at the level of seed binding sequences, promotes translational inhibition [119].

However, while some works suggest that translational inhibition is the primary mechanism triggered by microRNAs [120,121], other studies point to mRNA decay as the main mediator of gene silencing [122,123]. In some cases, the two mechanisms coexist [124,125] together with mRNA destabilization by deadenylation of the poly(A) tail [126] present on the 3' end of the mRNA. Moreover, according to kinetic studies carried out *in vitro* as well as *in vivo* in Drosophila, translational inhibition and mRNA decay are probably part of a sequential mechanism in which inhibition takes place first and is then is followed by mRNA deadenylation and decay to consolidate gene silencing [127-129].

Transcription of miRNAs is typically performed by the RNA polymerase II. The miRNA primary transcripts, named pri-miRNAs, consist of an imperfectly paired stem of about 33 base-pairs, with a terminal loop and two flanking segments. Then, two sequential processing reactions trim the pri-miRNA transcript into the mature miRNA. The first processing step takes place in the nucleus by the RNA-binding protein DGCR8 (DiGeorge Critical region) and the RNase III enzyme Drosha, that excises the stem-loop from pri-miRNAs to form the pre-miRNA product. In animals, the pre-miRNA is then exported to the cytoplasm where the RNase III enzyme Dicer performs the second cleavage reaction. Dicer excises the terminal loop from the pre-miRNA stem to produce a mature miRNA duplex of approximately 22 base-pair length [115]. The mature miRNA duplex associates with Argonaute (Ago) proteins in the RNA-induced silencing complex (RISC), where one miRNA strand of the duplex is retained while the other is discarded and degraded. To exert gene silencing, miRNA-associated Ago2 recruits the SDE3 helicase Mov10 [130,131], and components of the GW182 family of Trinucleotide repeat-containing-proteins (a group of genes that is composed of three paralogs in mammals: Tnrc6A, Tnrc6B and Tnrc6C). Thanks to the presence of tryptophan repeats, Tnrc proteins can bind several silencing effectors such as PolyA Binding proteins (PABP) and deadenylase complexes and are therefore essential for miRNA functioning [129,132,133], including translation repression of complimentary mRNA [134] (Fig. 4). Thus, miRNAs bound to Ago and Tnrc proteins can be considered the core components of the RISC complex, since impairing Ago2-Tnrc interaction prevents miR mediated gene-silencing both *in vitro* and *in vivo* [135].

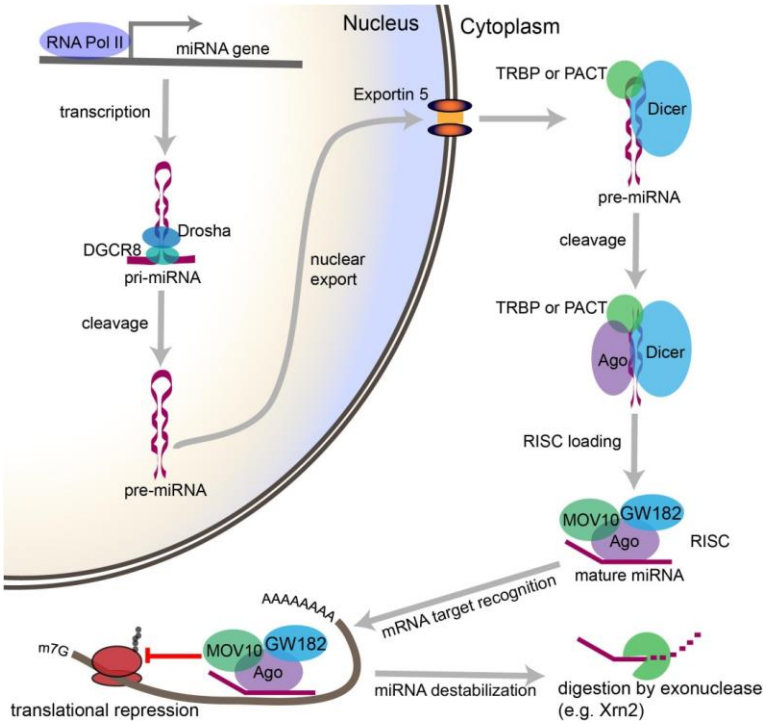

Figure 4: Overview of the miRNA processing pathway, from synthesis to target translational inhibition
From: Thomas K.T., et al., Front.Mol.Neurosci. 2018

Several studies indicate that miRNAs play critical regulatory roles in different biological processes such as neurite outgrowth and synaptogenesis. Interestingly, the production of mature miRNAs from their precursors can take place at the synaptic level, where they can regulate synaptic functions without requiring changes in mRNA expression [136]. Processing of miRNA, can also be triggered by neuronal activity. In particular, stimulation of individual synapse can lead to local pre-miR181a processing in the dendritic shaft close to the stimulated synapse, allowing a local reduction in target protein synthesis [137]. For this reason, miRNAs represent an essential layer of regulation to fine-tune expression profiles of genes necessary for activity-dependent synaptic plasticity. Accordingly, miRNAs have been recognized as key players in the formation and retrieval of memory and contribute to the structural plasticity of dendritic spines associated with LTP and LTD [138,139].

7. microRNAs in development and developmental disorders

miRNAs are essential regulators of the transcriptional network of the developing human brain and are probably involved in the onset of neurodevelopmental disorders. Indeed, many miRNAs are differentially expressed across different developmental periods (infancy, early childhood, late childhood and

adolescence). Moreover, differential expression of miRNAs between brain regions increases over developmental time, suggesting a role for miRNAs in regional specialization during brain maturation. Furthermore, putative gene targets of the differentially expressed miRNAs are involved in biological processes related to transcriptional regulation, neurodevelopment and neurodevelopmental disorders [140].

Profiling studies on the rat cortex during development have highlighted that sets of microRNAs share the same dynamic of expression throughout development. Some are continuously expressed across all developmental phases (for instance miR9 and let7), while others are selectively expressed over a short period. The second group might be involved in specific processes taking place during cortical development such as proliferation, differentiation, migration and network formation [141]. Indeed, microRNA-depleted neural stem cells can self-renew for several days *in vitro*, but they are not able to differentiate. This suggests that microRNA depletion (mediated by Dicer deletion) mostly affects cell-fate transition and maturation toward a more restricted progenitor cell type [142]. Considering that the extent of expression regulation exerted by a single microRNAs is relatively mild, it is likely that groups of co-expressed microRNAs cooperate to achieve the fine-tuned control required for the precise coordination of phase transition. On the other hand, a single microRNA can efficiently regulate a specific function by targeting several genes involved in the same pathway or exerting redundant functions [141].

MicroRNAs have been proven essential also for the control of physiological plasticity in adult neurons. In general, synaptic suppression seems to be one of the prominent functions of microRNAs at the synaptic level. For instance, miR138 can regulate the palmitoylation status of several proteins functioning at the synapse [143], while miR375 can downregulate BDNF to inhibit dendritic growth [144]. However, evidence of positive regulation of target gene expression at the synaptic levels have also been reported. For instance, miR124 enhances long-term facilitation by de-repressing the activity-dependent transcription factor CREB [145].

MicroRNAs can control synaptic transmission at multiple steps: from neurotransmitter synthesis to signal termination. Indeed, microRNAs regulate expression of various neurotransmitter receptors (including glutamate and GABA receptors) [146-149] as well as neurotransmitter release by targeting components of the SNARE complex or proteins regulating pre-synaptic calcium levels [150-152]. Neurotransmitter reuptake is another step of neuronal signaling that can be regulated by microRNAs. For example, miR16 can increase the efficacy of serotonin signaling by downregulation of the serotonin transporter SERT [153].

Consistent with the fact that microRNAs action affects gene expression in every stage of neurodevelopment, their dysregulation is involved in the onset of several neurodevelopmental disorders, including autism [154,155], epilepsy [156] and Fragile X syndrome [157]. Moreover, several miRNAs have been

found dysregulated in DS and Ts65Dn samples. However, among the 29 microRNAs encoded on chromosome 21, only a 5 (miR99a, let7c, miR125b-2, miR155 and miR802) have been detected at the expected ratio of 1.5 in DS compared to controls [158]. Nevetheless, since single microRNAs can regulate multiple target RNAs, these five miRNAs could potentially regulate the expression of more than 3600 genes, playing an important role in the developmental and functional defects as well as in the phenotypic variation observed in people with DS [158,159]. Among the many, Methyl-CpG-binding protein transcription factor 2 (MeCP2) is one of the most interesting targets of HSA21-triplicated miRNAs. Indeed, MeCP2 is involved in many brain functions including neurogenesis and spine formations, and its mutation leads to Rett syndrome [160,161]. The 3'UTR of MeCP2 harbors two binding sequences for miR155 and miR802 in addition to a single seed-binding sequence for miR125b and let-7c. Indeed, its levels were found decreased in trisomic samples from humans and Ts65Dn mice [162].

In agreement with the Amplified Developmental Instability hypothesis, several studies found that also other microRNAs, lying outside chromosome 21, are dysregulated in Ts65Dn and DS samples compared to controls. A study in the cerebrum of adult Ts65Dn mice found 20 microRNAs (including miR195 and miR497) whose expression was decreased in Ts65Dn brains. Interestingly, these down-regulated microRNAs were disomic. On the other hand, among the trisomic microRNAs, only miR-155 displayed a 1.8 fold increase, whereas no differences were detected in the expression levels of the other four microRNAs [163]. Accordingly, a study focusing on the lymphocytes from children with trisomy 21 found that not all the triplicated microRNAs were up-regulated at ratios higher than 1.5, whereas 114 microRNAs encoded outside chromosome 21 were differentially expressed [164]. Lin et al. characterized the expression profile of both microRNAs and protein in fetal cord blood samples, aiming to understand the functions of dysregulated microRNAs that are important for embryonic development. They found 344 differentially expressed microRNAs (including miR101, miR16 and miR195) and 505 differentially expressed proteins [165]. Another study carried out a correlation analysis of microRNAs and gene expression profiles in fetal hippocampal tissues to identify a network dysregulation that could cause cognitive impairment in DS. They found a total of 995 pairs of altered microRNAs and predicted targets whose functional analysis revealed a prominent role in the regulation of transcription [166]. Moreover, a study comparing the transcriptome of Ts65Dn and WT hippocampi found eleven differentially expressed microRNAs. Among these, six were up-regulated (miR-210, miR155, miR214, miR138, miR423-5p and mi223) while five were down-regulated (miR7b, miR181c, miR369-5p, miR361 and miR135b). Notably, the down-regulated miR7b targets the Fos gene, an important regulator of cell signaling and synaptic plasticity [167].

Many other neurological disorders are associated with altered gene expression regulation by miRNAs [168]. MicroRNAs are differentially expressed during all phases of epileptogenesis both in humans and in animal models of the pathology. In this context, microRNAs targeting ion channels are crucial. Indeed, ion channels can modulate intrinsic neuronal excitability. For instance, miR33, which is down-regulated in animal models of epilepsy, targets two $GABA_AR$ subunits (α4 and β2) as well as KCC2 transporter, indicating an essential role of miR33 in regulating inhibitory signaling in the brain [156].

Several single nucleotide polymorphisms (SNP) in the gene encoding for miR137 are associated with an increased risk of schizophrenia. In particular, alleles linked to elevated risk of schizophrenia are associated with low miR137 levels. Conversely other SNPs, associated with higher miR137 levels, are considered protective [169,170]. Moreover, also miR195-5p levels have been found reduced in patients with schizophrenia [171].

Fragile-X syndrome is also linked to microRNA pathway dysfunction. Indeed, the fragile X mental retardation protein (FMRP) participates in pri-miRNA processing by up-regulating Drosha at the translational level. Consequently, FMRP dysfunction results in the accumulation of pri-miRNAs and the reduction of pre-miRNA levels [157]. Moreover, FMRP regulates diverse mechanisms in cooperation with specific microRNAs. For example, FMRP phosphorylation promotes miR125a association with AGO2 complex, and the interaction with PSD95 mRNA. Moreover, miR181d and FMRP cooperatively repress the translation of the proteins involved in axon elongation process (Map1 and Calm1). On the other hand, FMRP mRNA is targeted by microRNAs such as miR130b whose levels negatively correlates with FMRP protein in mouse embryonic neural precursor cells as well as in humans [172].

Concerning autism spectrum disorders (ASD), the identification of specific genetic variants unequivocally leading to the pathology has not been achieved yet. However, microdeletions and microduplications (collectively referred as copy number variations; CNVs) at multiple chromosomal loci seem to be implicated in the disorder. Aiming to explain the genetic heterogeneity underlying ASD, a study investigated the involvement of microRNAs encoded in CNVs and identified ten microRNAs (including miR195 and miR497) as hub molecules. Many of these hub microRNAs formed regulatory loop with transcription factors and their downstream targets were involved in neurodevelopment and synapse formation [154].

8. Aim of the project

Deidda et al. found that NKCC1 chloride importer is upregulated both in Ts65Dn mice and in DS human samples [114], suggesting that modulation of NKCC1 expression could be a promising strategy to improve

cognition in DS. Since NKCC1 gene (Slc12a2) is not located on chromosome 21, and consequently it is not triplicated, the project aims to address the molecular mechanisms responsible for NKCC1 regulation in DS brains. In this case, it is also essential to understand the relation linking trisomy of chromosome 21 to NKCC1 upregulation.

Even though NKCC1 protein expression is highly dynamic during development and its changes have been extensively studied, the molecular mechanisms underlying NKCC1 developmental changes are currently unknown. Therefore, this study could also shed light on physiological regulation of NKCC1.

Moreover, dysregulation of chloride homeostasis is a major hallmark of many neurological and psychiatric conditions, including epilepsy, traumatic brain injury, ischemia, tuberous sclerosis, Rett syndrome, Fragile X, autism and chronic pain. Therefore, treatment of these pathologies could as well benefit from this study and the possibility to regulate NKCC1 levels by interfering with the molecular mechanisms underlying NKCC1 expression in physiology and/or pathology.

We hypothesize that understanding the mechanisms leading to NKCC1 differential expression in Ts65Dn neurons will allow us to manipulate its levels to restore physiological chloride concentration and possibly rescue cognitive impairment in Ts65Dn mice.

MATERIALS AND METHODS

1. Cloning and plasmid construction

The ~2.8 Kb mouse NKCC1 3'UTR was PCR-amplified from the genomic BAC clone RP24-109M9 (BACPAC Resources) and cloned in psiCHECK2 plasmid (Promega) downstream of Renilla luciferase (Rluc) coding sequence. This plasmid also expressed Firefly luciferase (Fluc) from a second promoter that serves as internal control. With this system, changes in the Rluc/Fluc ratio will reflect the degree of NKCC1 3'UTR post-transcriptional regulation.

To assess the repression activity of NKCC1 3'UTR specifically in neuron, we constructed a sensor plasmid (termed biSyn-EGFP-TOM) in which two identical expression cassettes bearing the neuro-specific human Synapsin promoters (hSyn) drive the expression of EGFP or tdTomato fluorescent proteins. NKCC1 3'UTR was sub-cloned downstream of EGFP sequence. Therefore, the EGFP/tdTomato ratio reflects changes in post-transcriptional regulation exerted by NKCC1 3'UTR. Mutations of miR497a-5p and miR101-3p seed-binding sequences on NKCC1 3'UTR was performed by standard PCR techniques.

2. Real-Time Quantitative PCR (RT-qPCR)

RT-qPCR was performed as previously described [73,173]. Total RNA was extracted with QIAzol reagent and purified on miRNeasy spin columns (Qiagen), which includes an in-column RNAse-free DNAse digestion for the removal of contaminating genomic DNA. RNA samples were quantified at 260 nm with a ND1000 Nanodrop spectrophotometer (Thermo Scientific). RNA purity was also determined by absorbance at 280 and 230 nm.

For mRNA analysis, reverse transcription was performed according to the manufacturer's recommendations on 1 µg of RNA with QuantiTect Reverse Transcription Kit (Qiagen). SYBR green RT-qPCR was performed in triplicate with 10 ng of template cDNA using QuantiTect master mix (Qiagen) on a 7900-HT Fast Real-time System (Applied Biosystem), using the following universal conditions: 5 min at 95 °C, 40 cycles of denaturation at 95 °C for 15 sec, and annealing/extension at 60 °C for 30 sec. Product specificity and occurrence of primer dimers were verified by melting curve analysis. Primers for mRNA detection (see table 1) were designed with Beacon Designer software (Premier Biosoft) in order to avoid template secondary structure and significant cross homologies regions with other genes by BLAST

search. For each target gene, primers were designed to target specific transcript variants annotated in RefSeq database (http://www.ncbi.nlm.nih.gov/refseq).

For miRNA analysis, we adopted the previously described poly(A) tailing method [174]. In brief, 2.5 µg of total RNA were first poly-adenylated with Poly(A) Polymerase (Ambion) and 0.2 µM ATP for 15 min at 37°C. Four-hundred ng of poly(A) tailed RNA were then reverse-transcribed with SuperScript™ III First-Strand Synthesis SuperMix (Invitrogen) and 3.75 µM of a PolyT anchor oligo (5′-GCGAGCACAGAATTAATACGACTCACTATAGGTTTTTTTTTTTTTTTTTTVN-3′) for 50 min at 50°C. SYBR green RT-qPCR for microRNA was performed in triplicate with 4 ng of template cDNA (as above) with a miRNA-specific forward primer (see table 2) and a universal adaptor reverse primer (5′-GCGAGCACAGAATTAATACGAC-3′).

In each experiment, no-template controls (NTC) and RT-minus controls were run in parallel to the experimental samples. PCR reaction efficiency for each primer pair was calculated by the standard curve method with serial dilution of cDNA. PCR efficiency calculated for each primer set was used for subsequent analysis. All experimental samples were detected within the linear range of the assay. Gene expression data were normalized by the multiple internal control gene method [175].

To determine an accurate normalization factor for data analysis the expression stability of different control genes was evaluated with GeNorm algorithm [175] available in qBasePlus software (Biogazelle). The tested control genes for mRNA analysis were: Gapdh (glyceraldehyde-3-phosphate dehydrogenase), Ppia (peptidylprolyl isomerase A) and Actb (β-actin). Normalization of miRNA expression data was similarly performed with small nucleolar RNAs (snoRNA) snord65, snord70, snord110 and U6 Small nuclear RNA (snRNA). Based on the relative expression stability of the control genes calculated by GeNorm analysis, expression data for mRNA analysis were normalized with Gapdh and Ppia, while expression data for miRNA analysis were normalized with snord70 and snord110. Calibration curves parameters, PCR reaction efficiency and amplicon information are listed in table 3A and 3B.

TABLE 1

Gene name	Accession Number	Forward primer	Reverse primer
Actb	NM_007393	AAGTGGTTACAGGAAGTCC	ATAATTTACACAGAAGCAATGC
Gapdh	NM_008084	GAACATCATCCCTGCATCCA	CCAGTGAGCTTCCCGTTCA
Ppia	NM_008907	CACTGTCGCTTTTCGCCGCTTG	TTTCTGCTGTCTTTGGAACTTTGTCTGC
Nkcc1 (Slc12A2)	NM_009194	GCTCTATCTAAGGACCTACCACCA	AGGCACTGAAGTACCATTCTGGAG
TNRC6c	NM_198022	CTCGTGGTCTCTGTCTTG	AATAACATCTTCAGTGCTAGGA

App	NM_001198823	CCGCCACAGCAGCCTCTG	AAATGGACACCGATGGGTAGTGAA
U6	NR_003027 (mouse) NR_004394 (human)	CGCTTCGGCAGCACATATAC	GCTTCACGAATTTGCGTGTC

TABLE 2

Gene name	Accession Number	Forward primer
mmu-Sno65	NR_028541	TTACCGGCAGATTGGTAGTG
mmu-Sno70	NR_028554	ACAAAAATTCGTCACTACCACTG
mmu-Sno110	NR_003078	AGATCACTGACGACTCCATGTG
mmu-miR101-3p	NR_029537	CGCAGTACAGTACTGTGATAACTGAA
mmu-miR15a-5p	NR_029733	TAGCAGCACATAATGGTTTGTGAA
mmu-miR15b-5p	NR_029529	TAGCAGCACATCATGGTTTACAAA
mmu-miR16-5p	NR_029734	TAGCAGCACGTAAATATTGGCG
mmu-miR195-5p	NR_029581	TAGCAGCACAGAAATATTGGCAA
mmu-miR322-5p	NR_029756	AGCAGCAATTCATGTTTTGGA
mmu-miR497a-5p	NR_030444	CAGCAGCACACTGTGGTTTGTA
hsa-Sno65	NR_003054	ACCGGCAGATTGTGTAGTGG
hsa-Sno70	NR_003058	TTCGTCACTACCACTGAGACAAC
hsa-Sno110	NR_003078	ATCTGTCAATCCCCTGAGTGC
hsa-miR101-3p	NR_029836	CGCAGTACAGTACTGTGATAACTGAA
hsa-miR15a-5p	NR_029485	TAGCAGCACATAATGGTTTGTGAA
hsa-miR15b-5p	NR_029663	TAGCAGCACATCATGGTTTACAAA
hsa-miR16-5p	NR_029486	TAGCAGCACGTAAATATTGGCG
hsa-miR195-5p	NR_029712	TAGCAGCACAGAAATATTGGCAA
hsa-miR424-5p	NR_029946	CAGCAGCAATTCATGTTTTGAA
hsa-miR497a-5p	NR_030178	CAGCAGCACACTGTGGTTTGTA

TABLE 3A

Gene name	Organism	Accession number	Amplicon length (bp)	Final primer concentration (µM)	Calibration curve (Slope/R^2)	Calculated PRC efficiency (%)
Actb	mouse	NM_007393	123	0.1	-3.130/0.986	108.7
Gapdh	mouse	NM_008084	77	0.2	-3.370/0.999	98.0
Pppia	mouse	NM_008907	133	0.2	-3.321/0.994	100.0
Nkcc1 (Slc12A2)	mouse	NM_009194	101	0.2	-3.280/0.999	101.8
Tnrc6c	mouse	NM_198022	118	0.2	-3.306/0.999	96.6

App	mouse	NM_001198823	124	0.2	-3.236/0.994	103.7

TABLE 3B

Gene name	Organism	Accession number	Final primer concentration (μM)	Calibration curve (Slope/R^2)	Calculated PRC efficiency (%)
mmu-Sno65	mouse	NR_028541	0.2	-3.383/0.999	97.5
mmu-Sno70	mouse	NR_028554	0.2	-3.342/0.999	99.2
mmu-Sno110	mouse	NR_003078	0.2	-3.459/0.999	94.6
U6	mouse	NR_003027	0.2	-3.411/0.997	96.4
mmu-miR101-3p	mouse	NR_029537	0.2	-3.432/0.999	95.6
mmu-miR15a-5p	mouse	NR_029733	0.2	-3.262/0.999	102.6
mmu-miR15b-5p	mouse	NR_029529	0.2	-3.349/0.999	98.9
mmu-miR16-5p	mouse	NR_029734	0.2	-3.259/0.997	101.1
mmu-miR195-5p	mouse	NR_029581	0.2	-3.437/0.997	95.4
mmu-miR322-5p	mouse	NR_029756	0.2	.3.343/0.992	99.1
mmu-miR497a-5p	mouse	NR_030444	0.2	-3.336/0.986	99.4
hsa-Sno65	human	NR_003054	0.2	-3.283/0.996	101.6
hsa-Sno70	human	NR_003058	0.2	-3.23/0.999	103.9
hsa-Sno110	human	NR_003078	0.2	-3.514/0.928	92.56
U6	human	NR_004394	0.2	-3.346/0.998	99.01
hsa-miR101-3p	human	NR_029836	0.2	-3.432/0.999	95.6
hsa-miR15a-5p	human	NR_029485	0.2	-3.262/0.999	102.6
hsa-miR15b-5p	human	NR_029663	0.2	-3.349/0.999	98.9
hsa-miR16-5p	human	NR_029486	0.2	-3.259/0.997	101.1
hsa-miR195-5p	human	NR_029712	0.2	-3.437/0.997	95.4
hsa-miR424-5p	human	NR_029946	0.2	-3.426/0.934	95.8
hsa-miR497a-5p	human	NR_030178	0.2	-3.336/0.986	99.4

3. Human Brain Samples

Hippocampal samples from adult human Down syndrome patients and age/sex-matched non-trisomic controls were obtained from the Brain and Tissue Bank for Developmental Disorders at the University of Maryland, Baltimore (MD). Samples information are described in Table 4 and were previously reported [73].

TABLE 4

Case number	Disorder	Age (years)	Gender
1276	DS	13	M
5277	DS	19	M
5341	DS	25	M
5005	DS	39	F
M1960M	DS	19	M
4925	Control	13	M
1841	Control	19	M
605	Control	25	M
5606	Control	35	F
4782	Control	18	M

4. Primary cultures and transfection

Primary neuronal cultures were prepared from WT and Ts65Dn pups at postnatal day 2 (P2), as previously described [176,177]. In brief, brains were dissected under a stereomicroscope in ice-cold Dissection Buffer (DB) composed of Hank's Balanced Salt Solution (HBSS; Gibco) supplemented with 6 mg/mL glucose, 3 mg/mL bovine serum albumin (BSA), 5.5 mM $MgSO_4$, 5 µg/mL gentamycin and 10 mM Hepes, pH 7.4 (all from Sigma). Cortical or hippocampal tissue was minced and then enzymatically digested with 0.25% trypsin in HBSS (Gibco) containing 0.6 mg/mL Deoxyribonuclease I (DNAse; Sigma) for 5 min at 37°C. Tissue chunks were washed in DB, incubated for 5 min in DB supplemented with 1 mg/mL of Soybean trypsin inhibitor (Sigma) and mechanically dissociated in DB supplemented with 0.6 mg/mL DNAse. Cells were passed through a 40 µm cell strainer and then centrifuged (*110 x g* for 7 min at 4°C) to remove cellular debris. Cells were plated on glass coverslips, 6-wells plates or MEA coated with poly-L-lysine (Sigma; 0.1 mg/mL in 100 mM borate buffer, pH 8.5) at a density of 250-500 cells/mm^2. Neurons were maintained in a culture medium consisting of Neurobasal-A supplemented with 2% B27, 1% GlutaMax and 5 µg/mL gentamycin (all from Gibco) at 37 °C in humidified atmosphere (95% air, 5% CO_2).

Primary cortical glial cultures were prepared from WT and Ts65Dn pups at P4. In brief, brains were dissected under a stereomicroscope in ice-cold HBSS. Cortical tissue was minced and then enzymatically digested with 0.25% trypsin in HBSS containing 1 mg/mL DNAse for 15 min at 37°C. Tissue chunks were washed in Glial medium (MEM supplemented with 10% horse serum, 1% Pen-Strep, 33 mM glucose and 1% glutamine, all from Gibco) and then centrifuged for 5 minutes at 1200 rpm. Pellet was

resuspended in fresh glial medium and mechanically dissociated. Cells were passed through a 40 µm cell strainer and plated on petri dishes coated with poly-D-lysine (Sigma; 0.01 mg/mL in H_2O). A complete medium change was performed the next day. Cells were maintained at 37 °C in humidified atmosphere (95% air, 5% CO2) with half-medium change every week. Cells were harvested at 14-16 DIV.

microRNA mimics and inhibitors were purchased from Ambion (Thermo Fisher Scientific). For biochemistry experiments, neurons were plated in 6-wells plates and transfected at 6 DIV with 45 pmol (30 nM final concentration in well) of microRNA mimics (mirVana Control mimic, catalog number: 4464058; mirVana m497a-5p mimic, ID: MC11293; mirVana m101a-3p mimic, ID: MC11414) or microRNA inhibitors (mirVana Control inhibitor, catalog number: 4464076; mirVana m497a-5p inhibitor,: MH11293; mirVana miR101a-3p inhibitor, ID: MH11414). Cells were harvested two days after transfection. For MEA recording and MQAE imaging experiments, neurons were transfected at 13 DIV with 6.5 or 25 pmol of microRNA mimics, respectively (10 nM final concentration in wells for both). Chloride imaging and MEA recordings were performed three days after transfection. For simultaneous transfection experiments with two microRNA mimics, neurons were transfected with a 1:1 mixture of each microRNA mimic (thus maintain the unaltered total amount of transfected mimics).

The specific short interfering RNA (siRNA) against Tnrc6c (Silencer Select Tnrc6c siRNA, ID #s103983) and control siRNA (Silencer Select Control siRNA, catalog number: 4390843) were also purchased from Ambion. Neurons plated in 6-wells plates were transfected at 5 DIV with 25 pmol (16.7 nM final concentration in wells) of siRNA. Transfected neurons were lysed four days after transfection. All RNA transfections were performed with 0.1 µl/pmol RNA of Lipofectamine RNAiMAX (Thermo Fisher Scientific).

For imaging experiments with biSyn-EGFP-TOM sensor, neurons were co-transfected at 13 DIV with 0.5 µg of plasmid and 12.5 pmol (4.8 nM final concentration in well) of microRNA mimics with 0.5 µl Lipofectamine2000 (Thermo Fisher Scientific) following manufacturer's instructions. Neurons were fixed with 4% paraformaldehyde 2 days after transfection for subsequent image analysis.

For dual-luciferase assay, cortical neurons were plated in 24 well plates. Neurons were transfected at 7 DIV with 0.2 µg of psiCHECK-2-NKCC1-3'UTR plasmid and 0.2 µL of Lipofectamine2000. Dual-luciferase measurements were performed at 15 DIV.

5. RNA interference

Sequences used for RNA interferences (RNAi) experiments were selected with BLOCK-iT RNAi Designer (Invitrogen). For viral expression of artificial microRNAs (amiRs) against mouse NKCC1 (SLC12A2: NM_009194) two amiR sequences (NKCC1 amiR #1: TTAACATGCAGCGGACTAATA and NKCC1 amiR #2: ATCACCAGCAGCACAATCTGA) were first cloned into the pcDNA6.2-GW/EmGFP-miR plasmid using the BLOCK-iT Pol II miR RNAi kit (Invitrogen), as previously described [178,179]. The expression cassette thus consisted of a 5' miR flanking region, a target-specific stem-loop amiR sequence and a 3' miR flanking region. This amiR cassette can be expressed from the 3' Untranslated Region (UTR) of any reporter gene under the control of a RNA polymerase type II promoter [180]. As a negative control, we used the control amiR sequence from pcDNA6.2-GW/EmGFP-miR-neg-control plasmid (provided with the kit) containing a sequence that did not target any known vertebrate gene (Control amiR: AAATGTACTGCGCGTGGAGAC). The amiR expression cassettes were then sub-cloned in lentiviral vector (LV) plasmids derived from pCCL.sin.cPPT.PGK.GFP.WPRE [181] (kind gift by L. Naldini, TIGET, San Raffaele Scientific Institute, Milan, Italy) downstream of the green fluorescent protein EGFP under the control of the human phosphoglycerate kinase promoter (hPGK) or downstream of the red fluorescent protein mCherry under the control of the neuro-specific human synapsin promoter (hSyn).

For viral expression of the short interference RNA (shRNA) against APP, a pair of DNA oligos (listed in table 5) were in vitro annealed and cloned downstream of the human U6 Pol III promoter in the pRNAT-U6 plasmid (GenScript). The U6 expression cassette was then sub-cloned in the AAV-hSyn-tdTomato vector (an adeno-associated virus vector plasmid derived from pAAV-hSyn-EGFP; Addgene #50465).

TABLE 5

shRNA	Top oligo	Bottom oligo
APP-sh	GATCGGCTGCTTCTCCTACGTATTCTCGAAA GAATACGTAGGAGAAGCAGCCTTTTTTTA	AGCTTAAAAAAAGGCTGCTTCTCCTACGTA TTCTTTCGAGAATACGTAGGAGAAGCAGCC
Control-sh	GATCGGCTTACGCTGAGTACTTCGATCGAA ATCGAAGTACTCAGCGTAAGCCTTTTTTT	AGCTTAAAAAAAGGCTTACGCTGAGTACTT CGATTTCGATCGAAGTACTCAGCGTAAGCC

For viral expression of microRNA mimics we adopted a previously described strategy that minimizes passenger-strand-mediated off-target effects [182]. For each microRNA mimic, a pair of DNA oligos (listed in table 6) were in vitro annealed and cloned downstream of the human U6 Pol III promoter in the pRNAT-U6 plasmid (GenScript). The U6 expression cassettes were then sub-cloned in the AAV-hSyn-tdTomato vector.

TABLE 6

miR-mimic	Top oligo	Bottom oligo
miR-497a-mimic	GAACCACAGTGTGCTGCTGCTCCTGACC CAGCAGCAGCACACTGTGGTTCTTTTTTT	AAAAAAAGAACCACAGTGTGCTGCTGCTG GGTCAGGAGCAGCAGCACACTGTGGTTC
miR-101-mimic	GAGTTATCACAGTACTGTACTCCTGACC CAGTACAGTACTGTGATAACTCTTTTTTT	AAAAAAAGAGTTATCACAGTACTGTACTG GGTCAGGAGTACAGTACTGTGATAACTC
Control-miR	GTCCACGCGCAGTACATTTCTCCTGACC CAGAAATGTACTGCGCGTGGACTTTTTTT	AAAAAAAGTCCACGCGCAGTACATTTCTG GGTCAGGAGAAATGTACTGCGCGTGGAC

6. Viral preparations

VSVG-pseudotyped third-generation LVs were produced by transient co-transfection into HEK293T cells using the calcium phosphate transfection method. Supernatants were collected, passed through a 0.45 μm filter and purified by ultracentrifugation, as previously described [178,181]. LVs were titrated at concentrations ranging from 5.0 x 10^8 to 1.0 x 10^9 transducing units (TU)/mL by FACS analysis on HEK293T or Neuro2a cells by the limiting dilution method. Neuronal cultures were infected with lentiviruses at 7 DIV by using 5-10 multiplicity of infection (MOI) and used for experiments between 15 and 20 DIV. The efficiency of infection was estimated to range between 80 and 95% of cells.

AAV chimeric serotype 1/2 ($AAV_{1/2}$) vectors were produced using a slight modification of the adenovirus-free transient transfection methods described before [183,184]. Briefly, adherent HEK293 cells were transfected with three plasmids containing the adenovirus helper proteins, the AAV Rep and Cap genes, and the ITR-flanked transgene expression cassette. Three days after transfection, cells were harvested, lysed and treated with benzonase (Sigma). $AAV_{1/2}$ vectors were purified by affinity columns as previously described [185]. The final AAV products were formulated in sterile phosphate buffered saline containing 0.001% of pluronic F-68 (Sigma), and stored at -80°C. AAV vector were titrated at concentrations ranging from 1.8 x 10^{11} and 1.0 x 10^{12} viral genome (vg)/mL by qPCR assay. Neuronal cultures were infected with AAV vectors at 7 DIV with 1.2 x 10^8 vg for miR mimics and 1.0 x 10^9 vg for APP knock-down. Cultures were used for experiments between 15 and 20 DIV.

7. Biochemistry

Samples were lysed in ice-cold RIPA buffer (1% NP40, 0.5% Deoxycholic acid, 0.1% SDS, 150 mM NaCl, 1 mM EDTA, 50 mM Tris, pH 7.4) containing 1 mM PMSF, 10 mM NaF, 2 mM sodium orthovanadate and 1% (v/v) protease and phosphatase inhibitor cocktails (Sigma). Samples were clarified through centrifugation at *20,000 x g* at 4°C, and the protein concentration was determined using the BCA kit (Pierce). For immunoblot analysis, protein extracts were prepared in lithium-dodecyl-sulfate (LDS) sample buffer (ThermoFisher Scientific) containing 50 mM dithiothreitol (DTT). To avoid NKCC1 protein aggregation/precipitation, samples were not heat-treated before loading [186,187]. Equal amounts of proteins were run on 4-12% Bis-Tris, NuPAGE (ThermoFisher Scientific) or Criterion-XT (Bio-Rad) gels with MOPS buffer and transferred overnight at 4°C onto nitrocellulose membranes (GE Healthcare) with Tris-Glycine transfer buffer (25 mM Tris-base, 192 mM glycine, 20% methanol). Membranes were probed with mouse anti-NKCC1 (clone T4c, Developmental Studies Hybridoma Bank; 1:4,000), mouse anti-APP (clone 22C11 Sigma catalog nº MAB348 1:4,000), chicken anti-GAPDH (Sigma, catalog nº AB2302, 1:16,000) and rabbit anti-Actin (Sigma, catalog nº: A2066; 1:10,000), followed by HRP-conjugated goat secondary antibodies (ThermoFisher Scientific; 1:5,000). Chemiluminescent signals were revealed with SuperSignal West Pico substrate (Pierce) and digitally acquired on a LAS 4000 Mini imaging system (GE Healthcare). Band intensities were quantified using ImageQuant software (GE Healthcare). The specificity of the anti-NKCC1 antibody was previously verified on brain samples from NKCC1 deficient mice [73].

8. MQAE intracellular chloride imaging

Imaging of intracellular Cl^- in hippocampal neurons was performed with the fluorescent chloride-sensitive indicator MQAE [N-(Ethoxycarbonylmethyl)-6-Methoxyquinolinium-Bromide], as previously described [73]. MQAE dye detects Cl^- ions *via* diffusion-limited collisional quenching, resulting in a concentration-dependent decrease of fluorescence emission following an increase in Cl^- concentration [188]. Therefore, a decrease in MQAE fluorescence is indicative of a higher $[Cl^-]_i$ and *vice versa*. Hippocampal neurons at 15 DIV were loaded with 5 mM MQAE (Molecular Probes) for 30 minutes at 37°C. Coverslips were then transferred to a holding chamber and perfused (2 mL/min) with extracellular solution (NaCl 145 mM, KCl 5 mM, $CaCl_2$ 2 mM, $MgCl_2$ 1 mM, HEPES 10 mM, D-glucose 5.5 mM, pH 7.4) at 25°C for 5 minutes before imaging. Images were taken with a Nikon A1 scanning confocal microscope equipped with a 20X air-objective (NA 0.75). MQAE was excited with a 405 nm diode laser and fluorescence

collected with a 525/50 nm band-pass emission filter. All excitation and acquisition parameters (laser intensity, PMT offset and gain) were keep constant throughout experiments. Image analysis was performed with NIS-Elements software (Nikon) by measuring the mean fluorescent intensity of regions of interest (ROIs) covering on the cell body of individual neurons from 6 randomly-selected fields of view for each coverslip. For each experiment, the average fluorescent intensity of all ROIs from a coverslip was normalized to the average fluorescent intensity of control samples in the same experiment. Pseudo-color images were generated with ImageJ software (http://rsbweb.nih.gov/ij/).

9. Fluorescent sensor imaging

Fluorescence images in hippocampal neurons transfected with biSyn-GFP-Tom were taken with a Nikon A1 scanning confocal microscope equipped with a 10X air-objective (NA 0.45). GFP was excited with a 488 nm diode laser and fluorescence collected with a 525/50 nm band-pass emission filter. tdTomato was excited with a 546 nm diode laser and fluorescence was collected with a 595/50 nm band-pass emission filter. All excitation and acquisition parameters (laser intensity, PMT offset and gain) were keep constant throughout experiments. Images were automatically acquired with NIS-Elements software from 9 fields of view (arranged in a 3x3 array) for each coverslip,

Image analysis was semi-automatically performed with NIS-Elements software with the "Object Count" and the "Automatic Measurement Results" tools. ROIs were automatically detected on neuronal cell bodies using a fixed intensity threshold on the red channel. To calculate GFP/tdTomato ratio, the mean fluorescence intensity of GFP and tdTomato were measured for each ROI. For each experiment, the average GFP/tdTomato ratio of all ROIs from a coverslip was normalized to the average fluorescent intensity of control samples (WT neurons transfected with biSyn-GFP-Tom NKCC1-3'UTR plasmid and control miR) in the same experiment. Pseudo-color images of GFP/tdTomato ratio shown in figure 14, 18 and 19 were generated with NIS-Elements software (Nikon).

10. Luciferase assay

Luciferase measurements were performed with Dual-luciferase assay kit (Promega), following the manufacturer's instructions on a Victor 3 plate reader (Perkin Elmer). Briefly, neurons were lysed in the provided lysis buffer and firefly luciferase luminescence was measured after addition of its specific substrate. Then, renilla luciferase luminescence was measured upon addition of Stop and Glow substrate (that also inhibits firefly luciferase activity).

11. Micro-Electrode Array recordings

Microelectrode arrays (Multichannel Systems, Germany) consisted of 60 TiN/SiN planar round electrodes (30 μm diameter; 200 μm center-to-center inter-electrode distance) divided into 6 separated wells. Each well contained 9 recording electrodes, arranged in a 3 × 3 square grid, and one big ground electrode. The activity of all cultures was recorded by means of the MEA60 System. After 1200x amplification, signals were sampled at 10 kHz and acquired through the data acquisition card and MC-Rack software (Multichannel Systems). To reduce thermal stress of the cells during the experiment, MEAs were kept at 37 °C through a controlled thermostat (Multichannel Systems) in an experimental setup equipped with a custom-made incubator chamber (maintaining an humidified atmosphere consisting of 95% air and 5% CO_2). All recordings were carried out in culture maintained in their original medium. Cultures were transferred to the recording setup and acclimatized for 20 minutes before beginning the recordings to allow the culture to adapt to the new environment and reach a stable level of activity [189-191].

Spontaneous network activity of cultures was first recorded for 30 minutes. To assess the synchronicity of the neuronal networks, we computed the cross-correlation function between each pair of spike trains recorded from active channels. The cross-correlation function represents the probability of observing a spike in one channel i at time (t+τ, τ=3 ms) given that there is a spike in a second channel i+1 at time t. To quantify the strength of correlation between each pair of electrodes, we evaluated the correlation peak (C_{peak}).

Spontaneous bursting activity was detected using a custom burst detection method [192,193]. According to those algorithms, in order to detect bursts, two thresholds were fixed: the first one was the maximum inter-spike interval (ISI) allowed for spikes within a burst (maxISI, usually set at 100 ms); the second one was defined as the minimum number of consecutive spikes belonging to a burst (minSpikes, usually set at 5).

After recording basal activity, bicuculline (BIC) or GABA (both 20 μM; Sigma) were applied and activity was recorded for an additional 30 minutes. The drugs were added to the bath solution by directly pipetting in the medium. Since we noticed that mechanical perturbation due to the pipette injection in the medium could cause a temporary instability of the firing rate, we discarded the first 10 minutes at the beginning of the 30-minutes recording phase.

Data analysis was performed off-line with Matlab software (The Mathworks, USA) using the custom software package SPYCODE [194]. The steps in the analysis are described briefly below.

Raw traces were high-pass-filtered (>300 Hz) to isolate spikes from the low fluctuation of the signal (LFP). We computed the spike detection as previously described [195].

To characterize the activity level of the analyzed networks, we calculated the mean firing rate (MFR), which is defined as the mean number of spikes per second measured over the total recording time. We considered electrodes active if they recorded a firing rate greater than 0.02 spikes per second. The low threshold guarantees that only electrodes that are not covered by cells and those with very few spikes are excluded and that all others are retained.

We computed the percentage of variation with respect to basal condition for each active electrode as follows:

$$\%\, Variation\ Ch = \frac{MFRdrug - MFRbasal}{MFRbasal}$$

In order to evaluate statistical differences in MFR variation for each recorded channel, and to avoid setting an arbitrary threshold of significance, we used bootstrap method.[196]

For the bootstrap analysis, the peak train for each time segment (basal or drug) was divided into 1-minute bins. The MFRs recorded during each 1-minute bin for the two time segments for each well were randomly shuffled into two groups for 10,000 times. The differences between the means of the randomly shuffled groups produced a null distribution (Fig. 5). For each channel, we computed the real difference between the basal and the drug values and assessed whether it fell outside the 95% confidence interval of the null distribution.

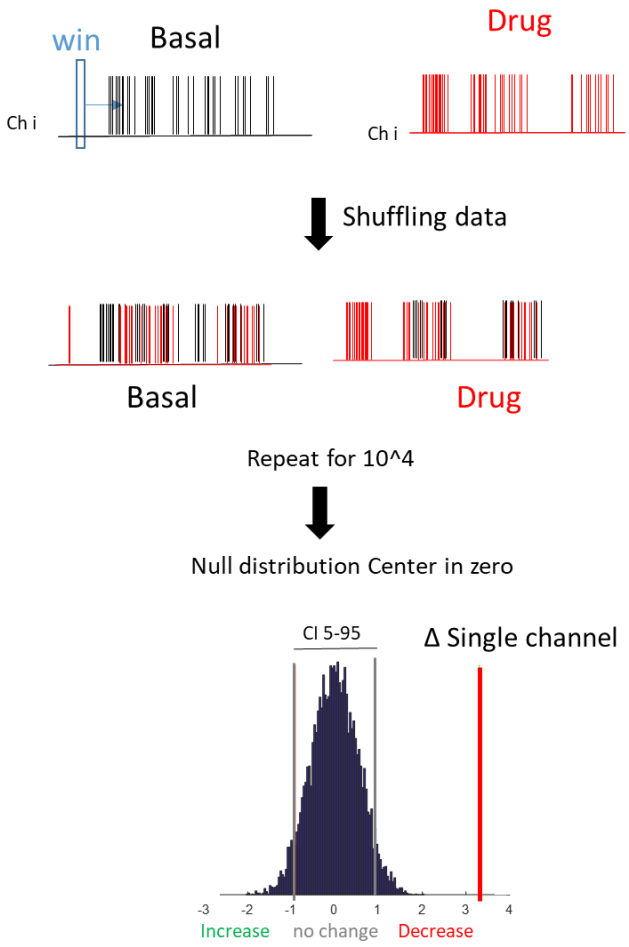

Figure 5: Bootstrap analysis method. The spike train for each channel was measured in 1-minute bins and shuffled 10,000 times. The differences between the means of the two randomly shuffled groups produced a null distribution. For each channel, we computed the real difference between the basal and the drug values and assessed whether it fell outside the 95% confidence interval of the null distribution.

12. Animals

Ts65Dn colony [41] was maintained by crossing Ts65Dn female to C57BL/6JEi x C3SnHeSnJ (B6EiC3) F1 males (Jackson Laboratories; Bar Harbor, USA). Animals were genotyped by PCR as previously described [197]. A veterinarian was employed to monitor health and comfort of the animals. Mice were housed in a temperature-controlled room with a 12:12 hour dark/light cycle and ad libitum access to water and food.

13. Statistical analysis

Except where otherwise stated, the results are presented as the means ± SEM. Statistical analysis was performed using SigmaPlot (Systat) or GraphPad (Prism) software. Where appropriate, the statistical significance was assessed using the following parametric test: paired Student's t-test, two-way ANOVA or two-way repeated-measures (RM) ANOVA followed by all pairwise Turkey's *post hoc* test. In case normal distribution or equal variance assumptions were not valid, statistical significance was evaluated using Wilcoxon signed-rank test (non-parametric) or two-way ANOVA and two-way RM-ANOVA on ranked transformed data. P values < 0.05 were considered significant.

RESULTS

1. NKCC1 expression in trisomic neuronal culture

Previous reports have indicated that NKCC1 chloride importer is upregulated in brains from Ts65Dn mice and Down syndrome persons [114]. Since chloride homeostasis regulated by NKCC1 expression levels influences cognitive behaviors, we were interested in understanding the cause of NKCC1 upregulation. As a first step, we assessed whether NKCC1 is upregulated also in Ts65Dn neurons in culture. To this aim, we analyzed the levels of NKCC1 protein in hippocampal and cortical primary neuronal cultures prepared from WT and Ts65Dn mice. At 15 days *in vitro* (DIV), neurons were lysed and NKCC1 protein expression was measured by western immunoblot. In line with previous *in vivo* results [114], western immunoblot analysis showed that the upregulation of NKCC1 is reproduced in both cortical and hippocampal trisomic neuronal cultures (Fig. 6).

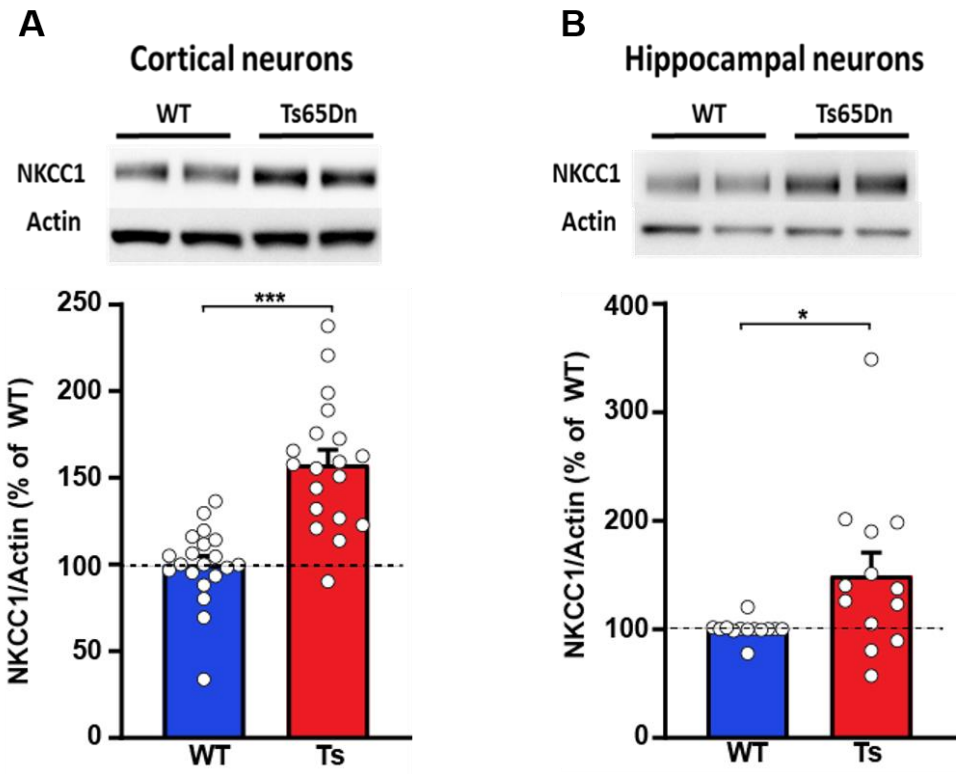

Figure 6: NKCC1 expression is increased in Ts65Dn cultured neurons. (A) *Top*: Representative immunoblot for NKCC1 in protein extracts from Ts65Dn and WT cortical neurons at 15 DIV. *Bottom*: Quantification of NKCC1 protein (expressed as percentage of WT neurons) showed increased NKCC1 expression in Ts65Dn compared to WT cortical neurons. Actin was used as loading control. **(B)** *Top*: Representative immunoblot for NKCC1 in protein extracts from Ts65Dn and WT hippocampal neurons at 15 DIV. *Bottom*: Quantification of NKCC1 protein (expressed as percentage of WT neurons) showed increased NKCC1 expression in Ts65Dn compared to WT hippocampal neurons. Actin was used as loading control. All data shown are means (± SEM). Each dot represents a single well obtained from 9 independent neuronal cultures. *p<0.05; *** p<0.001, unpaired Student's t-test.

These data indicate that primary cultures reproduce the phenotype observed *in vivo*, representing a suitable model to investigate the molecular mechanisms responsible for NKCC1 upregulation in DS. Interestingly, analysis of either NKCC1 mRNA expression by Real-Time quantitative PCR (RT-qPCR) or protein expression by immunoblot in primary cortical astrocyte cultures from WT and Ts65Dn mice did not show any significant difference (Fig. 7), indicating that altered regulation of NKCC1 expression is specific to trisomic neurons.

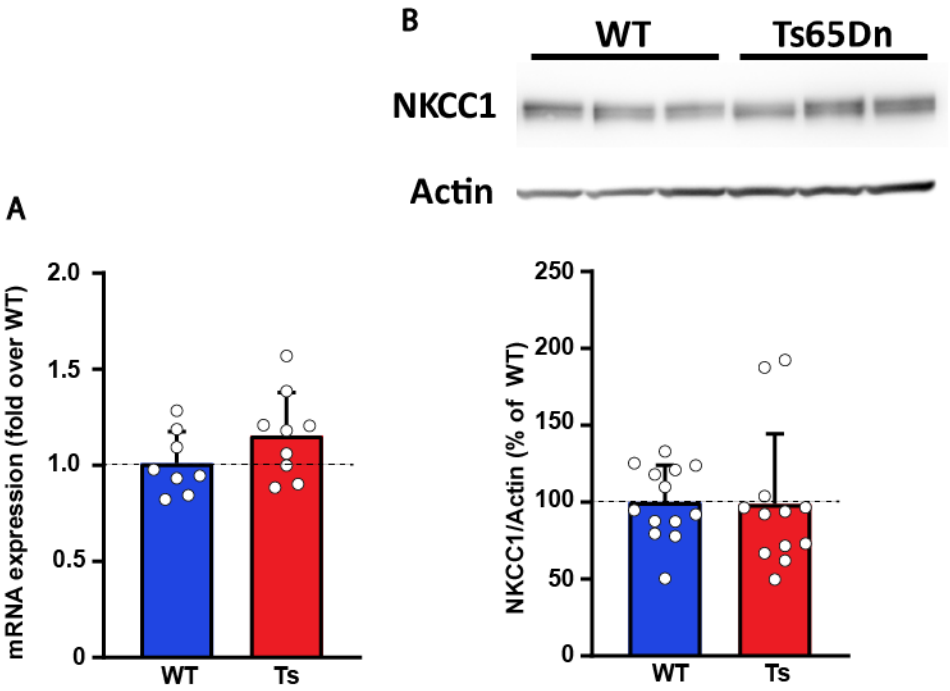

Figure 7: Similar NKCC1 mRNA and protein expression in cortical astrocyte cultures from WT and Ts65Dn mice. (A) RT-qPCR analysis of NKCC1 mRNA (expressed as fold over WT cells) showed similar NKCC1 expression in Ts65Dn compared to WT astrocytes. **(B)** *Top*: Representative immunoblot for NKCC1 in protein extracts from Ts65Dn and WT astrocytes at 15 DIV. *Bottom*: Quantification of NKCC1 protein (expressed as percentage of WT cells) showed similar NKCC1 expression in Ts65Dn compared to WT astrocytes. Actin was used as loading control. All data shown are means (± SEM). Each dot represents a single well obtained from 4 independent cultures.

Since previous studies have shown that the expression of NKCC1 and KCC2 are developmentally regulated during neuronal maturation [55,198], we next evaluated the expression of both the cotransporters in Ts65Dn neurons during development between 2 and 21 DIV. We found that NKCC1 was expressed at all timepoints and significantly increased in Ts65Dn neurons at both 15 and 21 DIV. In contrast, KCC2 expression was almost undetectable at 2 DIV, and strongly increased thereafter. Interestingly, KCC2 expression appeared to be similar in the two groups between 7 and 21 DIV (Fig. 8).

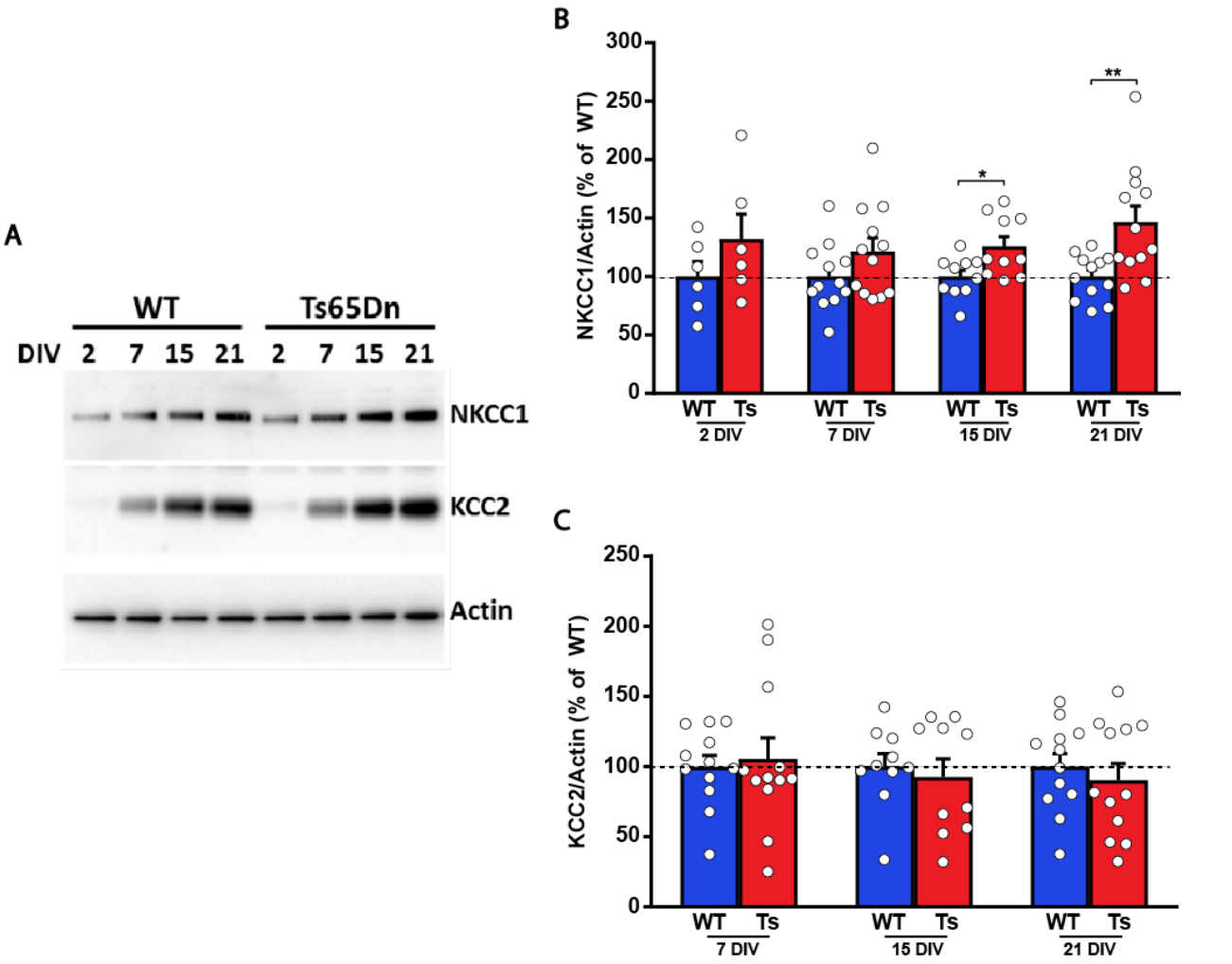

Figure 8: NKCC1 expression is increased in Ts65Dn neuronal cultures during development. **(A)** Representative immunoblot for NKCC1 and KCC2 in protein extracts from Ts65Dn and WT at different time points during neuronal development. **(B)** Quantification of NKCC1 protein (expressed as percentage of WT neurons at each time point) showed increased expression in Ts65Dn compared to WT neurons at both 15 and 21 DIV. Actin was used as loading control. **(C)** Quantification of KCC2 protein (expressed as percentage of WT neurons at each time point) showed similar expression in Ts65Dn compared to WT neurons in all time points. Actin was used as loading control. All data shown are means (± SEM). Each dot represents a single well obtained from 3 independent neuronal cultures. *p<0.05; ** p<0.01, unpaired Student's t-test.

2. NKCC1 upregulation causes intracellular chloride accumulation in Ts65Dn neurons.

To get insights into the functional consequences of NKCC1 upregulation in DS, we developed a Lentiviral-based RNA-interference (RNAi) strategy based on the expression of artificial microRNAs (amiR) to knockdown NKCC1 expression in trisomic neurons. We tested two different amiR sequences for their ability to reduce NKCC1 expression in WT and Ts65Dn neurons in culture. As shown in Fig. 9, NKCC1 expression was significantly reduced in both WT and Ts65Dn neurons by the two different amiR.

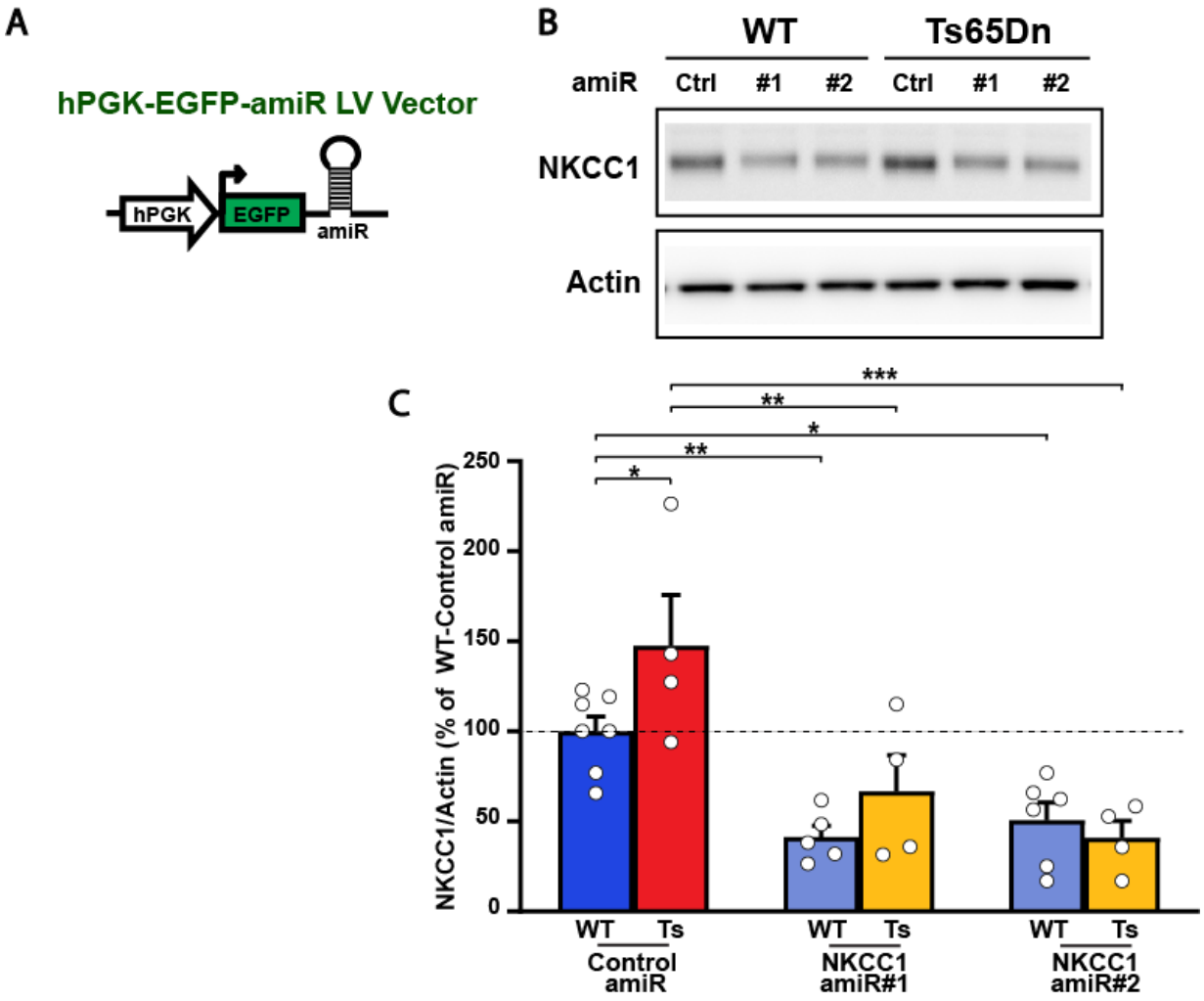

Figure 9: Lentiviral-based RNAi strategy reduces NKCC1 protein expression in both Ts65Dn and WT neuronal cultures. **(A)** Schematic representation of the lentiviral vector (LV) expressing either control or NKCC1 amiRs from the ubiquitous hPGK1 promoter. **(B)** Representative immunoblot for NKCC1 in protein extracts from LV-transduced Ts65Dn and WT neurons at 15 DIV. **(C)** Quantification of NKCC1 protein (expressed as percentage of WT neurons transduced with control amiR) showed increased NKCC1 expression in Ts65Dn compared to WT neurons. Expression of amiRs #1 and #2 induced significant NKCC1 knockdown in both WT and Ts65Dn neurons. Actin was used as internal standard. All data shown are means (± SEM). Each dot represents a single well obtained from 4 independent neuronal cultures. Two-way ANOVA: genotype [$F_{1,29}$=3.503, P=0.074]; treatment [$F_{2,29}$=19.942, P<0.001]; genotype x treatment [$F_{2,29}$= 2.256, P=0.127]. *p<0.05; **p<0.01; *** p<0.001, Two-way ANOVA followed by Tukey *post hoc* test.

Next, we measured changes in $[Cl^-]_i$ with the green fluorescent chloride-sensitive dye MQAE following NKCC1 knockdown in primary hippocampal neurons at 15 DIV. MQAE fluorescence is quenched by the presence of chloride ions. Therefore, an increase in $[Cl^-]_i$ is detected as a decrease in fluorescent signal. For these experiments, we expressed the NKCC1 amiRs together with the red fluorescent protein mCherry from the neuron-specific promoter hSyn (human Synapsin) to allow manipulation of $[Cl^-]_i$ selectively in neurons and its measurement by MQAE imaging. Intensity of fluorescence was measured on the cell bodies, to exclude the influence of the number of neurons present in different fields of view on mean fluorescence intensity. As previously reported for Ts65Dn brain slices [73], Ts65Dn cultured neurons transduced with control amiR showed decreased MQAE fluorescence (mirror of a higher $[Cl^-]_i$) compared to WT cells. Interestingly, NKCC1 knockdown by both amiRs significantly decreased $[Cl^-]_i$ in Ts65Dn neurons, indicating that NKCC1 upregulation drives intracellular chloride accumulation in trisomic neurons. NKCC1 knockdown in WT neurons also significantly decreased $[Cl^-]_i$ (Fig. 10).

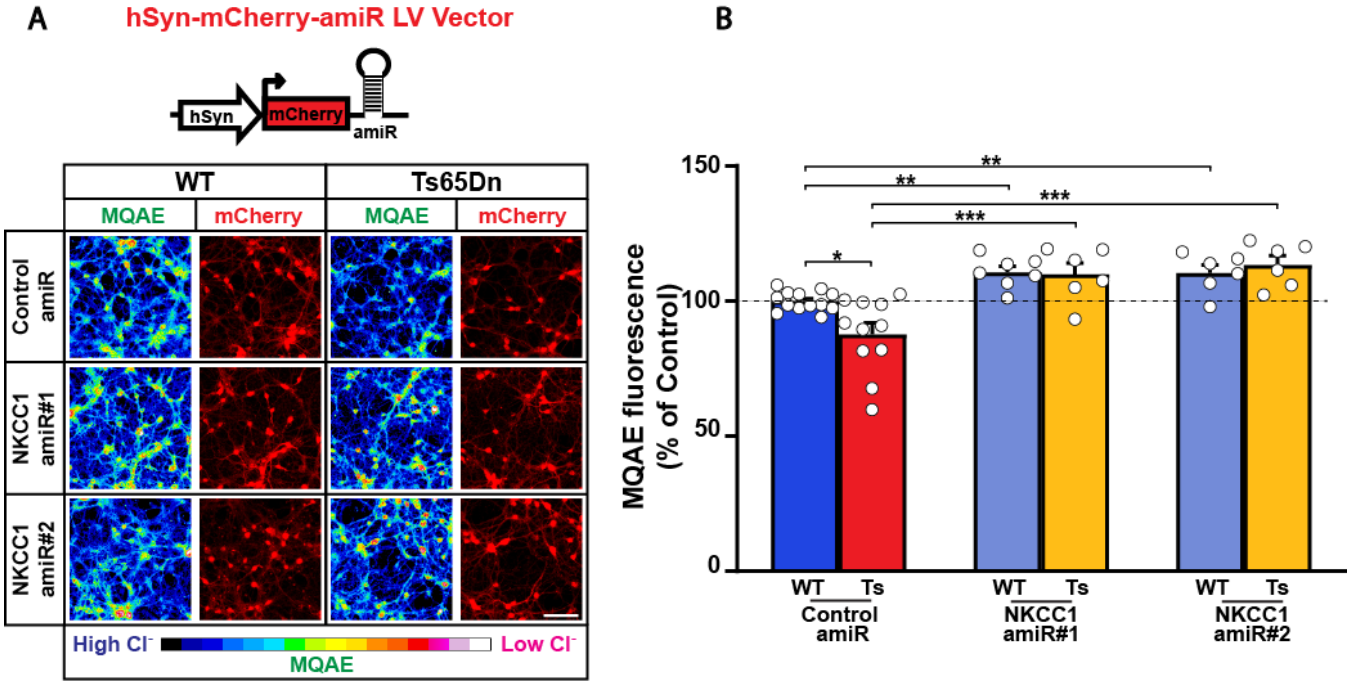

Figure 10: NKCC1 knockdown restores $[Cl^-]_i$ in Ts65Dn neurons (A) *Top*: Schematic representation of the LV expressing either control or NKCC1 amiRs from the neuron-specific hSyn promoter. *Bottom*: Representative images of LV-transduced WT and Ts65Dn hippocampal neurons at 15 DIV (expressing mCherry; red) during imaging experiments with the chloride-sensitive dye MQAE (pseudo-colors). Fluorescent intensity of the dye (color-coded on the bottom) is inversely proportional to $[Cl^-]_i$. **(B)** Quantification of $[Cl^-]_i$ with MQAE (expressed as percentage of WT neurons transduced with control amiR) showed lower fluorescent intensity (i.e. higher $[Cl^-]_i$) in Ts65Dn compared to WT neurons. NKCC1 knockdown by amiRs #1 or #2 significantly increased MQAE fluorescent intensity (i.e. decreased $[Cl^-]_i$) in both WT and Ts65Dn neurons. All data shown are means (± SEM).Each dot represents a single coverslip obtained from 6 independent neuronal cultures. Two-way ANOVA: genotype [$F_{1,48}$=0.394, P=0.533]; treatment [$F_{2,48}$=29.601, P<0.001]; genotype x treatment [$F_{2,48}$=1.891, P=0.163].. *p<0.05; **p<0.01; *** p<0.001, Two-way ANOVA followed by Tukey *post hoc* test.

3. Post-transcriptional regulation of NKCC1 expression in trisomic neurons.

As a first step in dissecting the mechanisms of NKCC1 regulation, we measured NKCC1 mRNA levels by RT-qPCR. In line with previous *in vivo* results in Ts65Dn mouse brains [114], we found that the expression of NKCC1 mRNA was similar between Ts65Dn and WT cortical and hippocampal primary neurons (Fig. 11). These results suggest that increased NKCC1 expression in Ts65Dn neurons is likely due to changes in post-transcriptional regulation rather than to enhanced transcription.

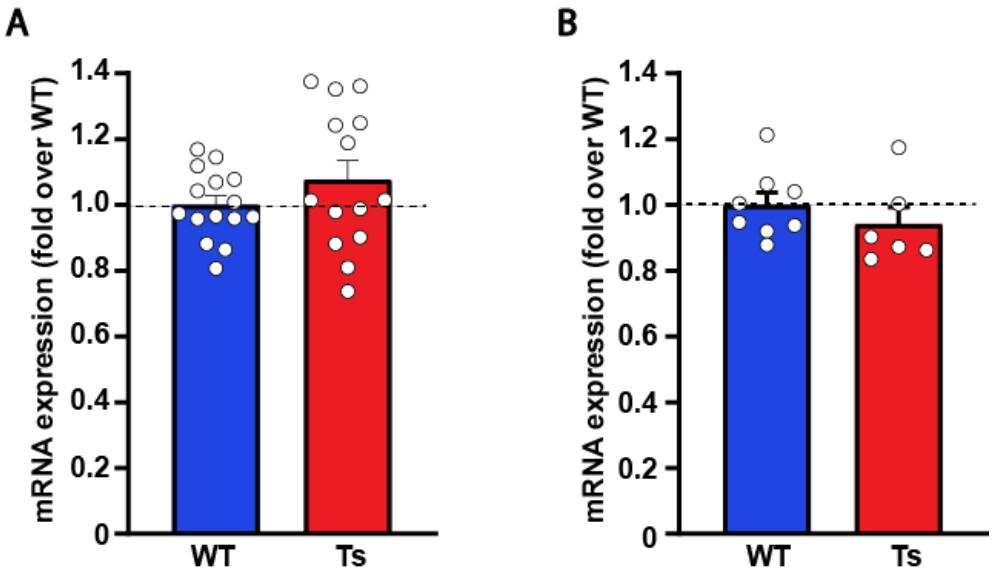

Figure 11: Similar NKCC1 mRNA expression in cortical and hippocampal neuronal cultures from WT and Ts65Dn mice. (A) RT-qPCR analysis of NKCC1 mRNA (expressed as fold over WT cells) showed similar NKCC1 expression in Ts65Dn compared to WT cortical neurons at 15 DIV. All data shown are means (± SEM). Each dot represents a single well obtained from 4 independent neuronal cultures **(B)** RT-qPCR analysis of NKCC1 mRNA (expressed as fold over WT cells) showed similar NKCC1 expression in Ts65Dn compared to WT hippocampal neurons at 15 DIV. All data shown are means (± SEM). Each dot represents a single well obtained from 2 independent neuronal cultures.

Increased NKCC1 protein expression in trisomic neurons could also be potentially due to a slower turnover rate in Ts65Dn cells. To compare NKCC1 protein degradation rate in trisomic and WT neurons, we treated the cultures with Cycloheximide (Chx) to inhibit protein synthesis. Then we analyzed NKCC1 expression at two different time points (12 and 24 hours later). Surprisingly, we found that NKCC1 protein turnover rate in trisomic neurons was actually faster than in WT neurons (Fig. 12). Indeed, the slope of best-fit linear regression line for Ts65Dn samples was significantly different from the one

obtained for WT samples. Therefore, NKCC1 upregulation in Ts65Dn neurons does not seem to originate from a slower protein turnover rate.

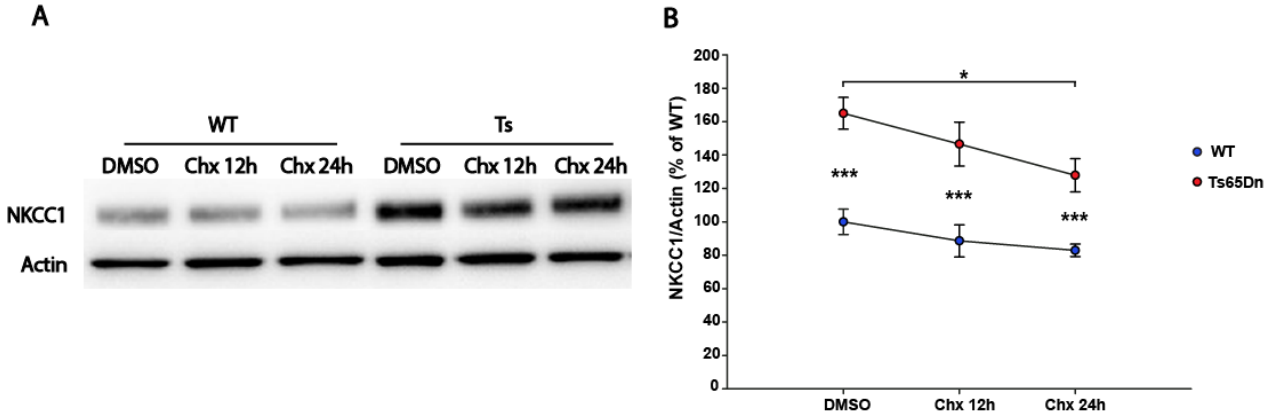

Figure 12: **NKCC1 protein turnover rate is increased in Ts65Dn neurons. (A)** Representative immunoblot for NKCC1 in protein extracts from Ts65Dn and WT neurons at 15 DIV after Cycloheximide (Chx) treatment for 12 or 24 hours. **(B)** Quantification of NKCC1 protein (expressed as percentage of WT neurons treated with DMSO) showed faster NKCC1 turnover in Ts65Dn neurons compared to WT. Actin was used as internal standard. All data shown are means (± SEM). Slope of the best-fit linear regression line was -0.712 ± 0.139 for WT and -1.546 ± 0.007 for Ts65Dn. Slopes were significantly different (*P*=0.027). Two-way ANOVA: genotype [$F_{1,57}$=88.783, P<0.001]; treatment [$F_{2,57}$=7.480, P=0.001]; genotype x treatment [$F_{2,57}$=0.0429 ,P=0.958]. *p<0.05; *** p<0.001, Two-way ANOVA followed by Tukey *post hoc* test.

Having established that increased NKCC1 protein expression in Ts65Dn neurons does not depend on differences in mRNA transcription or protein turnover, we hypothesized that the observed difference could depend on mechanisms affecting translationTranslational regulation often takes place at 3' untranslated regions (3'UTR) of genes. Considering that NKCC1 mRNA is characterized by the presence of a large 3'UTR (~2.8 kb) with a relatively high degree of conservation among mammals, we performed dual luciferase assay to test the influence of NKCC1 3'UTR on NKCC1 expression levels. To this aim, we cloned NKCC1 3'UTR downstream of Renilla luciferase (Rluc) in the psiCHECK2 plasmid, which also expresses Firefly luciferase (Fluc) as internal control. With this system, changes in the Rluc/Fluc ratio reflects the degree of post-transcriptional regulation exerted by the 3'UTR of NKCC1. Although this assay showed high variability, Ts65Dn cultures displayed a significantly higher value of the Rluc/Fluc ratio compared to WT. This was indicative of a loss of post-transcriptional repression exerted on the 3'UTR, which would result in enhanced NKCC1 expression in trisomic neurons (Fig. 13).

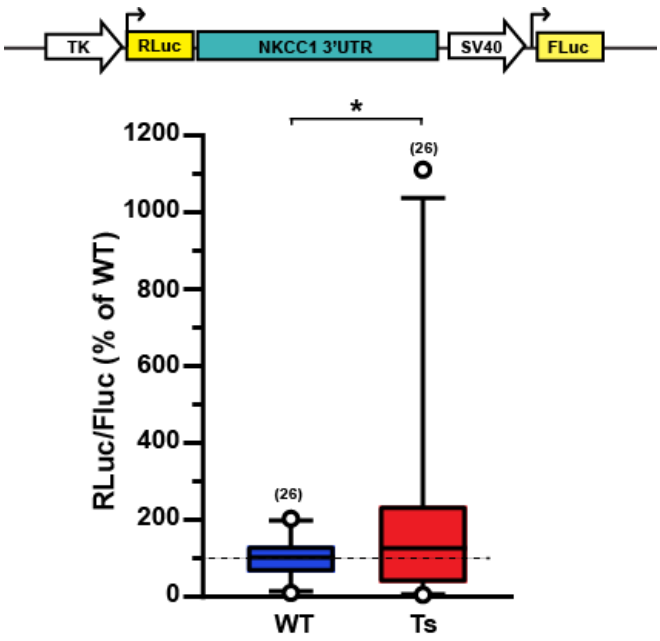

Figure 13: **Post-transcriptional regulation of NKCC1 3'UTR drives increased expression in Ts65Dn neurons.** *Top:* Scheme of the psiCHECK2 dual-luciferase plasmid used to assess NKCC1 3'UTR activity. *Bottom*: Rluc/Fluc ratio was increased in Ts65Dn neurons compared to WT. For each box plot, the central line indicates the median and the box limits indicate the 25th and 75th percentiles. Whiskers represent the 5th and the 95th percentiles. Number in parenthesis indicates the number of analysed samples for each experimental group obtained from 10 independent neuronal cultures. *p<0.05, unpaired Student's t-test.

We reasoned that the high variability observed in this assay could derive from two different sources. First, both Rluc and Fluc are expressed from ubiquitous promoters that will be active in both neurons and astrocytes in culture. Although, our neuronal cultures show ~10% astrocytes, these are transfected to high rate, therefore complicating the interpretation of the results. Second, the expression of Rluc and Fluc in this plasmid are under the control of two different promoters that could have different activity in different cell types including WT *versus* Ts65Dn neurons. To circumvent these limitations, we developed a neuro-specific sensor in which two identical transcription cassettes drive the expression of GFP and tdTomato fluorescent proteins under the control of the same neuron-specific Synapsin (Syn) promoter. In this sensor, NKCC1 3'UTR is cloned downstream of GFP while tdTomato serves as an internal control to normalize for transfection efficiency. Upon transfection in neurons, the GFP/tdTomato fluorescent signal ratio reflects the extent of translational repression exerted by NKCC1 3'UTR. With this assay, we confirmed the results obtained with the luciferase assay. Indeed the GFP/tdTomato ratio was significantly higher in trisomic neurons, indicating an impairment of post-transcriptional repression exerted on NKCC1-3'UTR (Fig 14).

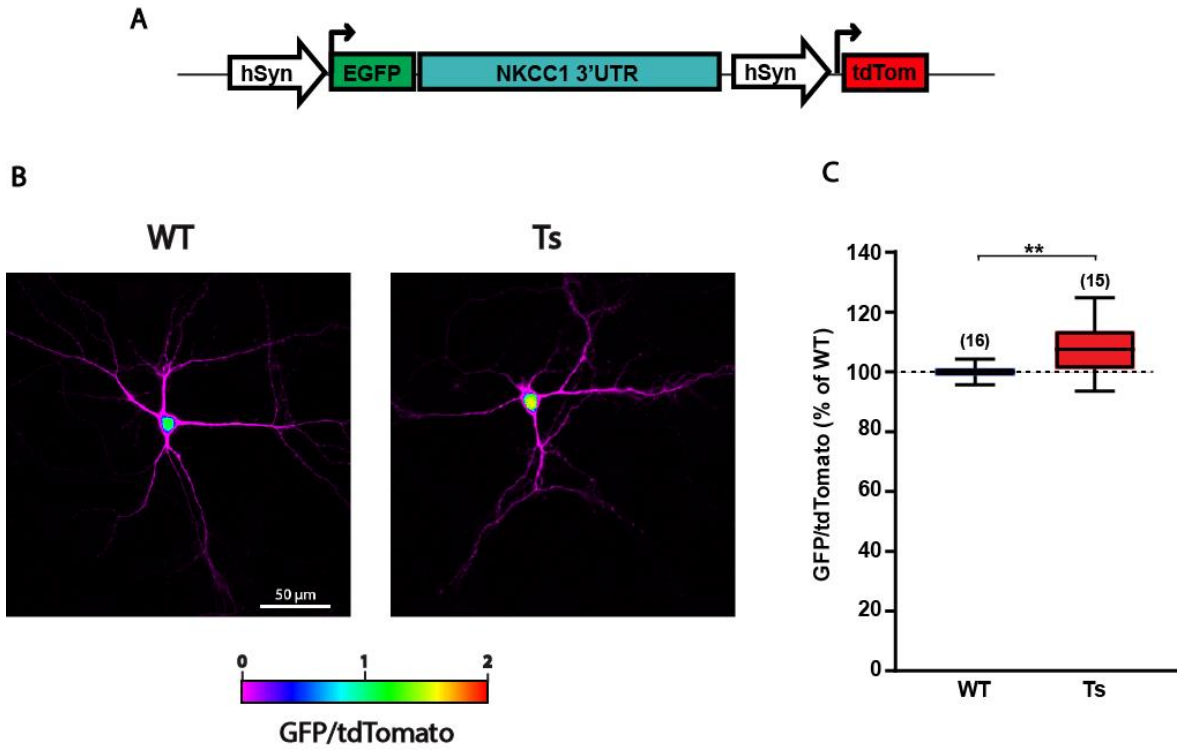

Figure 14: **Post-transcriptional regulation of NKCC1 3'UTR drives increased expression in Ts65Dn neurons. (A)** Scheme of the neuro-specific fluorescent sensor used to assess NKCC1 3'UTR repression activity. **(B)** Representative pseudo-color images of GFP/tdTomato ratio in WT and Ts65Dn neurons. **(C)** GFP/tdTomato ratio was increased in Ts65Dn neurons compared to WT. For each box plot, the central line indicates the median and the box limits indicate the 25th and 75th percentiles. Whiskers represent the 5th and the 95th percentiles. Number in parenthesis indicates the number of samples analyzed for each experimental group, deriving from 8 independent neuronal cultures. **p<0.01, unpaired Student's t-test.

Using the fluorescent sensor we found that the difference between WT and Ts65Dn in the ratio GFP/tdTomato was smaller than the difference in RLuc/FLuc obtained with luciferase assay. However, it should be noted that luciferase assay is affected by a greater variability compared to the measurement of fluorescence, probably due to the presence of signal collected from transfected astrocytes. Conversely, luciferase bioluminescence displays a wider dynamic range of measurement compared to fluorescence, partly explaining the smaller difference observed in Ts65Dn neurons compared to WT when performing the experiment using the fluorescent sensor.

4. microRNAs play a role in NKCC1 upregulation

Since 3'UTRs are the preferred site of action of microRNAs, we investigated the possible involvement of this class of regulatory noncoding RNAs in NKCC1 upregulation in trisomic neurons. To this aim, we inhibited microRNAs repressive activity by knockdown of the GW182 family member Tnrc6C (trinucleotide repeat containing protein 6C), an essential component of the RISC complex required for miRNA-dependent repression of translation of complimentary mRNAs [134] (Fig.15A). We transfected WT and Ts65Dn neurons with a specific short-interfering RNA (siRNA) and then assessed the changes in NKCC1 levels by western immunoblot. We found that Tnrc6C knockdown increased NKCC1 protein levels, demonstrating that NKCC1 expression is regulated by microRNAs in both WT and Ts65Dn neurons (Fig.15B).

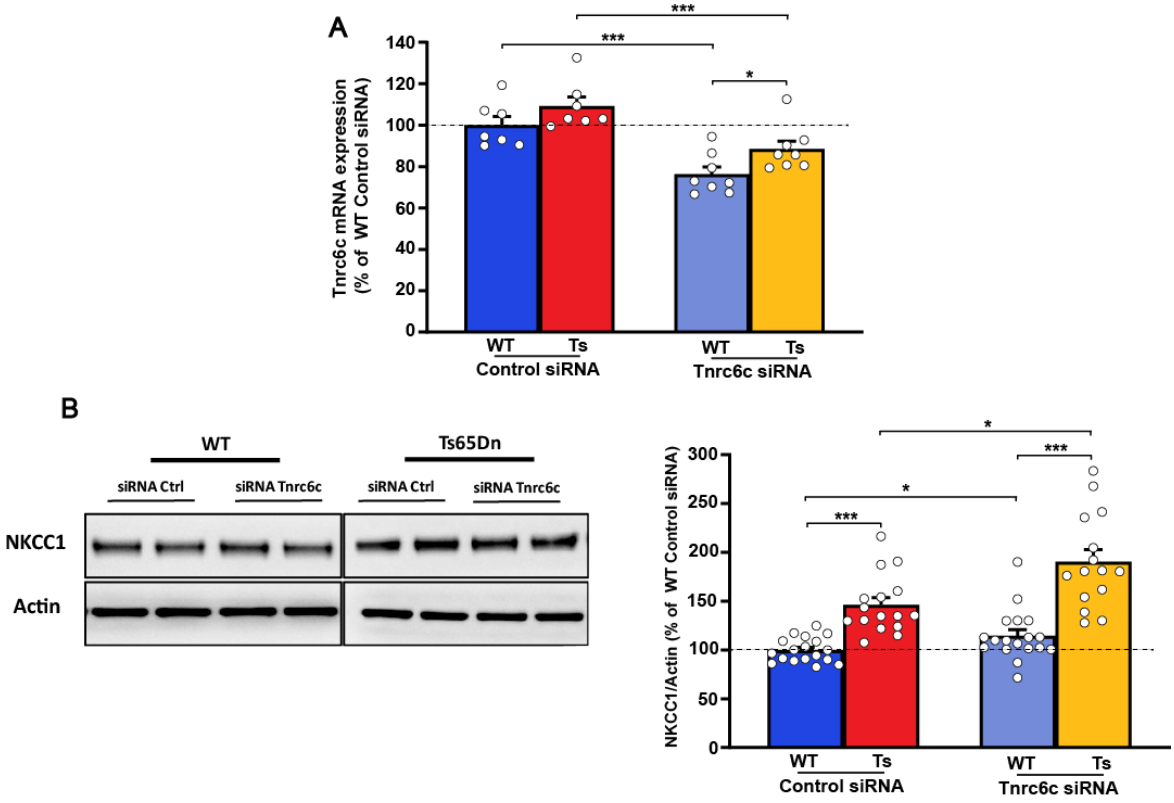

Figure 15: Tnrc6C regulates NKCC1 expression. (A) RT-qPCR analysis showed that Tnrc6C mRNA expression was significantly decreased after siRNA-mediated knockdown. All data shown are means (± SEM). Each dot represents a single well, obtained from 3 independent neuronal cultures. Two-way ANOVA: genotype [$F_{1,29}$=7.417, P=0.011]; treatment [$F_{1,29}$=31.960, P<0.001]; genotype x treatment [$F_{1,29}$=0.144 ,P=0.707]. **(B)** *Left:* Representative immunoblot for NKCC1 in protein extracts from Ts65Dn and WT neurons upon Tnrc6C knockdown. Right: Quantification of NKCC1 protein (expressed as percentage of WT neurons treated with control siRNA) showed higher NKCC1 expression after Tnrc6C knockdown in both Ts65Dn and WT neurons. Actin was used an internal standard. All data shown are means (± SEM). Each dot represents a single well, obtained from 8 independent neuronal cultures. Two-way ANOVA: genotype [$F_{1,66}$=103.031, P<0.001]; treatment [$F_{1,66}$=13.629, P<0.001]; genotype x treatment [$F_{1,66}$=0.0296 ,P=0.864]. *p<0.05; *** p<0.001, Two-way ANOVA followed by Tukey *post hoc* test.

After demonstrating that microRNAs are involved in NKCC1 regulation, we performed a bioinformatic analysis to predict potential miRNAs binding sites on NKCC1 3'UTR with TargetScan software [199] (Fig.16A). We found that several microRNAs are predicted to target NKCC1 3'UTR. In order to identify possible candidates microRNA (expressed at lower levels in trisomic samples) that could drive NKCC1 upregulation, we next performed an initial screening by RT-qPCR of the expression level of ~70 miRNAs predicted by the bioinformatics analysis to target NKCC1 3'UTR in WT and Ts65Dn brain samples (Fig.16B).

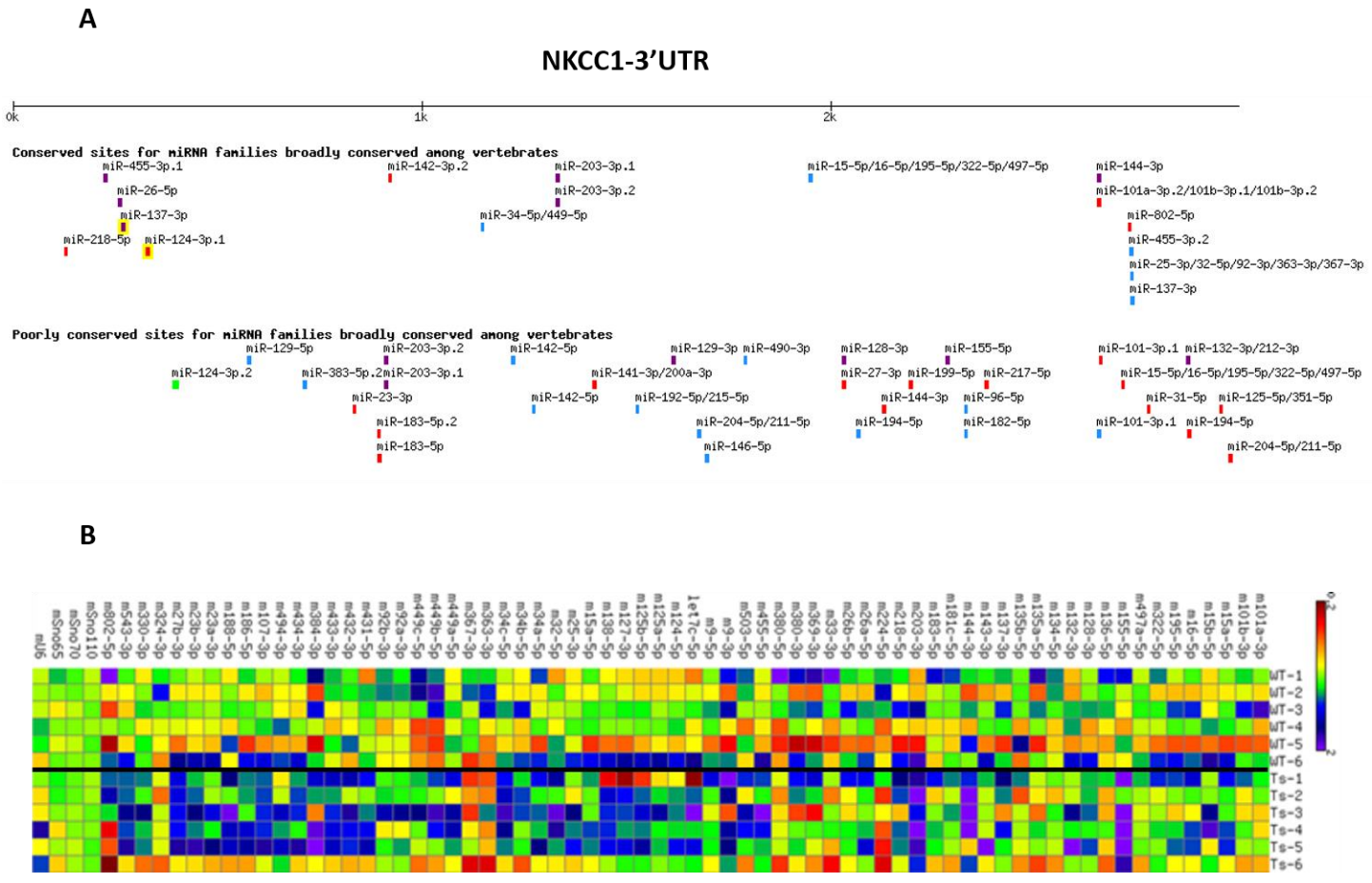

Figure 16: **Screening of potential miRNAs targeting NKCC1 3' UTR (A)** TargetScan analysis of potential miRNAs binding sites on NKCC1 3'UTR. **(B)** Heat-map showing miRNA expression of different microRNAs in the hippocampus of WT and Ts65Dn mice.

We found that miR497a-5p and miR101-3p were downregulated in Ts65Dn brains compared to WT. To confirm the results of this preliminary screening, we next assessed the expression of these two candidate miRNAs in primary neuronal cultures. Moreover, since miR497a-5p is a representative of a larger family of microRNAs sharing a nearly identical seed sequence, we also evaluated expression of other cognate miRNAs. RT-qPCR results showed that miR101-3p and miR497a-5p levels were in fact decreased in both Ts65Dn brains and neuronal cultures. We also found that miR15a-5p and miR15b-5p were decreased only in trisomic neuronal cultures (Fig. 17A and B). Interestingly, expression analysis in *post-mortem* human hippocampus from DS people also showed decreased expression of miR497a-5p, but not of miR101-3p (Fig 17C).

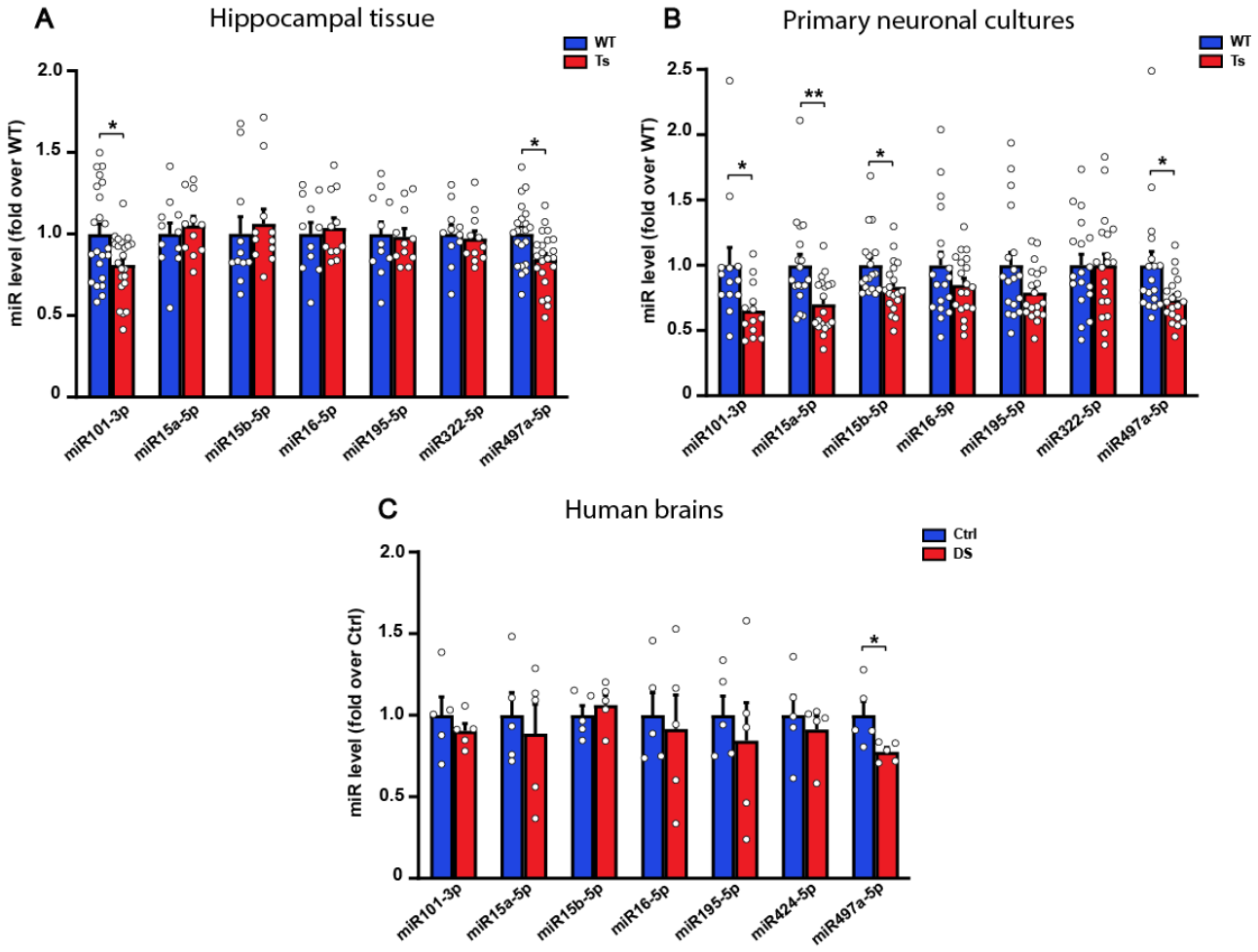

Fig.17: Expression of miR497a-5p and miR101-3p (A) RT-qPCR analysis showed the expression of miR497a-5p and miR101-3p was reduced in Ts65Dn hippocampus compared WT. **(B)** Expression of miR497a-5p, mir15a-5p, miR15b-5p and miR101-3p was reduced in Ts65Dn neuronal cultures compared WT. **(C)** Expression of miR497a-5p was reduced in the hippocampus of human DS patients compared to age/sex-matched controls. All data shown are means (± SEM). Each dot represents a single sample. For results shown in (B), samples derived from 3 independent neuronal cultures. *p<0.05, **p<0.01 unpaired Student's t-test.

5. Candidate microRNAs target NKCC1-3'UTR

In order to demonstrate the interaction of miR497a-5p and miR101-3p with NKCC1 3'UTR and evaluate their repression activity, we transfected the fluorescent NKCC1 3'UTR sensor in WT and Ts65Dn neurons together with candidate microRNA mimics. MicroRNA mimics are short, chemically modified double-stranded RNAs that mimic endogenous miRNAs. They are commonly used for functional analysis of microRNA activity by overexpression. We found that overexpression of miR497a-5p mimic effectively reduced the GFP/tdTomato ratio (mirroring reduced NKCC1 translation) in both WT and Ts65Dn neurons (Fig. 18 B and 19 B). Overexpression of miR101-3p mimic significantly decreased NKCC1 translation only in trisomic neurons (Fig. 18 D and 19 D)

Next, to study the interaction of endogenous microRNAs with NKCC1 3'UTR, we mutated NKCC1 3'UTR in the seed-binding sequences of miR101-3p and miR497a-5p to perturb miRNA-mRNA interaction and consequently prevent target repression.

Bioinformatics analysis with TargetScan predicted two biding sequences for miR497a-5p at position 1883 and 2636 (hereafter referred to as seed sequence number 1 and 2, respectively) and one miR101-3p binding site at position 2578 on NKCC1 3'UTR. In WT neurons, one by one mutation of the three seed sequences caused a significant increase in the GFP/tdTomato ratio. This indicated that the endogenous candidate microRNAs bind to NKCC1-3'UTR and exert a negative regulation of expression (Fig. 18 B and D). However, in trisomic neurons, none of the mutations produced a significant impact on GFP expression. This again pointed to impaired regulation exerted by these microRNAs in DS, probably due to their lower expression (Fig. 19 B and D). Moreover, mutation of the seed-binding sequence for miR101-3p and seed-binding sequence number 2 for miR497a-5p could prevent the interaction of exogenous microRNA mimics on NKCC1 3'UTR, abolishing their effect in both WT and Ts65Dn neurons (Fig. 18B and fig. 19B and D). This confirmed the site of action of both microRNA. Conversely, overexpression of miR497a-5p retained partial activity after mutation of its seed-binding sequence number 1 both in WT and Ts65Dn neurons. This indicated that this site probably plays a minor role in the interaction with the microRNA and in translational repression compared to binding sequence number 2 (Fig.18B and 19B).

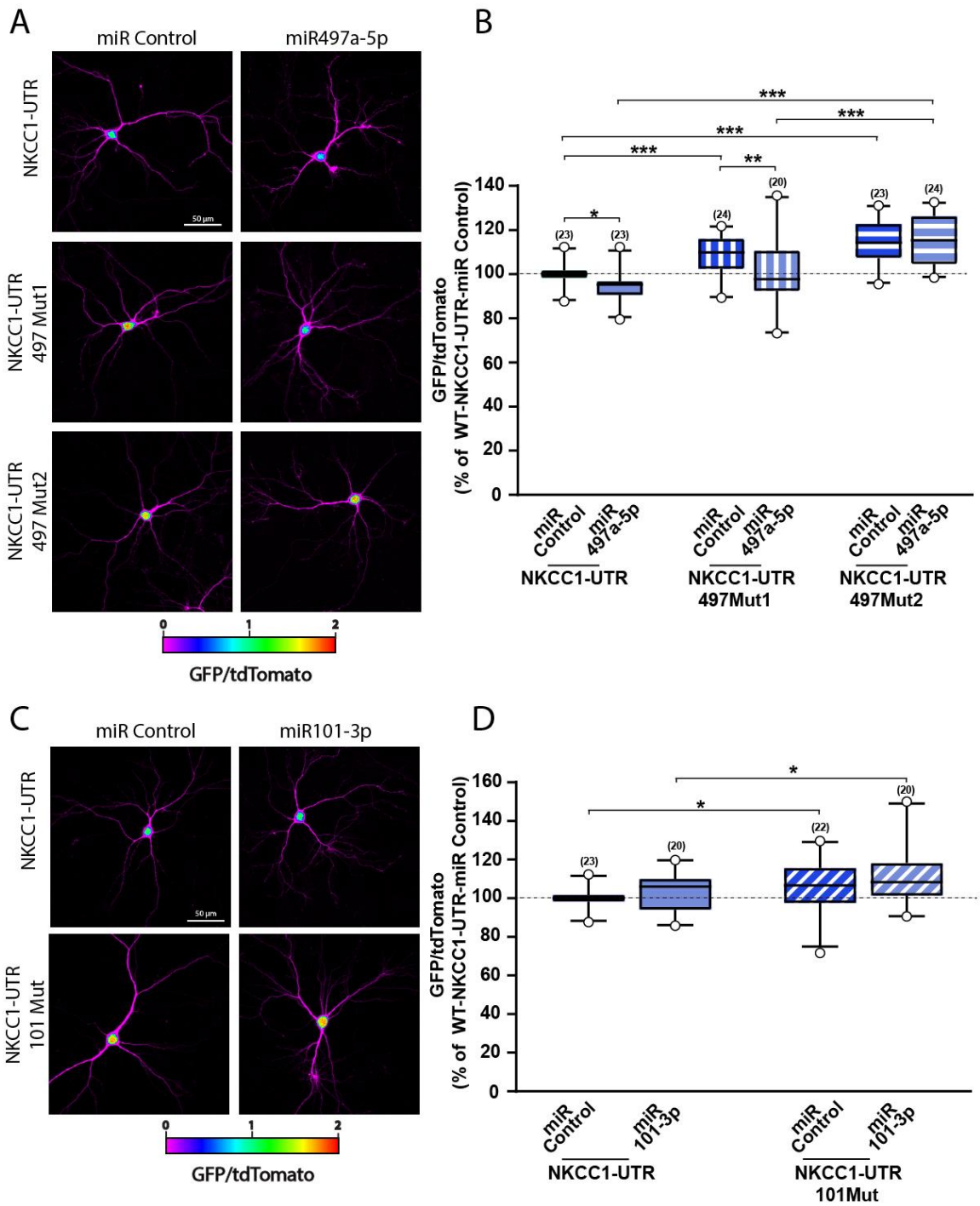

Figure 18: **miR-497a-5p and miR-101-3p regulate NKCC1 expression in WT neurons. (A)** Pseudo-color images of GFP/tdTomato ratio representing the interaction of miR497a-5p with native or mutated NKCC1 3'UTR **(B)** Mutation of miR497a-5p seed-binding sequences increases GFP/tdTomato ratio. Two-way ANOVA: sensor [$F_{2,136}$=41.827, P<0.001]; microRNA [$F_{1,136}$=10.011, P=0.002]; sensor x microRNA [$F_{2,136}$=4.020, P=0.020]. **(C)** Pseudo-color images of GFP/tdTomato ratio representing the interaction of miR101-3p with native or mutated NKCC1-3'UTR. **(D)** Mutation of miR101-3p seed-binding sequence increases GFP expression in wild-type neurons. Two-way ANOVA: sensor [$F_{1,84}$=10.232, P=0.02]; microRNA [$F_{1,84}$=1.884, P=0.174]; sensor x microRNA [$F_{1,84}$=0.0508, P=0.822]. For each box plot, the central line indicates the median and the box limits indicate the 25th and 75th percentiles. Whiskers represent the 5th and the 95th percentiles. Number in parenthesis indicates the number of samples for each experimental group, obtained from 12 independent neuronal cultures. *p<0.05; **p<0.01;*** p<0.001, Two-way ANOVA followed by Tukey *post hoc* test.

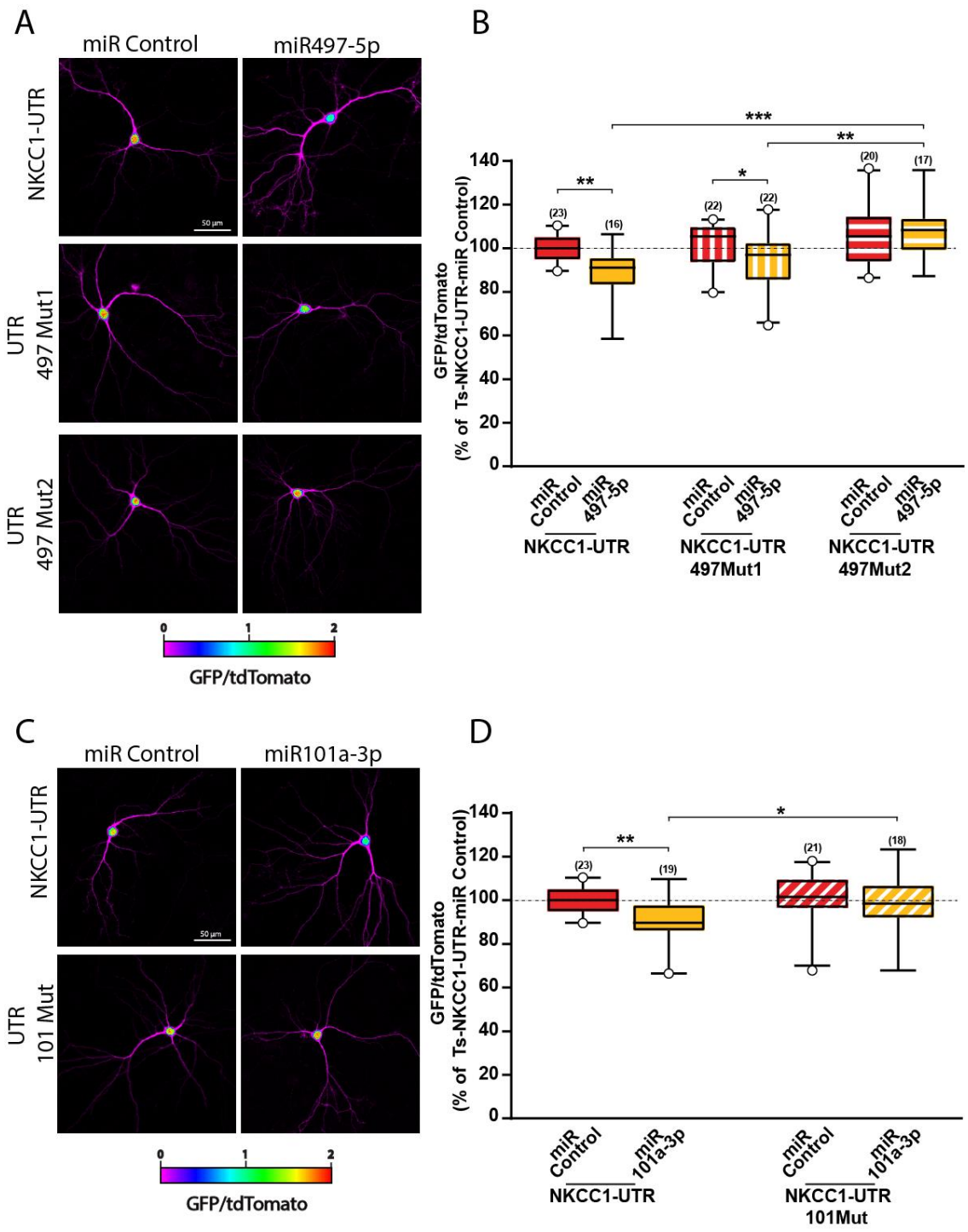

Figure 19: **miR497a-5p and miR101-3p regulate NKCC1 expression in Ts65Dn neurons. (A)** Pseudo-color images of GFP/tdTomato ratio representing the interaction of miR497a-5p with native or mutated NKCC1-3'UTR. **(B)** Overexpression miR497a-5p decreased GFP/tdTomato ratio by interacting mainly with seed-binding sequence number 2**.** Two-way ANOVA: sensor [$F_{2,118}$=11.834, P<0.001]; microRNA [$F_{2,118}$=7.583, P=0.007]; sensor x microRNA [$F_{2,118}$=3.185, P=0.045]. **(C)** Pseudo-color images of GFP/tdTomato ratio representing the interaction of miR101-3p with native or mutated NKCC1-3'UTR. **(D)** Overexpression of miR101-3p decreased GFP/tdTomato ratio. Two-way ANOVA: sensor [$F_{1,80}$=5.670, P=0.020]; microRNA [$F_{1,80}$=8.207, P=0.005]; sensor x microRNA [$F_{1,80}$=2.126, P=0.149]. For each box plot, the central line indicates the median and the box limits indicate the 25th and 75th percentiles. Whiskers represent the 5th and the 95th percentiles. Number in parenthesis indicates the number of samples for each experimental group, deriving from 12 independent neuronal cultures. *p<0.05; **p<0.01;*** p<0.001, Two-way ANOVA followed by Tukey *post hoc* test.

6. miR497a-5p and miR101-3p regulate chloride levels in primary neurons through the downregulation of NKCC1 expression

To finally investigate whether miR497a-5p and miR101-3p can eventually indeed regulate NKCC1 protein expression, we transfected candidate miRNAs mimics in primary cortical neurons and then performed western immunoblots to assess NKCC1 protein levels. We found that the exogenous delivery of both microRNAs significantly decreased NKCC1expression levels in trisomic neurons, restoring physiological level similar to the one of WT cells. Interestingly, simultaneous transfection with a 1:1 mixture of the two microRNA (to maintain unaltered the total amount of transfected mimics) did not elicit an additive effect on NKCC1 downregulation (Fig.20). This indicates that the action of the two microRNAs is not synergistic. Conversely, overexpression of the candidate microRNAs showed a minor effect, with only miR497a-5p demonstrating a small, but significant NKCC1 downregulation in WT neurons.

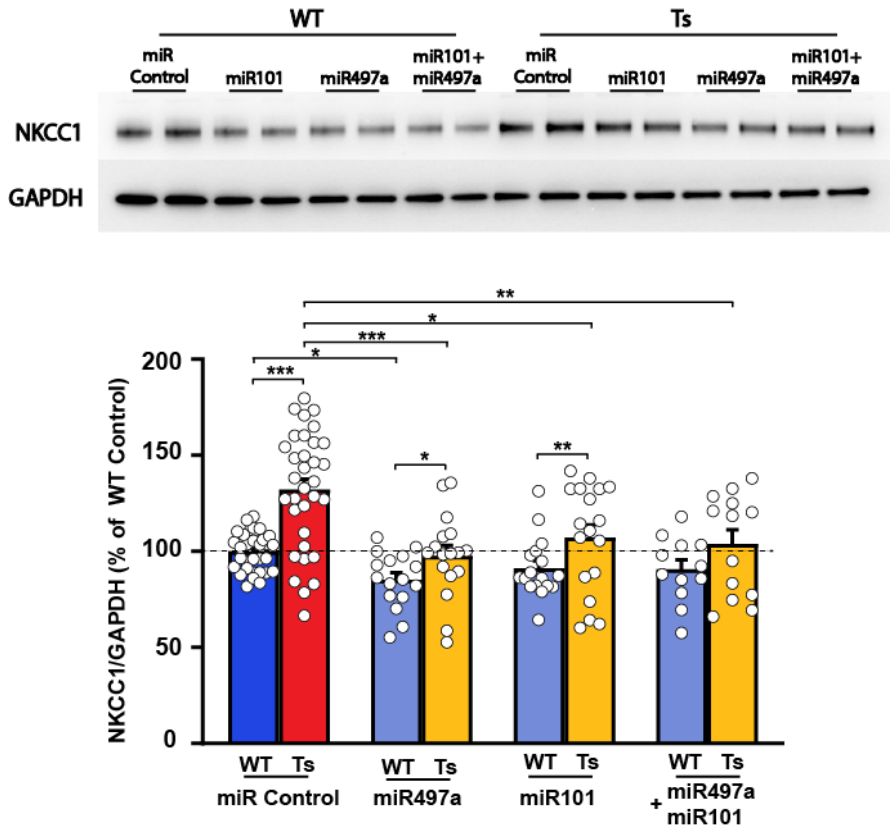

Fig.20: miR497a-5p and miR101-3p regulate NKCC1 protein expression in Ts65Dn neurons. *Top*: Representative immunoblot for NKCC1 in protein extracts from Ts65Dn and WT neurons upon miR497a-5p and miR101-3p transfection. *Bottom*: Quantification of NKCC1 protein (expressed as percentage of WT neurons treated with control mimic) showed NKCC1 downregulation mainly in Ts65Dn neurons after miR497a-5p and miR101-3p overexpression. GAPDH was used as internal standard. All data shown are means (± SEM). Each dot represents a single well of neurons, obtained from 15 independent neuronal cultures. Two-way ANOVA: genotype [$F_{1,157}$=22.639, P<0.001]; treatment [$F_{3,157}$=9.060, P<0.001]; genotype x treatment [$F_{3,157}$=0.385, P=0.764]. *p<0.05; **p<0.01; *** p<0.001, Two-way ANOVA followed by Tukey *post hoc* test.

To further strengthen these findings, we next performed the reverse experiment. We transfected short synthetic, single-stranded oligonucleotides (termed microRNA inhibitors) designed to bind and inhibit the interaction of endogenous miRNAs to their targets. Delivery of both anti-miR497a-5p or anti-miR101-3p inhibitors significantly increased NKCC1 protein expression in WT neurons, while displaying no effect on Ts65Dn neurons (Fig.21). This was likely because endogenous signaling by these microRNA is already impaired in trisomic cells. Importantly, these results are in line with the increase in GFP translation observed in experiments with the fluorescent sensor after mutating microRNAs seed-binding sequences to prevent their interaction with NKCC1 3'UTR (Fig.18 and 19).

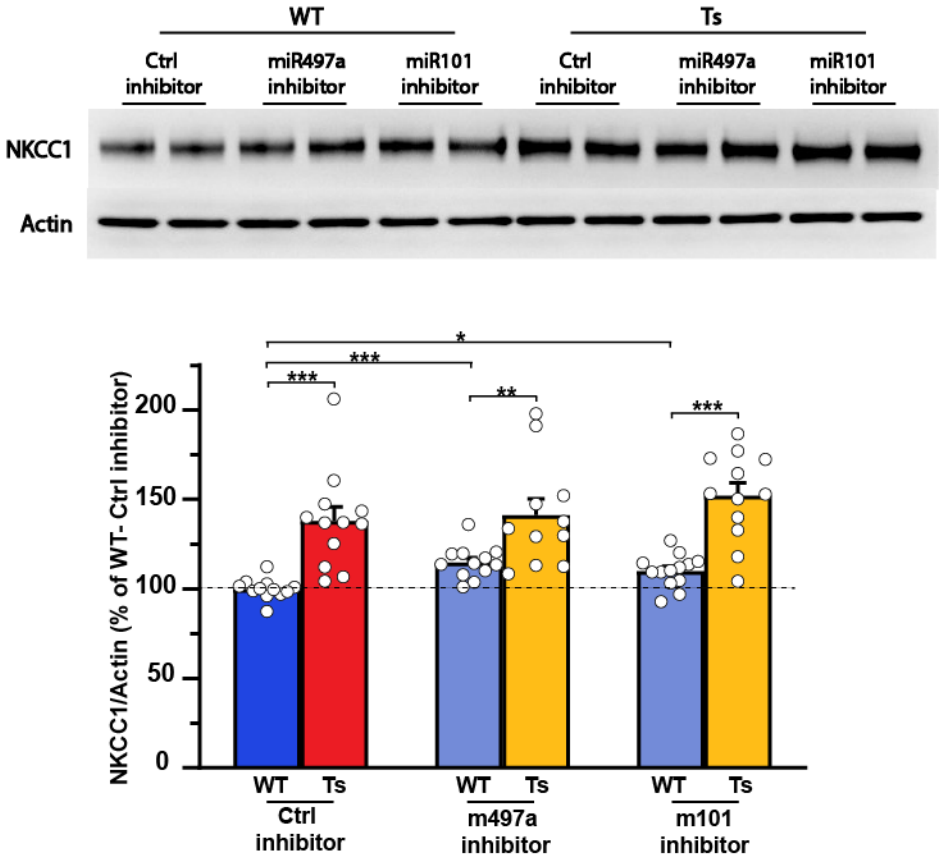

Fig.21: Delivery of miRNA inhibitors increase NKCC1 protein expression in WT neurons. *Top*: Representative immunoblot for NKCC1 in protein extracts from Ts65Dn and WT neurons upon miRNA inhibitors transfection. *Bottom*: Quantification of NKCC1 protein (expressed as percentage of WT neurons treated with control miRNA inhibitor) showed NKCC1 upregulation in WT but not Ts65Dn neurons after delivery of anti miR497a-5p and anti miR101-3p inhibitors. Actin was used as internal standard. All data shown are means (± SEM). Each dot represents a single well, obtained from 6 independent neuronal cultures. Two-way ANOVA: genotype [$F_{1,71}$=76,308, P<0.001]; treatment [$F_{2,71}$=5.978, P=0.004]; genotype x treatment [$F_{2,71}$=3.384, P=0.040]. *p<0.05; *** p<0.001, Two-way ANOVA followed by Tukey *post hoc* test.

Finally, to investigate the functional consequences of candidate miRNAs overexpression on $[Cl^-]_i$, we assessed intracellular chloride concentration in cultured primary hippocampal neurons using the chloride sensitive dye MQAE, whose fluorescence is quenched by the presence of chloride ions. In line with previous results, we found that Ts65Dn neurons transfected with control microRNA display increased levels of intracellular chloride compared to WT. Exogenous delivery of both miRNAs restored physiological $[Cl^-]_i$ in Ts65Dn neurons, without affecting chloride levels in WT neurons (Fig.22). Altogether, these results indicate that dysregulation of microRNAs in trisomic neurons leads to NKCC1 overexpression and subsequent alteration of chloride homeostasis.

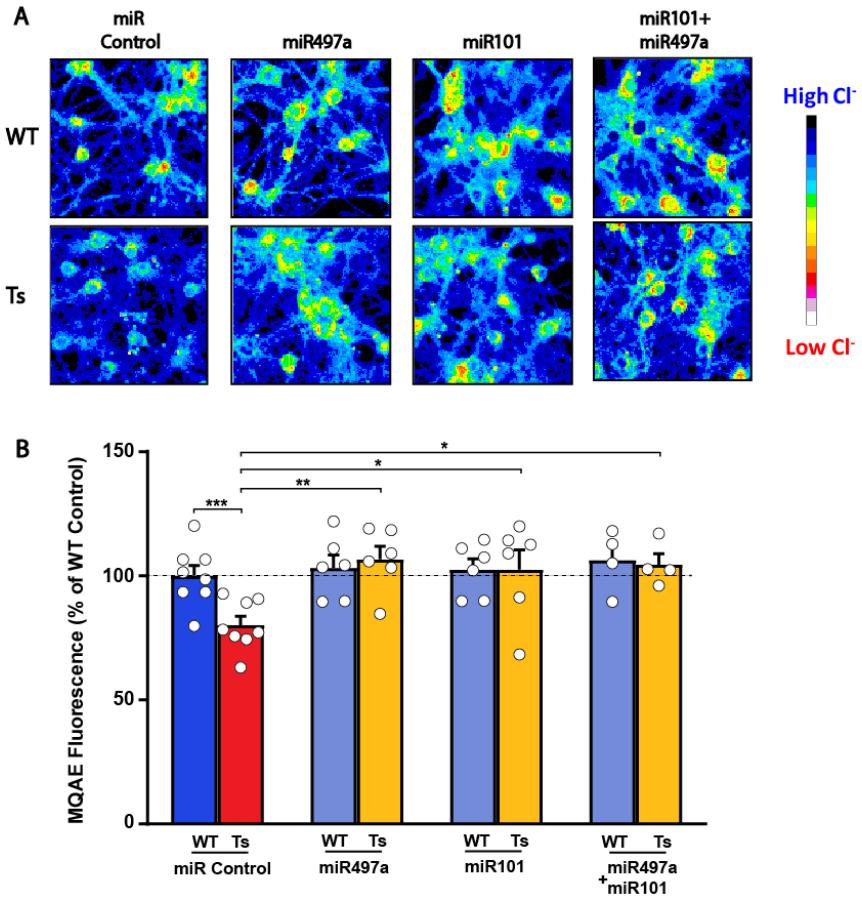

Fig.22: Overexpression of miR497a-5p and miR101-3p restored $[Cl^-]_i$ in Ts65Dn neurons. (A) Representative pseudo-color images of hippocampal neurons during intracellular Cl^- imaging with the fluorescent chloride-sensitive dye MQAE. Fluorescent intensity of the dye (color-coded on the right) is inversely proportional to $[Cl^-]_i$. **(B)** Quantification of $[Cl^-]_i$ with MQAE (expressed as percentage of WT neurons transduced with control miR) showed lower fluorescent intensity (i.e. higher $[Cl^-]_i$) in Ts65Dn compared to WT neurons. Overexpression of miR497a-5p and miR101-3p mimics restored $[Cl^-]_i$ in Ts65Dn neurons. All data shown are means (± SEM). Each dot represents a single well, obtained from 4 independent neuronal cultures. Two-way ANOVA: genotype [$F_{1,47}$=1.466, P=0.233]; treatment [$F_{3,47}$=4.543, P=0.008]; genotype x treatment [$F_{3,47}$=2.444, P=0.078]. *p<0.05; **p<0.01; Two-way ANOVA followed by Tukey *post hoc* test.

7. Overexpression of miR497a-5p and miR101-3p restore inhibitory GABAergic signaling in Ts65Dn neuronal networks

As a next step, we evaluated whether restoring $[Cl^-]_i$ in trisomic neurons through the overexpression of either miR497a-5p or miR101-3p could rescue $GABA_AR$ fully inhibitory signaling. To this aim, we used multi-electrode arrays (MEAs) to record the neuronal network activity from WT and Ts65Dn neurons in culture. First, we recorded basal neuronal activity at 16 DIV, three days after the transfection of miRNA mimics or the corresponding control. We found that the mean firing rate (MFR) and mean bursting rate (MBR) of action potentials were both increased in Ts65Dn compared to WT neuronal cultures (Fig.23 A and B). Interestingly, MFR and MBR were decreased in trisomic neuronal cultures transfected with miR101-3p mimic. Conversely, overexpression of miR101-3p mimic showed the opposite effect on MFR in WT neurons, while bursting activity was unchanged. Moreover, overexpression of miR497a-5p significantly decreased MBR of Ts65Dn neurons while having a smaller effect on MFR (Fig.23A and B). Interestingly, when we evaluated the firing synchrony of the neuronal network by measuring the peak of the cross-correlation function (C peak; see methods), we found that network synchrony was significantly lower in Ts65Dn networks compared to WT. However, overexpression of both microRNAs further decreased the synchrony of Ts65Dn cultures, broadening the difference between trisomic and WT neurons (Fig.23C).

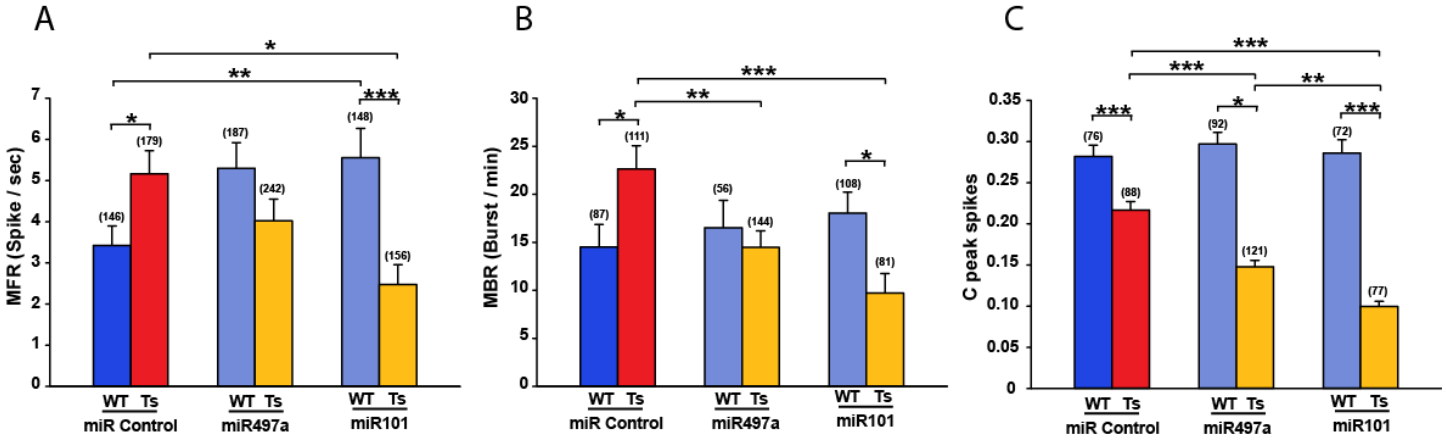

Fig.23: miR497a-5p and miR101-3p regulate basal firing parameters in Ts65Dn neuronal cultures. (A) Increased firing frequency in Ts65Dn neurons is rescued by miR101-3p overexpression. Conversely, miR101-3p overexpression increased the spiking frequency in WT neurons. Two-way ANOVA: genotype [$F_{1,1205}$=14.699, P<0.001]; treatment [$F_{2,1205}$=1.380, P=0.252]; genotype x treatment [$F_{2,1205}$=9.955, P<0.001]. **(B)** Increased burst rate in Ts65Dn neurons is rescued by overexpression of both miR497a-5p and miR101-3p, without affecting WT neurons. Two-way ANOVA: genotype [$F_{1,585}$=0.158, P=0.691]; treatment [$F_{2,585}$=2.237, P=0.108]; genotype x treatment [$F_{2,585}$=6.760, P=0.001]. **(C)** Network synchronization is decreased in trisomic cultures. Overexpression of miR497a-5p and 101-3p further decreases synchrony in trisomic neurons while having no effect in WT networks. Two-way ANOVA: genotype [$F_{1,3741}$=193.734, P<0.001]; treatment [$F_{2,3741}$=10.708, P<0.001]; genotype x treatment [$F_{2,3741}$=12.820, P<0.001]. *p<0.05; **p<0.01;*** p<0.001, Two-way ANOVA followed by Tukey *post hoc* test. All data shown are means (± SEM). Number in parenthesis indicates the number of electrodes recorded for each experimental group. Experiments were performed on 19 MEA for WT-miR-Control, 23 MEA for WT-miR497a, 17 MEA for WT-miR101, 22 MEA for Ts-miR-Control, 31 MEA for Ts-miR497a, 20 MEA for Ts-miR101.

Next, we recorded changes in neuronal network activity before and after the administration of drugs modulating GABAergic transmission.

At first, we tested whether overexpression of either microRNAs could restore inhibitory signaling upon bath application of exogenous GABA. We found that GABA application elicited a sharp decrease of MFR in virtually all recorded electrodes in WT hippocampal neurons. Conversely, only 75% of electrodes showed a decrease in MFR, while 13% showed even a significant increase in Ts65Dn hippocampal neurons (Fig. 24 A and B). This was indicative of a depolarizing effect of GABA. Accordingly, when we computed the mean ratio between MFR after GABA administration and basal MFR for each well, we noticed a significant increase of the ratio in Ts65Dn neurons transfected with control microRNA, compared to WT. However, since the majority of electrodes displayed decreased MFR, the mean MFR ratio computed on the whole well remained below 1, in spite of the presence of a population of neurons where $GABA_A$ receptor activation is depolarizing (Fig.24 C). Overexpression of either miR497a-5p or miR101-3p, achieved by transfection of microRNA mimics, completely rescued the inhibitory effect of exogenous GABA in Ts65Dn neurons returning MFR ratio to WT levels, and eliminating the population of neurons increasing the MFR after GABA administration (Fig. 24).

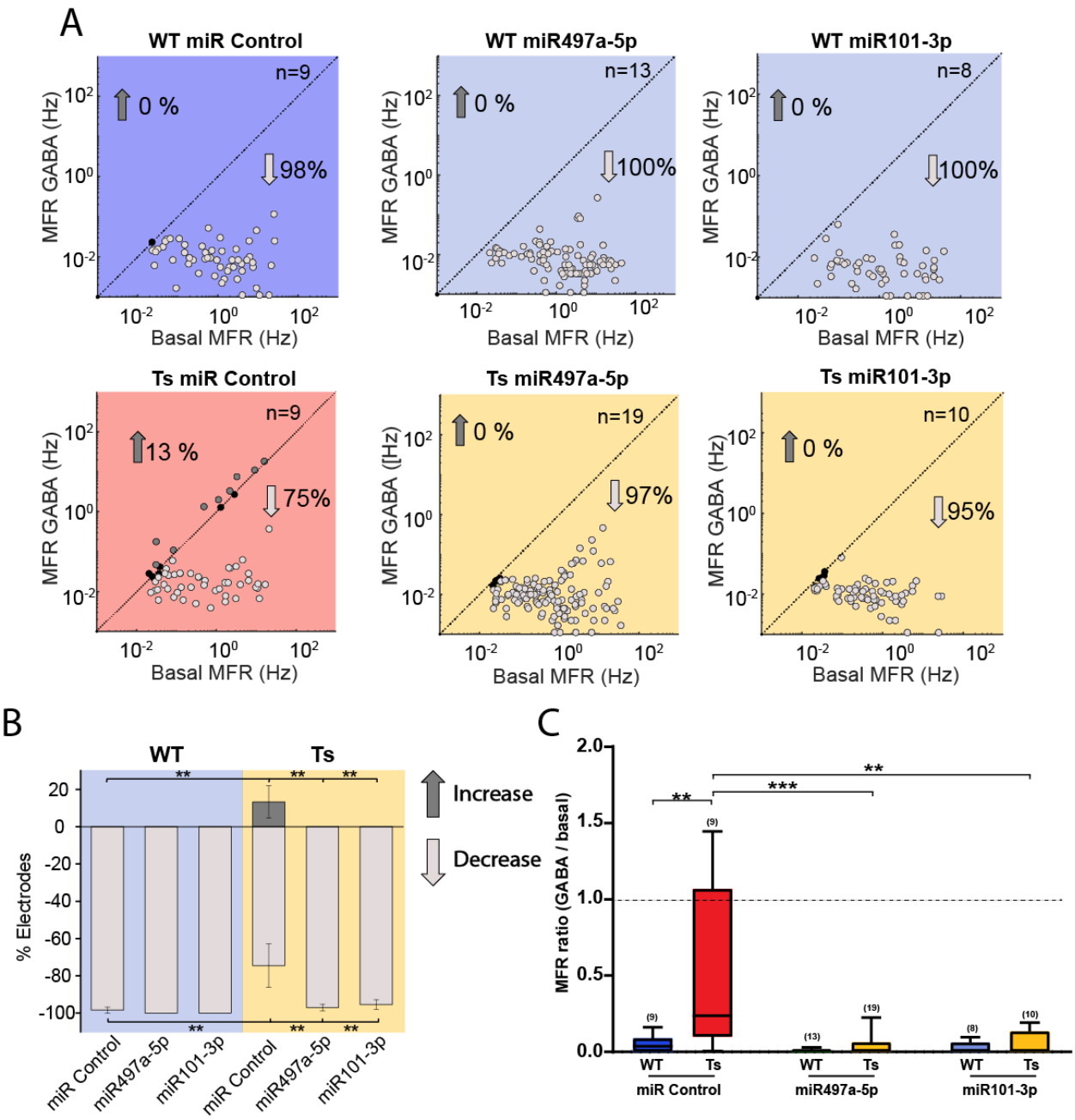

Fig.24: Overexpression of miR497a-5p and miR101-3p restored exogenous inhibitory GABAergic signalling in Ts65Dn neurons. (A) Mean firing rate (MFR) comparison for each recorded electrode (plotted as a dot) in basal conditions and after treatment with GABA (20 μM) in WT and Ts65Dn neurons. Dark and light grey dots indicate respectively electrodes showing a significant increase or decrease in the MFR. Black dots indicate electrodes showing no significant changes in MFR. Numbers of recorded MEA for each experimental group are indicated in the right top corner of each graph. **(B)** Quantification of the percentage of electrodes displaying an increase (dark grey) or decrease (light grey) in MFR after GABA administration showed a complete rescue of inhibitory signaling in Ts65Dn neurons upon overexpression of either miR497a-5p or miR101-3p. Data shown are means (± SEM). MFR increase, Two-way ANOVA: genotype [$F_{1,67}$=3.528, P=0.065]; treatment [$F_{2,67}$=3.342, P=0.042]; genotype x treatment [$F_{2,67}$=6.342, P=0.042].MFR decrease, Two-way ANOVA: genotype [$F_{1,67}$=3.388, P=0.072]; treatment [$F_{2,67}$=3.713, P=0.032]; genotype x treatment [$F_{2,67}$=3.713, P=0.032]. **(C)** Quantification of MFR ratio before and after GABA administration. For each box plot, central line represents the median and the box limits indicate the 25th and 75th percentiles. Whiskers represent the 5th and the 95th percentiles. Number in parenthesis indicates the number of wells recorded for each experimental group. Two-way ANOVA: genotype [$F_{1,67}$=8.261, P=0.006]; treatment [$F_{2,67}$=8.478, P<0.001]; genotype x treatment [$F_{2,67}$=1.383, P=0.259]. **p<0.01; *** p<0.001, Two-way ANOVA followed by Tukey *post hoc* test

We also performed the reverse experiment to test whether microRNAs overexpression could restore endogenous GABAergic inhibitory signaling as well.As expected, inhibition of endogenous GABAergic signaling with the $GABA_AR$ antagonist bicuculline (BIC) determined a significant increase of the MFR in 84% of active electrodes in WT cultures. Notably, in Ts65Dn neuronal network, application of bicuculline determined a decrease of MFR in 41% of electrodes, while only 48% showed an increase (Fig. 25 A and B). In addition, mean ratio between MFR after treatment with bicuculline and basal MFR was significantly lower in Ts65Dn neuronal networks compared to WT (Fig.25C). These results are consistent with the presence of a large population of trisomic neurons characterized by depolarizing GABAergic transmission. Importantly, in Ts65Dn cultures transfected with both miRNA mimics, the percentage of electrodes showing an increase in MFR upon bicuculline treatment and the mean value of MFR ratio were similar to the one seen in WT neurons. This indicates that endogenous inhibitory GABAergic signaling was restored (Fig 25).

Altogether, the MEA experiments showed that miRNAs downregulation drives alteration in inhibitory GABAergic signaling in trisomic neuronal networks and that their overexpression restores physiological responses to the neurotransmitter.

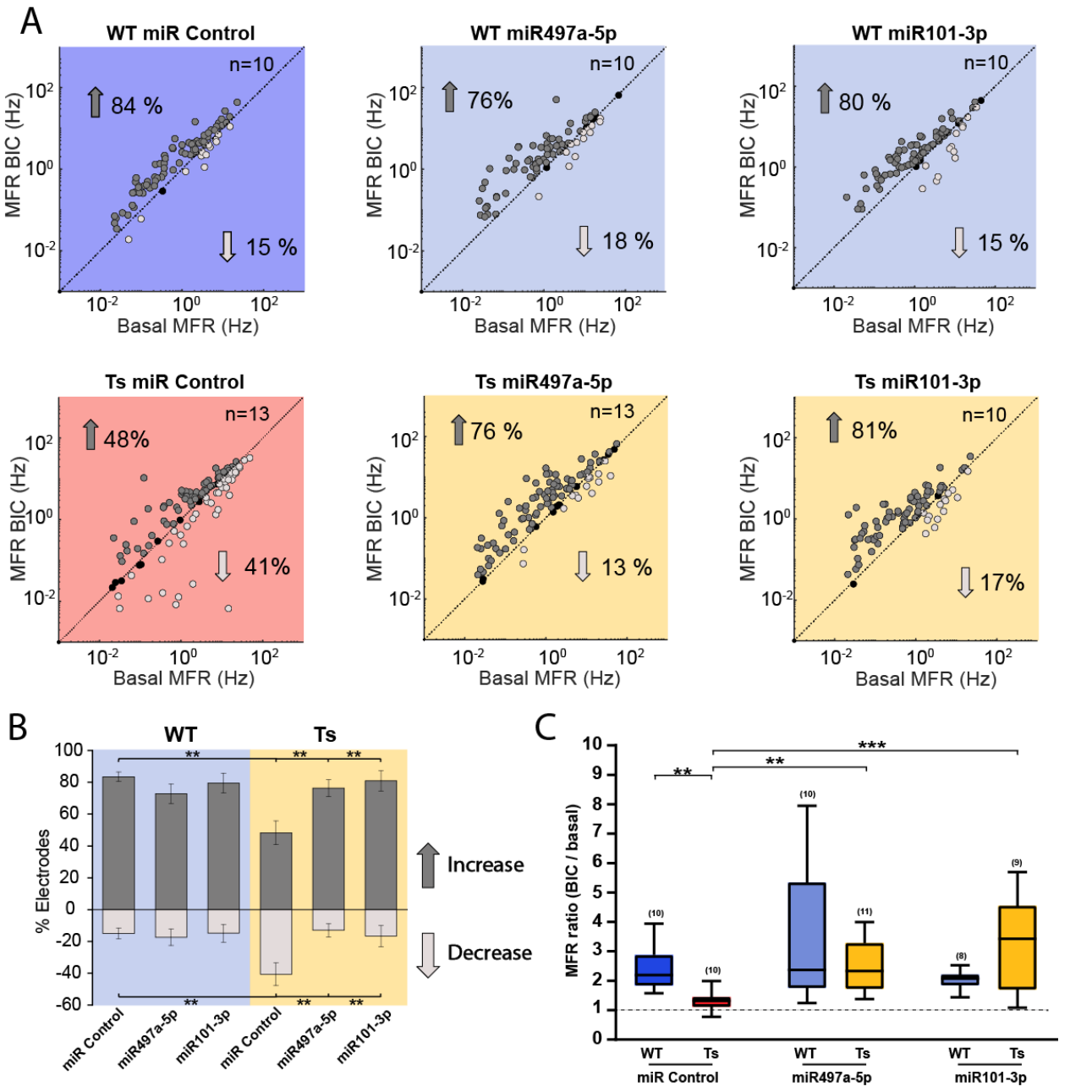

Fig.25: **Overexpression of miR497a-5p and miR101-3p restored endogenous inhibitory GABAergic signalling in Ts65Dn neurons. (A)** Mean firing rate (MFR) comparison for each recorded electrode (plotted as a dot) in basal conditions and after treatment with bicuculline (20 μM) in WT and Ts65Dn neurons. Dark and light grey dots indicate respectively electrodes showing a significant increase or decrease in the MFR. Black dots indicate electrodes showing no significant changes in MFR. Numbers of recorded MEA for each experimental group are indicated in the right top corner of each graph. **(B)** Quantification of the percentage of electrodes displaying an increase (dark grey) or decrease (light grey) in MFR after bicuculline administration showed a complete rescue of endogenous GABA inhibitory signaling in Ts65Dn neurons upon overexpression of either miR497a-5p or miR101-3p. Data shown are means (± SEM). MFR increase, Two-way ANOVA: genotype [$F_{1,66}$=4.109, P=0.047]; treatment [$F_{2,66}$=2.737, P=0.073]; genotype x treatment [$F_{2,66}$=6.484, P=0.003]. MFR decrease, Two-way ANOVA: genotype [$F_{1,66}$=2.783, P=0.100]; treatment [$F_{2,66}$=3.275, P=0.045]; genotype x treatment [$F_{2,66}$=4.088, P=0.022].. **(C)** Quantification of MFR ratio before and after bicuculline administration. For each box plot, central line represents the median and the box limits indicate the 25th and 75th percentiles. Whiskers represent the 5th and the 95th percentiles. Number in parenthesis indicates the number of wells recorded for each experimental group. Two-way ANOVA: genotype [$F_{1,57}$=1.473, P=0.23]; treatment [$F_{2,57}$=5.671, P=0.006]; genotype x treatment [$F_{2,57}$=6.456, P=0.003]. **p<0.01; *** p<0.001, Two-way ANOVA followed by Tukey *post hoc* test

8. Long-term overexpression of candidate microRNAs using viral vectors

Envisaging *in vivo* experiments, we constructed an adeno-associated viral vector that allowed us to achieve long-term overexpression of candidate microRNAs. In the expression vector, microRNA mimics are ubiquitously expressed on the 3' arm of the hairpin, under the control of the U6 promoter according to a previously described strategy that minimizes passenger-strand-mediated off-target effects [200]. Upon transduction, we performed western immunoblot to check whether AAV-mediated delivery of miR497a-5p and miR101-3p mimic was efficient in reducing NKCC1 levels. Similar to transient transfection with the same mimics, infection of cortical cultured neurons induced a significant decrease in NKCC1 levels in Ts65Dn neurons (Fig.26). In the next months, we will perform stereotaxic injection of these viral vectors in the hippocampus of Ts65Dn mice and WT littermates, aiming at reducing intracellular chloride accumulation and possibly rescuing learning and memory in this model of Down syndrome.

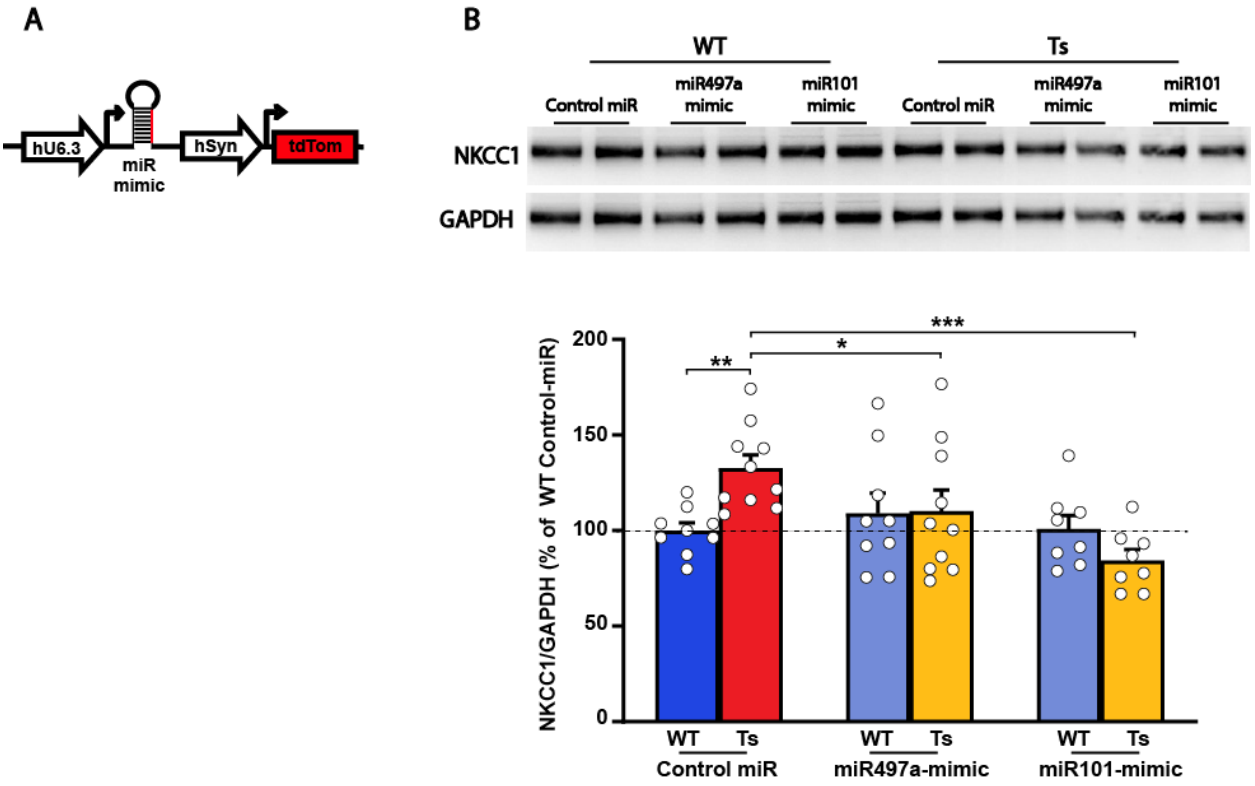

Fig.26: AAV-mediated microRNA mimics delivery decreases NKCC1 expression in Ts65Dn neurons. (A) Scheme of the AAV vector plasmid used to overexpress miR497a-5p or miR101-3p mimics. **(B)** *Top*: Representative immunoblot for NKCC1 in protein extracts from Ts65Dn and WT neurons upon AAV-mediated miRNA mimic overexpression. *Bottom*: Quantification of NKCC1 protein (expressed as percentage of WT neurons transduced with control miR) showed NKCC1 downregulation in Ts65Dn neurons after delivery of miR mimics. GAPDH was used as internal standard. All data shown are means (± SEM). Each dot represents a single well, obtained from 5 independent cultures. Two-way ANOVA: genotype [$F_{1,53}$=0.319, P=0.575]; treatment [$F_{2,53}$=5.315, P=0.008]; genotype x treatment [$F_{2,53}$=3.384, P=0.009]. *p<0.05; **p<0.01;*** p<0.001, Two-way ANOVA followed by Tukey *post hoc* test.

9. The DS-triplicated gene APP regulates NKCC1 *in trans* by competing for miR497a-5p and miR101-3p in Ts65Dn neurons

How does genome triplication lead to microRNA dysregulation in DS? To try addressing this question, we hypothesized that the overexpressed genes from the DS-triplicated chromosomal region in Ts65Dn mice could act as competitive endogenous RNAs (ceRNAs) for microRNA also targeting NKCC1. Indeed, mRNAs bearing seed-binding sequences for the same microRNAs can influence each other expression by competing for microRNAs binding [201,202]. Therefore, changes in the levels of one mRNA can influence the expression of other transcripts that share the binding site for the same microRNA. Bioinformatic analysis with TargetScan for possible DS-triplicated genes acting as ceRNAs, predicted three binding sites for candidate microRNAs on the 3'UTR of APP: one seed-binding sequence for miR497a-5p and two for miR101-3p. Accordingly, we found that AAV-mediated overexpression of both microRNA mimics could strikingly reduce APP levels both in WT and Ts65Dn neurons (Fig.27).

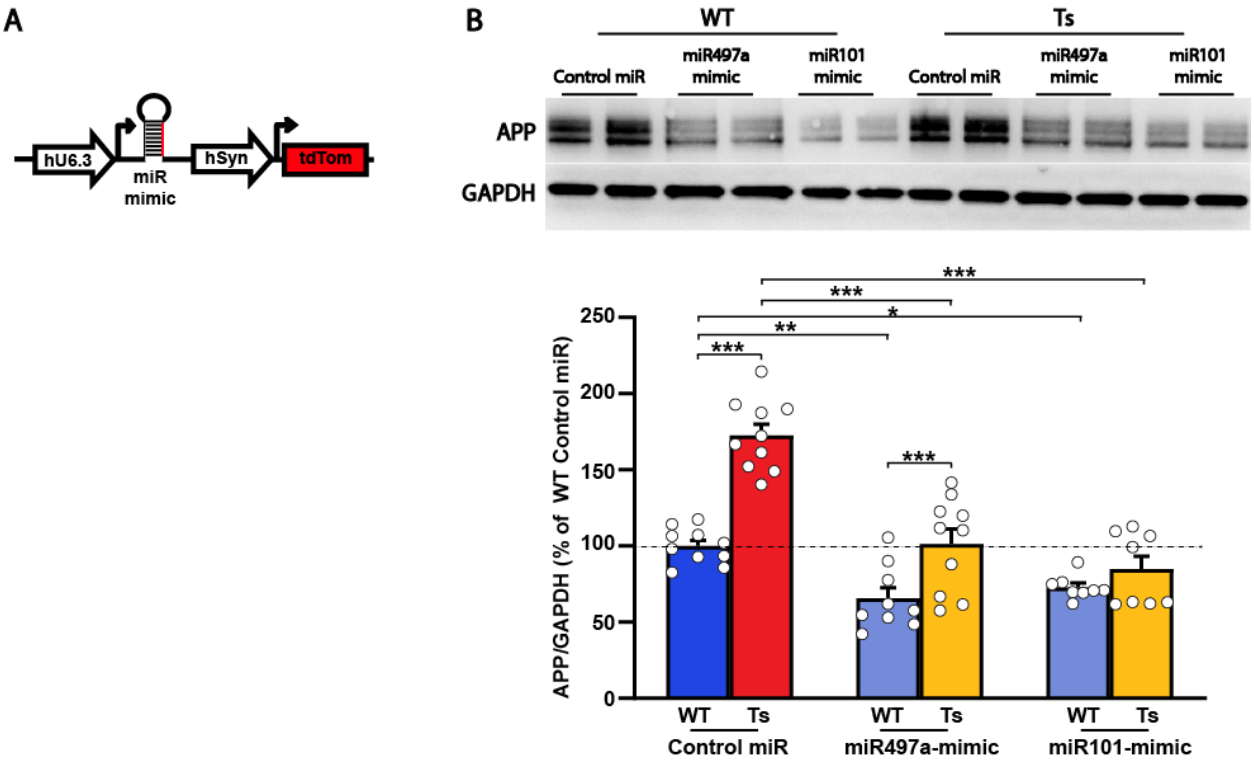

Fig.27: AAV-mediated overexpression of miR497a-5p and miR101-3p downregulate APP expression in Ts65Dn and WT neurons. (A) Scheme of the AAV vector plasmid used to overexpress miR497a-5p or miR101-3p mimics. **(B)** *Top:* Representative immunoblot for APP in protein extracts from Ts65Dn and WT neurons transduced with AAV vectors expressing miRNA mimic. *Bottom*: Quantification of APP protein (expressed as percentage of WT neurons transduced with control miR) showed APP downregulation in both WT and Ts65Dn neurons after delivery of miR mimics. GAPDH was used as internal standard. All data shown are means (± SEM). Each dot represents a single well, obtained from 5 independent cultures. Two-way ANOVA: genotype [$F_{1,54}$=47.440, P<0.001]; treatment [$F_{2,54}$=41.844, P<0.001]; genotype x treatment [$F_{2,54}$=9.226, P<0.001]. *p<0.05;**p<0.01, *** p<0.001, Two-way ANOVA followed by Tukey *post hoc* test.

The ceRNAs hypothesis postulates that 3'UTRs, in addition to the action exerted *in cis* on the upstream coding sequence, can also act *in trans* by sequestering microRNAs and preventing them to repress other targets [201,202]. Therefore, we thought that upregulation of the DS-triplicated gene APP could result in binding a higher amount of microRNAs, attenuating translational inhibition on other targets carrying seed-binding sequences for the same microRNAs, such as NKCC1 and Dyrk1A. To test this hypothesis, we designed a short interference RNA against APP and assessed possible changes in NKCC1 levels upon knockdown. Indeed, AVV-mediated APP knockdown caused a significant decrease in NKCC1 levels in trisomic neurons (Fig.28). Altogether, these data indicate that the DS-triplicated gene APP is targeted by the same microRNA regulating NKCC1 expression in neuron and that the expression level of the two proteins are related. This established a link between DS genomic triplication, microRNA dysregulation and NKCC1 upregulation and culminated in chloride homeostasis deficits and altered GABAergic signaling.

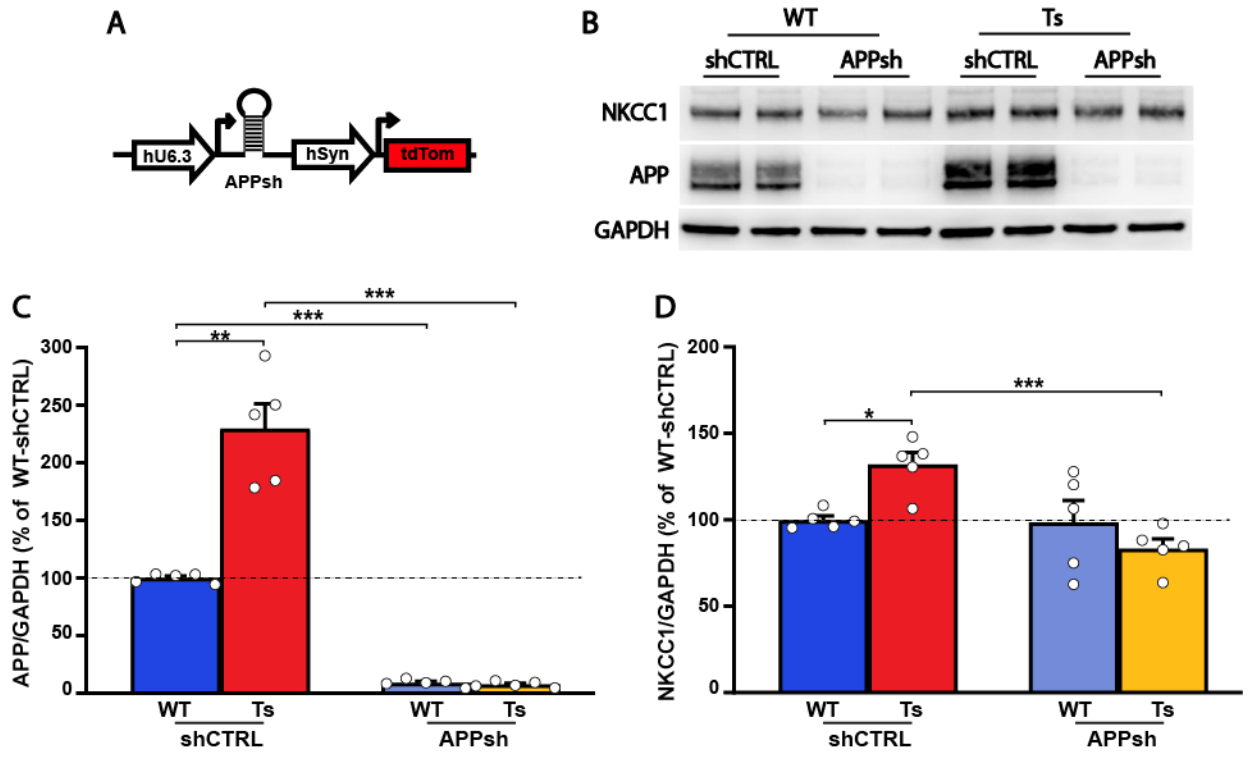

Fig.28: APP knockdown decreases NKCC1 expression in Ts65Dn neurons. (A) Scheme of the AAV vector plasmid used to express APP shRNA. **(B)** Representative immunoblot for NKCC1 and APP in protein extracts from Ts65Dn and WT neurons upon APP shRNA expression. **(C)** Quantification of APP protein (expressed as percentage of WT neurons transduced with control shRNA) showed a marked APP downregulation in both WT and Ts65Dn neurons upon delivery of APP shRNA. GAPDH was used as internal standard. Two-way ANOVA: genotype [$F_{1,19}$=3.200, P=0.093]; treatment [$F_{1,19}$=80.000, P<0.001]; genotype x treatment [$F_{1,19}$=7.200, P=0.016]. **(D)** Quantification of NKCC1 protein (expressed as percentage of WT neurons transduced with control shRNA) showed NKCC1 downregulation in Ts65Dn neurons after delivery of APP shRNA. GAPDH was used as internal standard. All data shown are means (± SEM). Each dot represents a single well, obtained from 2 independent cultures. Two-way ANOVA: genotype [$F_{1,19}$=1.180, P=0.293]; treatment [$F_{1,19}$=10.178, P=0.006]; genotype x treatment [$F_{1,19}$=9.012, P=0.008]. *p<0.05;** *** p<0.001, Two-way ANOVA followed by Tukey *post hoc* test.

DISCUSSION

DS is caused by the triplication of human chromosome 21 (HSA21) and it is the most common genetic form of intellectual disability. Cognitive deficits are the major hallmark of DS and represent the most debilitating aspect of the pathology, highly impinging on life quality of DS people and their families. Studies on DS mouse models have identified many alterations to explain DS-related cognitive impairments [5,35]. The Ts65Dn mouse is a widely used trisomic murine model of DS carrying a freely-segregating extra chromosome containing ~55% of mouse orthologues genes to HSA21 [41]. Although the Ts65Dn model presents some genetic limitations compared to the human syndrome [18,197], it recapitulates many DS-related abnormalities, including craniofacial dysmorphic features, cognitive impairment and altered hippocampus-dependent memory functions [41,203,204]. Currently, the Ts65Dn mouse is the only model that has been exploited for preclinical evaluation of pharmacotherapy for cognition in DS [36]. A number of studies have evaluated the contribution of different HSA21-derived genes to DS-related cognitive impairment by genetically restoring disomy of some triplicated genes or pharmacologically reducing their activity in Ts65Dn mice. In particular, much of the work on triplicated HSA21 orthologues in Ts65Dn mice has focused on a small set of genes: App [205-207], Girk2 [208,209], the dual specificity tyrosine-phosphorylation-regulated kinase 1A (Dyrk1A)[210-212], the bHLH transcription factors Olig1/Olig2 [90], and the phosphoinositide phosphatase synaptojanin 1 (Synj1)[213]. These studies have clearly showed that specific DS-related phenotypes critically arise from the triplication of different HSA21 dosage-sensitive genes in Ts65Dn mice. However, transcriptome profiling in brains of both Ts65Dn mice and DS patients have highlighted global gene expression dysregulation of hundreds of non-HSA21 transcripts as a secondary consequence of trisomy [25,32,214], greatly complicating the understanding of the underling neurophysiological alterations leading to cognitive disabilities [24]. In fact, although HSA21 does not contain any gene encoding for GABA receptors, a large body of evidence has pointed to altered signaling from $GABA_A$Rs and excitatory/inhibitory synaptic imbalance as major players in cognitive impairment in Ts65Dn mice [72,84,86,90,96]. In this framework, we have recently found that intracellular chloride accumulation shifts $GABA_A$R-mediated currents from hyperpolarizing to depolarizing and dampens the efficacy of GABA-mediated inhibition in the adult Ts65Dn mice [73]. Accordingly, MEA recordings of network activity in hippocampal cultures form Ts65Dn mice showed the presence of a population of neurons in which GABAergic signaling is depolarizing and therefore in which $GABA_A$R activation favors excitation. Although intracellular chloride imaging showed a decrease in chloride levels in most of Ts65Dn neurons, only 13% of the electrodes recording from Ts65Dn networks showed an increase in mean firing rate after GABA administration. However, it should be noted that GABA administration activates both $GABA_A$ channels and $GABA_B$ GPCR. In addition, since subunit 2 of

GIRK channel is triplicated in DS and DS mouse models, $GABA_B$/GIRK currents result increased in primary hippocampal neurons, enhancing GIRK-mediated shunting inhibition [72] and mitigating the increased neuronal excitability due to increased $[Cl^-]_i$.

Optimal neural network activity and brain functions critically depend on the correct balance between excitatory and inhibitory synaptic inputs. In fact, precise control of $[Cl^-]_i$ is necessary to ensure the efficacy of synaptic inhibition trough chloride-permeable $GABA_A$Rs. In mature neurons, low $[Cl^-]_i$ determines an inward (hyperpolarizing) flow of negatively charged chloride ions through $GABA_A$Rs [215]. However, relatively small changes in neuronal $[Cl^-]_i$ are sufficient to switch the polarity of GABAergic responses from hyperpolarizing to depolarizing [215,216]. Therefore, $[Cl^-]_i$ must be tightly controlled in neurons to ensure appropriate GABAergic inhibition and avoid catastrophic consequences on excitatory/inhibitory balance and neural network activity. Regulation of neuronal $[Cl^-]_i$ is mainly controlled by the opposite action of two major cation/chloride cotransporters: the Cl^- importer NKCC1 and exporter KCC2 [217,218]. During development, changes in the levels of the two cotransporters trigger the developmental GABAergic switch from depolarizing to hyperpolarizing [55]. Interestingly, alteration of neuronal chloride homeostasis due to changes in the expression or the transport activity of NKCC1 or KCC2 may also occur later in life and seems to be a common feature of a wide range of neurodevelopmental and neurological disorders [216] including: chronic pain [66], brain trauma [67-69], autism spectrum disorder [70,71], Rett syndrome [74,75], Parkinson disease [219], Fragile X syndrome [71,76], Huntington disease [77], Tuberous sclerosis [78], 22q11.2 microdeletion syndrome [79], maternal immune activation [80] and some form of epilepsy [81-83,220,221].
In our experiments, NKCC1 upregulation caused an intracellular chloride accumulation leading to a depolarizing effect of GABAergic transmission. Overexpression of both miR101-3p and miR497a-5p, restored the hyperpolarizing action of GABAergic transmission, through the downregulation of NKCC1 and the reestablishment of physiological chloride concentration in trisomic neurons.

Given its importance in brain physiology, many studies have addressed the mechanisms controlling KCC2 expression and activity. For instance, KCC2 activity is known to be regulated by post-translational modifications such as phosphorylation of key residues [222]. Serine 940 is one of the most important PKC phosphorylation sites on KCC2 C-terminal domain, and its phosphorylation status influences the cell surface stability and activity of the cotransporter [59]. Moreover, KCC2 functions are also regulated in an activity-dependent manner. Indeed, sustained neuronal stimulation or interictal-like activity can reduce KCC2 membrane levels through BDNF-dependent activation of the TrkB receptor or calpain protease cleavage [223,224]. Interestingly, KCC2 expression and surface targeting have been shown to be regulated by

the HSA21 gene APP. A first report showed that APP knockout in mice resulted in significant reductions in both total and membrane KCC2 levels, leading to a depolarizing shift in the GABA reversal potential. APP regulation of KCC2 was shown to be mediated by direct protein-protein interaction by acting on KCC2 phosphorylation and ubiquitination [64]. Conversely, a second report showed that overexpression of human APP in rat cortical neurons decreased KCC2 expression and depolarized the GABA reversal potential [225]. While both studies did not found any difference in NKCC1 expression and regardless of the contradictory results, it is interesting to notice that a DS-triplicated protein may be involved in the regulation of chloride homeostasis.

While these studies have investigated how APP protein modulated KCC2 levels, in our work we have highlighted that also APP mRNA could play a role in the regulation of chloride homeostasis. In our hypothesis, the ability of APP to regulate NKCC1 levels could be mediated by a variation in microRNA levels. According to recent studies, microRNAs degradation can take place after their loading into AGO protein when the pairing with target RNA induces the destabilization of the bound microRNA, a process known as target RNA-directed miRNA degradation (TDMD). In most of the cases, TDMD is triggered by an elevated degree of complementarity between the target RNA and the microRNA, especially at the 3'end of the microRNA. However other factors may play a role in determining if the mRNA-miRNA interaction will result in gene silencing or in TDMD, such as relative mRNA-miRNA abundances and interestingly, in some cases, high expression levels of the target may compensate for a low degree of complementarity. Moreover, the requirements for TDMD occurrence may differ for different microRNAs and in different cellular systems [226]. For instance, TDMD has been shown to be particularly effective in primary neurons [227]. For this reasons, we hypothesize that being overexpressed in Ts65Dn neurons, APP mRNA could, at least in part, mediate the degradation of microR101-3p and miR497a-5p, even though their complementarity does not extend to the 3' end of the microRNAs.

Intracellular chloride accumulation has been observed in several pathological conditions, causing an excitatory-inhibitory imbalance and disrupting neuronal communication.

Several neurodevelopmental disorders are associated with increased $[Cl^-]_i$, due to the dysregulation of one or both the chloride cotransporters. Indeed, enhanced NKCC1 and reduced KCC2 levels characterize different epilepsy syndromes, as shown in animal models and human tissue studies [228-231]. Animal models of others pathologies show dysregulation of KCC2 alone or of both NKCC1 and KCC2 [66,71,74,75,77,81,232]. Schizophrenia pathology has been associated with loss-of-function mutations of KCC2 and gain-of-function mutation of NKCC1 genes, implying a role for altered chloride levels in the pathogenesis of the disease [233,234]. On the other hand, in iPSC-derived neurons from Rett syndrome patients chloride reversal potential was depolarized due to only KCC2 reduction [75]. Accordingly, analysis of cerebrospinal fluid

from Rett syndrome patients found a decrease in KCC2 levels, while NKCC1 levels were not altered [235]. Interestingly, in DS, only the expression of NKCC1 was found enhanced, while no changes were found in KCC2, in both human and mouse brain samples [114].

According to the amplified developmental instability hypothesis, in addition to overexpression of triplicated genes in trisomic cells, a secondary contribution to the pathology will come from global dysregulation of gene expression. A recently reported example concerns the endocannabinoid system. The expression of the most abundant cannabinoid receptor in the brain (CB1R) was found increased in the excitatory terminals of the hippocampus in Ts65Dn mice. Nevertheless, CB1R mRNA levels did not differ between WT and Ts65Dn mice [236]. Similarly, we found that NKCC1 cotransporter was upregulated in Ts65Dn brains and primary neuronal cultures while its mRNA levels were unchanged. Interestingly, we also found that NKCC1 protein degradation was actually slightly faster in Ts65Dn neurons. The increase in degradation speed is limited and probably does not lead to any physiological consequence due to slow NKCC1 turn-over, however, this evidence indicates that decreased protein turnover cannot account for the observed increase in the transporter expression.
On the other hand, we found that in Ts65Dn neurons post-transcriptional repression exerted on the 3'UTR of NKCC1 was reduced and may therefore contribute to NKCC1 protein upregulation in DS.

Among the regulators binding to 3'UTRs of genes, microRNAs, control gene expression at the post-transcriptional level by mainly (although not exclusively) interacting with the 3'UTRs of target genes trough the RISC complex. Therefore, we reasoned that if NKCC1 levels are regulated by microRNA, interfering with their repression activity would affect NKCC1 expression. In fact, we found that inhibiting microRNA activity by knockdown of Tnrc6C, a fundamental component the RISC complex [135], increased NKCC1 protein expression.
MicroRNAs play an essential role during development, modifying protein expression with high spatial and temporal precision [140,237]. Indeed, many developmental disorders are associated with microRNA dysregulation. For instance, FMRP protein (whose mutation causes Fragile X syndrome) regulates some components of the microRNA pathway and its mutation is associated with altered microRNA profiling [157,172,238]. Additionally, a single nucleotide polymorphism (SNP) within the primary transcript of miR137 that modifies the levels of this microRNA, has been associated with schizophrenia risk [150,169]. Furthermore, microRNAs targeting ion channels can influence neuronal excitability, being involved in all stages of epileptogenesis [156,239,240]. In Down syndrome, in addition to microRNAs encoded on chromosome 21, many others have been reported to be dysregulated in different tissues [163,164,166,167,241]. Our RT-qPCR screening of microRNAs in Ts65Dn hippocampi and primary neuronal cultures as well as in human DS hippocampi, found two downregulated microRNAs predicted to target NKCC1 3'UTR:

miR497a-5p and miR101-3p. Interestingly, both microRNAs had been previously found to target NKCC1. miR101 was shown to regulate NKCC1 (together with other targets) during early development, leading to the establishment of balanced network excitability later in life. Indeed, transient inhibition of miR101 during development delayed the GABAergic developmental switch and resulted in increased neuronal excitability in adult mice [242]. miR497a-5p is part of a large family of microRNAs sharing the same seed sequence and mRNA targets: miR15a-5p, miR15b-5p, miR16-5p, miR195-5p, miR322-5p. Among these, miR15a-5p was shown to reduce NKCC1 translation during mouse inner ear development [243]. Interestingly, a large genome-wide screening experiment by high-throughput sequencing of RNA isolated by crosslinking immunoprecipitation (HITS-CLIP) showed Ago2-mediated interaction of both miR101-3p and components of the miR497a-5p family to NKCC1 mRNA in mouse brain [244]. Notably, both miR497a-5p and miR101-3p had already been found dysregulated in DS models [163,165,245].

By mutation, overexpression and downregulation studies, we demonstrated that both miR497a-5p and miR101-3p act as NKCC1 post-transcriptional repressors in neuronal cultures. Therefore, decreased levels of miR497a-5p and miR101-3p likely drive NKCC1 upregulation in trisomic neurons.

From a more functional point of view, we have found that re-expression of both microRNAs restores physiological chloride levels and GABAergic inhibitory signaling in trisomic neurons, indicating these small RNAs as possible tools for therapeutic intervention.

Clearly, other mechanisms are involved in NKCC1 regulation and compensatory mechanism may counteract the effect exerted by microRNAs on NKCC1-3'UTR. This could explain why, in WT neurons, NKCC1 protein does not increase to Ts65Dn levels after inhibition of miRISC functionality or upon microRNA antagonization.

Interestingly, we found that the triplicated gene APP shares with NKCC1 predicted binding sites for both miR497a-5p and miR101-3p. Therefore, restoring the expression of these microRNAs has the potential to normalize both APP and NKCC1 levels. Accordingly, we showed that overexpression of miR497a-5p and miR101-3p mimics downregulated APP in both WT and Ts65Dn neurons. This further increases microRNAs overexpression potential as a therapeutic option to treat cognitive impairment, acting simultaneously by restoring chloride homeostasis and reducing APP levels to delay early-onset Alzheimer's disease observed in people with Down syndrome.

The observation that triplicated genes can impact on the entire transcriptome not only through the expression of upregulated transcription factors and regulatory proteins but also in a coding-independent manner through the upregulation of mRNA transcripts, may have a more mechanistic implication regarding how chromosome 21 triplication may affect *in trans* the expression of other genes. According to the “competitive endogenous RNA” (ceRNA) hypothesis, mRNAs bearing seed-binding sequences for

the same microRNAs influence each other by competing for a limited pool of these microRNAs. Therefore, changes in the levels of one of the predicted microRNA targets can relieve or potentiate microRNA repression on competitive targets [201,202]. For example, many ceRNAs couples are expressed with stage-specificity and can act sequentially or synergistically to tune and coordinate specific functions during brain development. Moreover, their competition for microRNAs can mediate the crosstalk between different signaling pathways [246]. Competition can take place between protein-coding or non-coding RNAs such as pseudogenes and circular RNAs (circRNAs). For instance, PTENP1 is a pseudogene sharing microRNA-binding elements with the tumor suppressor gene PTEN (phosphatase and tensin homolog). Overexpression of PTENP1-3'UTR leads to growth inhibition and increased levels of PTEN by competing for the same microRNAs. On the other hand, copy number losses at the PTENP1 locus have been identified in sporadic colon cancer, suggesting a tumor suppression function for PTENP1 [247]. Additionally, also circRNAs can efficiently act as microRNA sponges and have been involved in brain pathologies. For instance, the circRNA antisense to the cerebellar degeneration-related protein 1 transcript (CDR1as) harbors more than 70 microRNA-binding elements for miR7, and has therefore been named ciRS-7. The main role of ciRs-7 is to bind miR7 and its ectopic expression phenocopied miR7 knockdown, causing morphological midbrain deficits [248,249]. Interestingly, ciRS-7 is downregulated in the hippocampus and cortex of Alzheimer's disease patients. ciRS-7 downregulation has been associated with a de-repression of miR7 function and the downregulation of its known downstream target ubiquitin conjugating enzyme E2A (UBE2A), involved in ubiquitin-mediated degradation of amyloid peptides [250]. miR7 can also target α-synuclein mRNA, a protein involved in Parkinson's disease pathogenesis [251]. Therefore, ciRS-7 could possibly be involved in a ceRNA network contributing to the progression of neurodegenerative diseases [248,252].

Moreover, Valluy et al. found that a particular transcript of UBE3A gene (Ube3a1), whose duplication is frequently observed in autism, can possibly act as a ceRNA during development to regulate dendrite growth and prevent premature spine maturation[253]. Therefore, the ceRNA mechanism possibly plays a role also in the onset of neurodevelopmental disorders.

In our context, due to the presence of a supernumerary copy of the APP gene, a higher amount of miR497a-5p and/or miR101-3p may bind to APP 3'UTR, leading to a lack of repression exerted on other microRNA targets, including NKCC1. Therefore, we hypothesized that variations in the levels of free miR497a-5p and miR101-3p (due to APP triplication) could represent the missing link between the trisomy of chromosome 21 and NKCC1 upregulation. In fact, our preliminary data, obtained through the downregulation of APP with a specific shRNA, indicate that knockdown of APP downregulates NKCC1 protein in Ts65Dn neurons, establishing a direct connection between trisomy and GABAergic dysfunctions. However, further experiments are needed to establish whether the decrease in miR497a-5p

and miR101-3p occurs as a consequence of their binding to APP 3'UTR (possibly through the TDMD process) or if the reduction of miRNA levels and APP competition for binding are independent phenomena. Interestingly, APP has already been shown to play a role in cortical development by suppressing the levels of a specific microRNA (miR574-5p). In this case, the authors hypothesize that APP protein is acting through transcriptional inhibition, however, the specific molecular mechanism involved in the suppression of miR574-5p is not fully clarified in the study [254].

In conclusion, we identified a lack of microRNA-mediated inhibition of translation as the cause of NKCC1 upregulation, which leads to intracellular chloride accumulation in the Ts65Dn model of DS. Defective translational repression derives from the downregulation of miR497a-5p and miR101-3p in trisomic neurons. Interestingly, four triplicated genes, APP, Dyrk1A, RUNX1 and BACE2, are predicted targets of these two microRNAs. This implies that, as predicted by competitive endogenous RNA hypothesis, the 3'UTR of those genes probably act *in trans*, by binding the shared microRNAs, resulting in the de-repression of NKCC1. Accordingly, our preliminary results obtained with APP shRNA show that APP downregulation causes a decrease in NKCC1 levels.

Using molecular biology and biochemical approaches as well as MEA recordings, we have demonstrated that overexpression of miR497a-5p and miR101-3p can reduce NKCC1 levels, restoring physiological $[Cl^-]_i$ and the hyperpolarizing action of endogenous GABAergic transmission. Therefore, this approach has the potential to rescue the cognitive deficits characterizing Ts65Dn model. We decided to perform these experiments using tranfection of miRNA mimics as a first approach, due to their immediate availability. However, this approach carries some limitations as it only allows a short-term evaluation of miRNA activity and the percentage of transfected neurons can be low compared to neuronal cultures transduced with viral vectors. For this reason, we are performing validation experiments using viral vectors to overexpress microRNAs in order to perform measurements with higher targeting efficacy and on a longer time-scale and to better evaluate the consequences of miR497a-5p and miR101-3p long-term overexpression. In addition, to improve data reliability, we will perform further experiments trying to overcome the limitations affecting the study. For instance, even though all the experiment were carried out using a control microRNA, bearing a scramble sequence, we will repeat the key experiments using a non-related microRNA (which is not predicted to target any of the proteins involved in the study) as an additional negative control.

Moreover, to better elucidate the molecular mechanisms linking APP to NKCC1 we will separately overexpress APP coding sequence and APP-3' UTR to investigate whether the effect on NKCC1 is mediated by 3'UTR RNA.

A further step will require understanding whether the ceRNA action exerted by APP is associated to TDMD, causing the observed decrease in miRNAs levels, or the two phenomena are independent. To address this point, we will check variations in miR497a-5p and miR101-3p levels in WT and trisomic neurons after APP knock-down and APP-3'UTR overexpression

Eventually, to test the ability of microRNAs overexpression to rescue cognitive impairment and their value as a target for future therapy, we will perform stereotaxic injection in the hippocampus of WT and Ts65Dn mice and then perform behavioral tests to assess mice memory and learning performances.

BIBLIOGRAPHY

1 Down, J. L. H. Observations on an ethnic classification of idiots. *Clinical Lecture Reports, London Hospital* **3**, 259-262 (1866).

2 Lejeune, J., Gautier, M. & Turpin, R. [Study of somatic chromosomes from 9 mongoloid children]. *C R Hebd Seances Acad Sci* **248**, 1721-1722 (1959).

3 Megarbane, A. *et al.* The 50th anniversary of the discovery of trisomy 21: the past, present, and future of research and treatment of Down syndrome. *Genet Med* **11**, 611-616, doi:10.1097/GIM.0b013e3181b2e34c (2009).

4 Dierssen, M. Down syndrome: the brain in trisomic mode. *Nature reviews. Neuroscience* **13**, 844-858 (2012).

5 Contestabile, A., Benfenati, F. & Gasparini, L. Communication breaks-Down: from neurodevelopment defects to cognitive disabilities in Down syndrome. *Prog Neurobiol* **91**, 1-22 (2010).

6 Pinter, J. D. *et al.* Amygdala and hippocampal volumes in children with Down syndrome: a high-resolution MRI study. *Neurology* **56**, 972-974, doi:10.1212/wnl.56.7.972 (2001).

7 Pinter, J. D., Eliez, S., Schmitt, J. E., Capone, G. T. & Reiss, A. L. Neuroanatomy of Down's syndrome: a high-resolution MRI study. *Am J Psychiatry* **158**, 1659-1665 (2001).

8 Teipel, S. J. *et al.* Age-related cortical grey matter reductions in non-demented Down's syndrome adults determined by MRI with voxel-based morphometry. *Brain* **127**, 811-824, doi:10.1093/brain/awh101 (2004).

9 Teipel, S. J. *et al.* Relation of corpus callosum and hippocampal size to age in nondemented adults with Down's syndrome. *Am J Psychiatry* **160**, 1870-1878 (2003).

10 Contestabile, A. *et al.* Cell cycle alteration and decreased cell proliferation in the hippocampal dentate gyrus and in the neocortical germinal matrix of fetuses with Down syndrome and in Ts65Dn mice. *Hippocampus* **17**, 665-678, doi:10.1002/hipo.20308 (2007).

11 Guidi, S. *et al.* Neurogenesis impairment and increased cell death reduce total neuron number in the hippocampal region of fetuses with Down syndrome. *Brain Pathol* **18**, 180-197, doi:10.1111/j.1750-3639.2007.00113.x (2008).

12 Wisniewski, H. M., Silverman, W. & Wegiel, J. Ageing, Alzheimer disease and mental retardation. *J Intellect Disabil Res* **38 (Pt 3)**, 233-239 (1994).

13 Becker, L. E., Armstrong, D. L. & Chan, F. Dendritic atrophy in children with Down's syndrome. *Ann Neurol* **20**, 520-526 (1986).

14 Ferrer, I. & Gullotta, F. Down's syndrome and Alzheimer's disease: dendritic spine counts in hippocampus. *Acta Neuropathol* **79**, 680-685 (1990).

15 Takashima, S., Becker, L. E., Armstrong, D. L. & Chan, F. Abnormal neuronal development in the visual cortex of the human fetus and infant with down's syndrome. A quantitative and qualitative Golgi study. *Brain Res* **225**, 1-21 (1981).

16 Vuksic, M., Petanjek, Z., Rasin, M. R. & Kostovic, I. Perinatal Growth of Prefrontal Layer III Pyramids in Down Syndrome. *Pediatr Neurol* **27**, 36-38 (2002).

17 Whittle, N., Sartori, S. B., Dierssen, M., Lubec, G. & Singewald, N. Fetal Down syndrome brains exhibit aberrant levels of neurotransmitters critical for normal brain development. *Pediatrics* **120**, e1465-1471, doi:10.1542/peds.2006-3448 (2007).

18 Gupta, M., Dhanasekaran, R. & Gardiner, K. J. Mouse models of Down syndrome: gene content and consequences. *Mamm Genome* **doi:10.1007/s00335-016-9661-8** (2016).
19 Hattori, M. *et al.* The DNA sequence of human chromosome 21. *Nature* **405**, 311-319, doi:10.1038/35012518 (2000).
20 Antonarakis, S. E. Down syndrome and the complexity of genome dosage imbalance. *Nat Rev Genet* **18**, 147-163, doi:10.1038/nrg.2016.154 (2017).
21 Olson, L. E., Richtsmeier, J. T., Leszl, J. & Reeves, R. H. A chromosome 21 critical region does not cause specific Down syndrome phenotypes. *Science* **306**, 687-690, doi:10.1126/science.1098992 (2004).
22 Letourneau, A. & Antonarakis, S. E. Genomic determinants in the phenotypic variability of Down syndrome. *Prog Brain Res* **197**, 15-28, doi:10.1016/b978-0-444-54299-1.00002-9 (2012).
23 Olson, L. E. *et al.* Trisomy for the Down syndrome 'critical region' is necessary but not sufficient for brain phenotypes of trisomic mice. *Hum Mol Genet* **16**, 774-782, doi:10.1093/hmg/ddm022 (2007).
24 Antonarakis, S. E., Lyle, R., Chrast, R. & Scott, H. S. Differential gene expression studies to explore the molecular pathophysiology of Down syndrome. *Brain Res Brain Res Rev* **36**, 265-274 (2001).
25 Olmos-Serrano, J. L. *et al.* Down Syndrome Developmental Brain Transcriptome Reveals Defective Oligodendrocyte Differentiation and Myelination. *Neuron* **89**, 1208-1222, doi:10.1016/j.neuron.2016.01.042 (2016).
26 Letourneau, A. *et al.* Domains of genome-wide gene expression dysregulation in Down's syndrome. *Nature* **508**, 345-350, doi:10.1038/nature13200 (2014).
27 Ait Yahya-Graison, E. *et al.* Classification of human chromosome 21 gene-expression variations in Down syndrome: impact on disease phenotypes. *Am J Hum Genet* **81**, 475-491, doi:10.1086/520000 (2007).
28 Laufer, B. I., Hwang, H., Vogel Ciernia, A., Mordaunt, C. E. & LaSalle, J. M. Whole genome bisulfite sequencing of Down syndrome brain reveals regional DNA hypermethylation and novel disorder insights. *Epigenetics* **14**, 672-684, doi:10.1080/15592294.2019.1609867 (2019).
29 Mendioroz, M. *et al.* Trans effects of chromosome aneuploidies on DNA methylation patterns in human Down syndrome and mouse models. *Genome Biol* **16**, 263, doi:10.1186/s13059-015-0827-6 (2015).
30 Reinholdt, L. G. *et al.* Meiotic behavior of aneuploid chromatin in mouse models of Down syndrome. *Chromosoma* **118**, 723-736, doi:10.1007/s00412-009-0230-8 (2009).
31 Sobol, M. *et al.* Transcriptome and Proteome Profiling of Neural Induced Pluripotent Stem Cells from Individuals with Down Syndrome Disclose Dynamic Dysregulations of Key Pathways and Cellular Functions. *Mol Neurobiol*, doi:10.1007/s12035-019-1585-3 (2019).
32 Lockstone, H. E. *et al.* Gene expression profiling in the adult Down syndrome brain. *Genomics* **90**, 647-660, doi:10.1016/j.ygeno.2007.08.005 (2007).
33 Gupta, M., Dhanasekaran, A. R. & Gardiner, K. J. Mouse models of Down syndrome: gene content and consequences. *Mamm Genome* **27**, 538-555, doi:10.1007/s00335-016-9661-8 (2016).
34 Davisson, M. T. *et al.* Evolutionary breakpoints on human chromosome 21. *Genomics* **78**, 99-106, doi:10.1006/geno.2001.6639 (2001).
35 Rueda, N., Florez, J. & Martinez-Cue, C. Mouse models of Down syndrome as a tool to unravel the causes of mental disabilities. *Neural Plast* **2012**, 584071, doi:10.1155/2012/584071 (2012).

36 Gardiner, K. J. Pharmacological approaches to improving cognitive function in Down syndrome: current status and considerations. *Drug Des Devel Ther* **9**, 103-125 (2014).

37 Li, Z. *et al.* Duplication of the entire 22.9 Mb human chromosome 21 syntenic region on mouse chromosome 16 causes cardiovascular and gastrointestinal abnormalities. *Hum Mol Genet* **16**, 1359-1366, doi:10.1093/hmg/ddm086 (2007).

38 Yu, T. *et al.* Effects of individual segmental trisomies of human chromosome 21 syntenic regions on hippocampal long-term potentiation and cognitive behaviors in mice. *Brain Res* **1366**, 162-171, doi:10.1016/j.brainres.2010.09.107 (2010).

39 O'Doherty, A. *et al.* An aneuploid mouse strain carrying human chromosome 21 with Down syndrome phenotypes. *Science* **309**, 2033-2037 (2005).

40 Sago, H. *et al.* Genetic dissection of region associated with behavioral abnormalities in mouse models for Down syndrome. *Pediatr Res* **48**, 606-613 (2000).

41 Reeves, R. H. *et al.* A mouse model for Down syndrome exhibits learning and behaviour deficits. *Nat Genet* **11**, 177-184 (1995).

42 Fernandez, F. & Garner, C. C. Episodic-like memory in Ts65Dn, a mouse model of Down syndrome. *Behav Brain Res* **188**, 233-237, doi:10.1016/j.bbr.2007.09.015 (2008).

43 Chakrabarti, L., Galdzicki, Z. & Haydar, T. F. Defects in embryonic neurogenesis and initial synapse formation in the forebrain of the Ts65Dn mouse model of Down syndrome. *J Neurosci* **27**, 11483-11495, doi:10.1523/jneurosci.3406-07.2007 (2007).

44 Chakrabarti, L. *et al.* Olig1 and Olig2 triplication causes developmental brain defects in Down syndrome. *Nat Neurosci* **13**, 927-934, doi:10.1038/nn.2600 (2010).

45 Padgett, C. L. & Slesinger, P. A. GABAB receptor coupling to G-proteins and ion channels. *Adv Pharmacol* **58**, 123-147, doi:10.1016/s1054-3589(10)58006-2 (2010).

46 Rost, B. R. *et al.* Activation of metabotropic GABA receptors increases the energy barrier for vesicle fusion. *J Cell Sci* **124**, 3066-3073, doi:10.1242/jcs.074963 (2011).

47 Bohme, I., Rabe, H. & Luddens, H. Four amino acids in the alpha subunits determine the gamma-aminobutyric acid sensitivities of GABAA receptor subtypes. *J Biol Chem* **279**, 35193-35200, doi:10.1074/jbc.M405653200 (2004).

48 Caraiscos, V. B. *et al.* Tonic inhibition in mouse hippocampal CA1 pyramidal neurons is mediated by alpha5 subunit-containing gamma-aminobutyric acid type A receptors. *Proc Natl Acad Sci U S A* **101**, 3662-3667, doi:10.1073/pnas.0307231101 (2004).

49 Farrant, M. & Nusser, Z. Variations on an inhibitory theme: phasic and tonic activation of GABA(A) receptors. *Nat Rev Neurosci* **6**, 215-229, doi:10.1038/nrn1625 (2005).

50 Cellot, G. & Cherubini, E. Functional role of ambient GABA in refining neuronal circuits early in postnatal development. *Front Neural Circuits* **7**, 136 (2013).

51 Ben-Ari, Y. Excitatory actions of gaba during development: the nature of the nurture. *Nature reviews. Neuroscience* **3**, 728-739, doi:10.1038/nrn920 (2002).

52 Ben-Ari, Y. The GABA excitatory/inhibitory developmental sequence: a personal journey. *Neuroscience* **279**, 187-219, doi:10.1016/j.neuroscience.2014.08.001 (2014).

53 Ben-Ari, Y. NKCC1 Chloride Importer Antagonists Attenuate Many Neurological and Psychiatric Disorders. *Trends Neurosci* **40**, 536-554, doi:10.1016/j.tins.2017.07.001 (2017).

54 Schulte, J. T., Wierenga, C. J. & Bruining, H. Chloride transporters and GABA polarity in developmental, neurological and psychiatric conditions. *Neurosci Biobehav Rev* **90**, 260-271, doi:10.1016/j.neubiorev.2018.05.001 (2018).

55 Ben-Ari, Y., Gaiarsa, J. L., Tyzio, R. & Khazipov, R. GABA: a pioneer transmitter that excites immature neurons and generates primitive oscillations. *Physiol Rev* **87**, 1215-1284, doi:10.1152/physrev.00017.2006 (2007).

56 Sulis Sato, S. *et al.* Simultaneous two-photon imaging of intracellular chloride concentration and pH in mouse pyramidal neurons in vivo. *Proc Natl Acad Sci U S A* **114**, E8770-e8779, doi:10.1073/pnas.1702861114 (2017).

57 Raimondo, J. V., Richards, B. A. & Woodin, M. A. Neuronal chloride and excitability - the big impact of small changes. *Curr Opin Neurobiol* **43**, 35-42, doi:10.1016/j.conb.2016.11.012 (2017).

58 Chew, T. A. *et al.* Structure and mechanism of the cation-chloride cotransporter NKCC1. *Nature* **572**, 488-492, doi:10.1038/s41586-019-1438-2 (2019).

59 Lee, H. H. *et al.* Direct protein kinase C-dependent phosphorylation regulates the cell surface stability and activity of the potassium chloride cotransporter KCC2. *J Biol Chem* **282**, 29777-29784, doi:10.1074/jbc.M705053200 (2007).

60 Mahadevan, V. *et al.* Kainate receptors coexist in a functional complex with KCC2 and regulate chloride homeostasis in hippocampal neurons. *Cell Rep* **7**, 1762-1770, doi:10.1016/j.celrep.2014.05.022 (2014).

61 Pressey, J. C. *et al.* A kainate receptor subunit promotes the recycling of the neuron-specific K(+)-Cl(-) co-transporter KCC2 in hippocampal neurons. *J Biol Chem* **292**, 6190-6201, doi:10.1074/jbc.M116.767236 (2017).

62 Banke, T. G. & Gegelashvili, G. Tonic activation of group I mGluRs modulates inhibitory synaptic strength by regulating KCC2 activity. *J Physiol* **586**, 4925-4934, doi:10.1113/jphysiol.2008.157024 (2008).

63 Kahle, K. T. *et al.* WNK3 modulates transport of Cl- in and out of cells: implications for control of cell volume and neuronal excitability. *Proc Natl Acad Sci U S A* **102**, 16783-16788, doi:10.1073/pnas.0508307102 (2005).

64 Chen, M. *et al.* APP modulates KCC2 expression and function in hippocampal GABAergic inhibition. *Elife* **6**, doi:10.7554/eLife.20142 (2017).

65 Okabe, A. *et al.* Amygdala kindling induces upregulation of mRNA for NKCC1, a Na(+), K(+)-2Cl(-) cotransporter, in the rat piriform cortex. *Neurosci Res* **44**, 225-229, doi:10.1016/s0168-0102(02)00093-7 (2002).

66 Ferrini, F. *et al.* Morphine hyperalgesia gated through microglia-mediated disruption of neuronal Cl(-) homeostasis. *Nat Neurosci* **16**, 183-192, doi:10.1038/nn.3295 (2013).

67 Jayakumar, A. R. *et al.* Na-K-Cl cotransporter-1 in the mechanism of cell swelling in cultured astrocytes after fluid percussion injury. *J Neurochem* **117**, 437-448, doi:10.1111/j.1471-4159.2011.07211.x (2011).

68 Lu, K. T. *et al.* Inhibition of the Na+ -K+ -2Cl- -cotransporter in choroid plexus attenuates traumatic brain injury-induced brain edema and neuronal damage. *Eur J Pharmacol* **548**, 99-105, doi:10.1016/j.ejphar.2006.07.048 (2006).

69 Karimy, J. K. *et al.* Inflammation-dependent cerebrospinal fluid hypersecretion by the choroid plexus epithelium in posthemorrhagic hydrocephalus. *Nat Med* **23**, 997-1003, doi:10.1038/nm.4361 (2017).

70 Lemonnier, E. *et al.* A randomised controlled trial of bumetanide in the treatment of autism in children. *Transl Psychiatry* **11**, e202, doi:10.1038/tp.2012.124 (2012).

71 Tyzio, R. *et al.* Oxytocin-mediated GABA inhibition during delivery attenuates autism pathogenesis in rodent offspring. *Science* **343**, 675-679 (2014).

72 Contestabile, A., Magara, S. & Cancedda, L. The GABAergic Hypothesis for Cognitive Disabilities in Down Syndrome. *Front Cell Neurosci* **11**, 54 (2017).

73 Deidda, G. *et al.* Reversing excitatory GABAAR signaling restores synaptic plasticity and memory in a mouse model of Down syndrome. *Nature Medicine* **21**, 318-326 (2015).

74 Banerjee, A. *et al.* Jointly reduced inhibition and excitation underlies circuit-wide changes in cortical processing in Rett syndrome. *Proc Natl Acad Sci U S A* **113**, E7287-E7296 (2016).

75 Tang, X. *et al.* KCC2 rescues functional deficits in human neurons derived from patients with Rett syndrome. *Proc Natl Acad Sci U S A* **113**, 751-756 (2016).

76 He, Q. *et al.* Critical period inhibition of NKCC1 rectifies synapse plasticity in the somatosensory cortex and restores adult tactile response maps in fragile X mice. *Mol Psychiatry*, doi:10.1038/s41380-018-0048-y (2018).

77 Dargaei, Z. *et al.* Restoring GABAergic inhibition rescues memory deficits in a Huntington's disease mouse model. *Proc Natl Acad Sci U S A* **115**, E1618-E1626, doi:10.1073/pnas.1716871115 (2018).

78 Talos, D. M. *et al.* Altered inhibition in tuberous sclerosis and type IIb cortical dysplasia. *Ann Neurol* **71**, 539-551, doi:10.1002/ana.22696 (2012).

79 Amin, H., Marinaro, F., De Pietri Tonelli, D. & Berdondini, L. Developmental excitatory-to-inhibitory GABA-polarity switch is disrupted in 22q11.2 deletion syndrome: a potential target for clinical therapeutics. *Scientific reports* **7**, 15752, doi:10.1038/s41598-017-15793-9 (2017).

80 Corradini, I. *et al.* Maternal Immune Activation Delays Excitatory-to-Inhibitory Gamma-Aminobutyric Acid Switch in Offspring. *Biol Psychiatry* **83**, 680-691 (2018).

81 Nardou, R. *et al.* Neuronal chloride accumulation and excitatory GABA underlie aggravation of neonatal epileptiform activities by phenobarbital. *Brain* **134**, 987-1002, doi:10.1093/brain/awr041 (2011).

82 Huberfeld, G. *et al.* Perturbed chloride homeostasis and GABAergic signaling in human temporal lobe epilepsy. *Journal of Neuroscience* **27**, 9866-9873 (2007).

83 Pallud, J. *et al.* Cortical GABAergic excitation contributes to epileptic activities around human glioma. *Science translational medicine* **6**, 244ra289, doi:10.1126/scitranslmed.3008065 (2014).

84 Costa, A. C. & Grybko, M. J. Deficits in hippocampal CA1 LTP induced by TBS but not HFS in the Ts65Dn mouse: a model of Down syndrome. *Neurosci Lett* **382**, 317-322 (2005).

85 Fernandez, F. *et al.* Pharmacotherapy for cognitive impairment in a mouse model of Down syndrome. *Nat Neurosci* **10**, 411-413, doi:10.1038/nn1860 (2007).

86 Fernandez, F. *et al.* Pharmacotherapy for cognitive impairment in a mouse model of Down syndrome. *Nature Neuroscience* **10**, 411-413 (2007).

87 Rueda, N., Florez, J. & Martinez-Cue, C. Chronic pentylenetetrazole but not donepezil treatment rescues spatial cognition in Ts65Dn mice, a model for Down syndrome. *Neurosci Lett* **433**, 22-27, doi:10.1016/j.neulet.2007.12.039 (2008).

88 Bhattacharyya, A., McMillan, E., Chen, S. I., Wallace, K. & Svendsen, C. N. A critical period in cortical interneuron neurogenesis in down syndrome revealed by human neural progenitor cells. *Dev Neurosci* **31**, 497-510, doi:10.1159/000236899 (2009).

89 Huo, H. Q. *et al.* Modeling Down Syndrome with Patient iPSCs Reveals Cellular and Migration Deficits of GABAergic Neurons. *Stem Cell Reports* **10**, 1251-1266, doi:10.1016/j.stemcr.2018.02.001 (2018).

90 Chakrabarti, L. *et al.* Olig1 and Olig2 triplication causes developmental brain defects in Down syndrome. *Nat Neurosci* **13**, 927-934 (2010).

91 Parrini, M. *et al.* Aerobic exercise and a BDNF-mimetic therapy rescue learning and memory in a mouse model of Down syndrome. *Scientific reports* **7**, 16825 (2017).

92 Best, T. K., Cramer, N. P., Chakrabarti, L., Haydar, T. F. & Galdzicki, Z. Dysfunctional hippocampal inhibition in the Ts65Dn mouse model of Down syndrome. *Experimental Neurology* (2012).

93 Hanson, J. E., Blank, M., Valenzuela, R. A., Garner, C. C. & Madison, D. V. The functional nature of synaptic circuitry is altered in area CA3 of the hippocampus in a mouse model of Down's syndrome. *J. Physiology* **579** (2007).

94 Stagni, F. *et al.* Pharmacotherapy with fluoxetine restores functional connectivity from the dentate gyrus to field CA3 in the Ts65Dn mouse model of down syndrome. *PLoS One* **8**, e61689 (2013).

95 Kleschevnikov, A. M. *et al.* Increased efficiency of the GABAA and GABAB receptor-mediated neurotransmission in the Ts65Dn mouse model of Down syndrome. *Neurobiol Dis* **45**, 683-691 (2012).

96 Kleschevnikov, A. M. *et al.* Hippocampal long-term potentiation suppressed by increased inhibition in the Ts65Dn mouse, a genetic model of Down syndrome. *J Neurosci* **24**, 8153-8160 (2004).

97 Mitra, A., Blank, M. & Madison, D. V. Developmentally altered inhibition in Ts65Dn, a mouse model of Down syndrome. *Brain Res* **1440**, 1-8, doi:10.1016/j.brainres.2011.12.034 (2012).

98 Hattori, M. *et al.* The DNA sequence of human chromosome 21. *Nature* **405**, 311-319 (2000).

99 Ohira, M. *et al.* Gene identification in 1.6-Mb region of the Down syndrome region on chromosome 21. *Genome Res* **7**, 47-58 (1997).

100 Harashima, C. *et al.* Elevated expression of the G-protein-activated inwardly rectifying potassium channel 2 (GIRK2) in cerebellar unipolar brush cells of a Down syndrome mouse model. *Cell Mol Neurobiol* **26**, 719-734 (2006).

101 Harashima, C. *et al.* Abnormal expression of the G-protein-activated inwardly rectifying potassium channel 2 (GIRK2) in hippocampus, frontal cortex, and substantia nigra of Ts65Dn mouse: a model of Down syndrome. *J Comp Neurol* **494**, 815-833 (2006).

102 Bony, G. *et al.* Non-hyperpolarizing GABAB receptor activation regulates neuronal migration and neurite growth and specification by cAMP/LKB1. *Nature communications* **4**, 1800, doi:10.1038/ncomms2820 (2013).

103 Best, T. K., Siarey, R. J. & Galdzicki, Z. Ts65Dn, a mouse model of Down syndrome, exhibits increased GABAB-induced potassium current. *Journal of Neurophysiology* **97**, 892-900 (2007).

104 Best, T. K., Cramer, N. P., Chakrabarti, L., Haydar, T. F. & Galdzicki, Z. Dysfunctional hippocampal inhibition in the Ts65Dn mouse model of Down syndrome. *Exp Neurol* **233**, 749-757, doi:10.1016/j.expneurol.2011.11.033 (2012).

105 Rueda, N., Florez, J. & Martınez-Cue, C. Chronic pentylenetetrazole but not donepezil treatment rescues spatial cognition in Ts65Dn mice, a model for Down syndrome. *Neuroscience Letters* **433**, 22-27 (2008).

106 Deidda, G., Bozarth, I. F. & Cancedda, L. Modulation of GABAergic transmission in development and neurodevelopmental disorders: investigating physiology and pathology to gain therapeutic perspectives. *Front Cell Neurosci* **8**, 119, doi:10.3389/fncel.2014.00119 (2014).

107 Colas, D. *et al.* Short-term treatment with the $GABA_A$ receptor antagonist pentylenetetrazole produces a sustained pro-cognitive benefit in a mouse model of Down's syndrome. *British Journal of Pharmacology* **169** 963-973 (2013).

108 Martinez-Cue, C. *et al.* Reducing GABAA alpha5 receptor-mediated inhibition rescues functional and neuromorphological deficits in a mouse model of down syndrome. *J Neurosci* **33**, 3953-3966, doi:10.1523/JNEUROSCI.1203-12.2013 (2013).

109 Braudeau, J. *et al.* Chronic Treatment with a Promnesiant GABA-A alpha5-Selective Inverse Agonist Increases Immediate Early Genes Expression during Memory Processing in Mice and Rectifies Their Expression Levels in a Down Syndrome Mouse Model. *Advances in pharmacological sciences* **2011**, 153218, doi:10.1155/2011/153218 (2011).

110 Braudeau, J. *et al.* Specific targeting of the GABA-A receptor alpha5 subtype by a selective inverse agonist restores cognitive deficits in Down syndrome mice. *Journal of psychopharmacology* **25**, 1030-1042, doi:10.1177/0269881111405366 (2011).

111 Potier, M. C., Braudeau, J., Dauphinot, L. & Delatour, B. Reducing GABAergic inhibition restores cognitive functions in a mouse model of Down syndrome. *CNS Neurol Disord Drug Targets* **13**, 8-15 (2014).

112 Hanson, J. E., Blank, M., Valenzuela, R. A., Garner, C. C. & Madison, D. V. The functional nature of synaptic circuitry is altered in area CA3 of the hippocampus in a mouse model of Down's syndrome. *J Physiol* **579**, 53-67, doi:10.1113/jphysiol.2006.114868 (2007).

113 Szemes, M., Davies, R. L., Garden, C. L. & Usowicz, M. M. Weaker control of the electrical properties of cerebellar granule cells by tonically active GABAA receptors in the Ts65Dn mouse model of Down's syndrome. *Mol Brain* **6**, 33, doi:10.1186/1756-6606-6-33 (2013).

114 Deidda, G. *et al.* Reversing excitatory GABAAR signaling restores synaptic plasticity and memory in a mouse model of Down syndrome. *Nat Med* **21**, 318-326, doi:10.1038/nm.3827 (2015).

115 Carthew, R. W. & Sontheimer, E. J. Origins and Mechanisms of miRNAs and siRNAs. *Cell* **136**, 642-655, doi:10.1016/j.cell.2009.01.035 (2009).

116 Sharp, P. A. The centrality of RNA. *Cell* **136**, 577-580, doi:10.1016/j.cell.2009.02.007 (2009).

117 Hutvagner, G. & Zamore, P. D. A microRNA in a multiple-turnover RNAi enzyme complex. *Science* **297**, 2056-2060, doi:10.1126/science.1073827 (2002).

118 Zeng, Y., Yi, R. & Cullen, B. R. MicroRNAs and small interfering RNAs can inhibit mRNA expression by similar mechanisms. *Proc Natl Acad Sci U S A* **100**, 9779-9784, doi:10.1073/pnas.1630797100 (2003).

119 Jo, M. H. *et al.* Human Argonaute 2 Has Diverse Reaction Pathways on Target RNAs. *Mol Cell* **59**, 117-124, doi:10.1016/j.molcel.2015.04.027 (2015).

120 Olsen, P. H. & Ambros, V. The lin-4 regulatory RNA controls developmental timing in Caenorhabditis elegans by blocking LIN-14 protein synthesis after the initiation of translation. *Dev Biol* **216**, 671-680, doi:10.1006/dbio.1999.9523 (1999).

121 Pillai, R. S. *et al.* Inhibition of translational initiation by Let-7 MicroRNA in human cells. *Science* **309**, 1573-1576, doi:10.1126/science.1115079 (2005).

122 Hendrickson, D. G. *et al.* Concordant regulation of translation and mRNA abundance for hundreds of targets of a human microRNA. *PLoS Biol* **7**, e1000238, doi:10.1371/journal.pbio.1000238 (2009).
123 Guo, H., Ingolia, N. T., Weissman, J. S. & Bartel, D. P. Mammalian microRNAs predominantly act to decrease target mRNA levels. *Nature* **466**, 835-840, doi:10.1038/nature09267 (2010).
124 Zdanowicz, A. *et al.* Drosophila miR2 primarily targets the m7GpppN cap structure for translational repression. *Mol Cell* **35**, 881-888, doi:10.1016/j.molcel.2009.09.009 (2009).
125 Bagga, S. *et al.* Regulation by let-7 and lin-4 miRNAs results in target mRNA degradation. *Cell* **122**, 553-563, doi:10.1016/j.cell.2005.07.031 (2005).
126 Beilharz, T. H. *et al.* microRNA-mediated messenger RNA deadenylation contributes to translational repression in mammalian cells. *PLoS One* **4**, e6783, doi:10.1371/journal.pone.0006783 (2009).
127 Djuranovic, S., Nahvi, A. & Green, R. miRNA-mediated gene silencing by translational repression followed by mRNA deadenylation and decay. *Science* **336**, 237-240, doi:10.1126/science.1215691 (2012).
128 Mathonnet, G. *et al.* MicroRNA inhibition of translation initiation in vitro by targeting the cap-binding complex eIF4F. *Science* **317**, 1764-1767, doi:10.1126/science.1146067 (2007).
129 Fabian, M. R. *et al.* Mammalian miRNA RISC recruits CAF1 and PABP to affect PABP-dependent deadenylation. *Mol Cell* **35**, 868-880, doi:10.1016/j.molcel.2009.08.004 (2009).
130 Kenny, P. J. *et al.* MOV10 and FMRP regulate AGO2 association with microRNA recognition elements. *Cell Rep* **9**, 1729-1741, doi:10.1016/j.celrep.2014.10.054 (2014).
131 Ashraf, S. I., McLoon, A. L., Sclarsic, S. M. & Kunes, S. Synaptic protein synthesis associated with memory is regulated by the RISC pathway in Drosophila. *Cell* **124**, 191-205, doi:10.1016/j.cell.2005.12.017 (2006).
132 Fabian, M. R. & Sonenberg, N. The mechanics of miRNA-mediated gene silencing: a look under the hood of miRISC. *Nat Struct Mol Biol* **19**, 586-593, doi:10.1038/nsmb.2296 (2012).
133 Eulalio, A., Helms, S., Fritzsch, C., Fauser, M. & Izaurralde, E. A C-terminal silencing domain in GW182 is essential for miRNA function. *Rna* **15**, 1067-1077, doi:10.1261/rna.1605509 (2009).
134 Chekulaeva, M. *et al.* miRNA repression involves GW182-mediated recruitment of CCR4-NOT through conserved W-containig motifs. *Nat Struct Mol Biol* **18**, 1218-1226 (2011).
135 Takimoto, K., Wakiyama, M. & Yokoyama, S. Mammalian GW182 contains multiple Argonaute-binding sites and functions in microRNA-mediated translational repression. *Rna* **15**, 1078-1089, doi:10.1261/rna.1363109 (2009).
136 Lugli, G., Larson, J., Martone, M. E., Jones, Y. & Smalheiser, N. R. Dicer and eIF2c are enriched at postsynaptic densities in adult mouse brain and are modified by neuronal activity in a calpain-dependent manner. *J Neurochem* **94**, 896-905, doi:10.1111/j.1471-4159.2005.03224.x (2005).
137 Sambandan, S. *et al.* Activity-dependent spatially localized miRNA maturation in neuronal dendrites. *Science* **355**, 634-637, doi:10.1126/science.aaf8995 (2017).
138 Hu, Z. & Li, Z. miRNAs in synapse development and synaptic plasticity. *Curr Opin Neurobiol* **45**, 24-31, doi:10.1016/j.conb.2017.02.014 (2017).
139 Garza-Manero, S., Pichardo-Casas, I., Arias, C., Vaca, L. & Zepeda, A. Selective distribution and dynamic modulation of miRNAs in the synapse and its possible role in Alzheimer's Disease. *Brain Res* **1584**, 80-93, doi:10.1016/j.brainres.2013.12.009 (2014).

140 Ziats, M. N. & Rennert, O. M. Identification of differentially expressed microRNAs across the developing human brain. *Mol Psychiatry* **19**, 848-852, doi:10.1038/mp.2013.93 (2014).

141 Barca-Mayo, O. & De Pietri Tonelli, D. Convergent microRNA actions coordinate neocortical development. *Cell Mol Life Sci* **71**, 2975-2995, doi:10.1007/s00018-014-1576-5 (2014).

142 De Pietri Tonelli, D. *et al.* miRNAs are essential for survival and differentiation of newborn neurons but not for expansion of neural progenitors during early neurogenesis in the mouse embryonic neocortex. *Development* **135**, 3911-3921, doi:10.1242/dev.025080 (2008).

143 Siegel, G. *et al.* A functional screen implicates microRNA-138-dependent regulation of the depalmitoylation enzyme APT1 in dendritic spine morphogenesis. *Nat Cell Biol* **11**, 705-716, doi:10.1038/ncb1876 (2009).

144 Abdelmohsen, K. *et al.* miR-375 inhibits differentiation of neurites by lowering HuD levels. *Mol Cell Biol* **30**, 4197-4210, doi:10.1128/mcb.00316-10 (2010).

145 Rajasethupathy, P. *et al.* Characterization of small RNAs in Aplysia reveals a role for miR-124 in constraining synaptic plasticity through CREB. *Neuron* **63**, 803-817, doi:10.1016/j.neuron.2009.05.029 (2009).

146 Edbauer, D. *et al.* Regulation of synaptic structure and function by FMRP-associated microRNAs miR-125b and miR-132. *Neuron* **65**, 373-384, doi:10.1016/j.neuron.2010.01.005 (2010).

147 Karr, J. *et al.* Regulation of glutamate receptor subunit availability by microRNAs. *J Cell Biol* **185**, 685-697, doi:10.1083/jcb.200902062 (2009).

148 Zhao, C. *et al.* Computational prediction of MicroRNAs targeting GABA receptors and experimental verification of miR-181, miR-216 and miR-203 targets in GABA-A receptor. *BMC Res Notes* **5**, 91, doi:10.1186/1756-0500-5-91 (2012).

149 Higa, G. S. *et al.* MicroRNAs in neuronal communication. *Mol Neurobiol* **49**, 1309-1326, doi:10.1007/s12035-013-8603-7 (2014).

150 Thomas, K. T., Gross, C. & Bassell, G. J. microRNAs Sculpt Neuronal Communication in a Tight Balance That Is Lost in Neurological Disease. *Front Mol Neurosci* **11**, 455, doi:10.3389/fnmol.2018.00455 (2018).

151 Wei, C. *et al.* miR-153 regulates SNAP-25, synaptic transmission, and neuronal development. *PLoS One* **8**, e57080, doi:10.1371/journal.pone.0057080 (2013).

152 Earls, L. R. *et al.* Age-dependent microRNA control of synaptic plasticity in 22q11 deletion syndrome and schizophrenia. *J Neurosci* **32**, 14132-14144, doi:10.1523/jneurosci.1312-12.2012 (2012).

153 Baudry, A., Mouillet-Richard, S., Schneider, B., Launay, J. M. & Kellermann, O. miR-16 targets the serotonin transporter: a new facet for adaptive responses to antidepressants. *Science* **329**, 1537-1541, doi:10.1126/science.1193692 (2010).

154 Vaishnavi, V., Manikandan, M., Tiwary, B. K. & Munirajan, A. K. Insights on the functional impact of microRNAs present in autism-associated copy number variants. *PLoS One* **8**, e56781, doi:10.1371/journal.pone.0056781 (2013).

155 Nakata, M. *et al.* MicroRNA profiling in adults with high-functioning autism spectrum disorder. *Mol Brain* **12**, 82, doi:10.1186/s13041-019-0508-6 (2019).

156 Gross, C. & Tiwari, D. Regulation of Ion Channels by MicroRNAs and the Implication for Epilepsy. *Curr Neurol Neurosci Rep* **18**, 60, doi:10.1007/s11910-018-0870-2 (2018).

157 Wan, R. P. *et al.* Involvement of FMRP in Primary MicroRNA Processing via Enhancing Drosha Translation. *Mol Neurobiol* **54**, 2585-2594, doi:10.1007/s12035-016-9855-9 (2017).

158 Bras, A., Rodrigues, A. S., Gomes, B. & Rueff, J. Down syndrome and microRNAs. *Biomed Rep* **8**, 11-16, doi:10.3892/br.2017.1019 (2018).

159 Alexandrov, P. N., Percy, M. E. & Lukiw, W. J. Chromosome 21-Encoded microRNAs (mRNAs): Impact on Down's Syndrome and Trisomy-21 Linked Disease. *Cell Mol Neurobiol* **38**, 769-774, doi:10.1007/s10571-017-0514-0 (2018).

160 Kaufmann, W. E., Johnston, M. V. & Blue, M. E. MeCP2 expression and function during brain development: implications for Rett syndrome's pathogenesis and clinical evolution. *Brain Dev* **27 Suppl 1**, S77-s87, doi:10.1016/j.braindev.2004.10.008 (2005).

161 Bienvenu, T. & Chelly, J. Molecular genetics of Rett syndrome: when DNA methylation goes unrecognized. *Nat Rev Genet* **7**, 415-426, doi:10.1038/nrg1878 (2006).

162 Elton, T. S., Sansom, S. E. & Martin, M. M. Trisomy-21 gene dosage over-expression of miRNAs results in the haploinsufficiency of specific target proteins. *RNA Biol* **7**, 540-547, doi:10.4161/rna.7.5.12685 (2010).

163 He, X. J. *et al.* Detection and functional annotation of misregulated microRNAs in the brain of the Ts65Dn mouse model of Down syndrome. *Chinese medical journal* **126**, 108-113 (2013).

164 Xu, Y. *et al.* Identification of dysregulated microRNAs in lymphocytes from children with Down syndrome. *Gene* **530**, 278-286, doi:10.1016/j.gene.2013.07.055 (2013).

165 Lin, H. *et al.* Integrated microRNA and protein expression analysis reveals novel microRNA regulation of targets in fetal down syndrome. *Mol Med Rep* **14**, 4109-4118, doi:10.3892/mmr.2016.5775 (2016).

166 Shi, W. L. *et al.* Integrated miRNA and mRNA expression profiling in fetal hippocampus with Down syndrome. *J Biomed Sci* **23**, 48, doi:10.1186/s12929-016-0265-0 (2016).

167 Keck-Wherley, J. *et al.* Abnormal microRNA expression in Ts65Dn hippocampus and whole blood: contributions to Down syndrome phenotypes. *Dev Neurosci* **33**, 451-467, doi:10.1159/000330884 (2011).

168 Siew, W. H., Tan, K. L., Babaei, M. A., Cheah, P. S. & Ling, K. H. MicroRNAs and intellectual disability (ID) in Down syndrome, X-linked ID, and Fragile X syndrome. *Front Cell Neurosci* **7**, 41, doi:10.3389/fncel.2013.00041 (2013).

169 Genome-wide association study identifies five new schizophrenia loci. *Nat Genet* **43**, 969-976, doi:10.1038/ng.940 (2011).

170 Guella, I. *et al.* Analysis of miR-137 expression and rs1625579 in dorsolateral prefrontal cortex. *J Psychiatr Res* **47**, 1215-1221, doi:10.1016/j.jpsychires.2013.05.021 (2013).

171 Mellios, N., Huang, H. S., Grigorenko, A., Rogaev, E. & Akbarian, S. A set of differentially expressed miRNAs, including miR-30a-5p, act as post-transcriptional inhibitors of BDNF in prefrontal cortex. *Hum Mol Genet* **17**, 3030-3042, doi:10.1093/hmg/ddn201 (2008).

172 Zhou, Y., Hu, Y., Sun, Q. & Xie, N. Non-coding RNA in Fragile X Syndrome and Converging Mechanisms Shared by Related Disorders. *Front Genet* **10**, 139, doi:10.3389/fgene.2019.00139 (2019).

173 Pozzi, D. *et al.* REST/NRSF-mediated intrinsic homeostasis protects neuronal networks from hyperexcitability. *EMBO J* **32**, 2994-3007, doi:emboj2013231 [pii]

10.1038/emboj.2013.231 (2013).

174 Shi, R. & Chiang, V. L. Facile means for quantifying microRNA expression by real-time PCR. *Biotechniques* **39**, 519-525 (2005).

175 Vandesompele, J. *et al.* Accurate normalization of real-time quantitative RT-PCR data by geometric averaging of multiple internal control genes. *Genome Biol* **3**, RESEARCH0034 (2002).

176 Beaudoin, G. M., 3rd *et al.* Culturing pyramidal neurons from the early postnatal mouse hippocampus and cortex. *Nature protocols* **7**, 1741-1754, doi:10.1038/nprot.2012.099 (2012).

177 Valente, P. *et al.* Cell adhesion molecule L1 contributes to neuronal excitability regulating the function of voltage-gated Na+ channels. *J Cell Sci* **129**, 1878-1891 (2016).

178 Pozzi, D. *et al.* REST/NRSF-mediated intrinsic homeostasis protects neuronal networks from hyperexitability. *EMBO Journal* **13**, 2994-3007 (2013).

179 Thalhammer, A. *et al.* Alternative Splicing of P/Q-Type Ca2+ Channels Shapes Presynaptic Plasticity. *Cell Rep* **20**, 333-343 (2017).

180 Chung, K. H. *et al.* Polycistronic RNA polymerase II expression vectors for RNA interference based on BIC/miR-155. *Nucleic Acids Res* **34**, e53 (2006).

181 Follenzi, A., Ailles, L. E., Bakovic, S., Geuna, M. & Naldini, L. Gene transfer by lentiviral vectors is limited by nuclear translocation and rescued by HIV-1 pol sequences. *Nat Genet* **25**, 217-222 (2000).

182 Gu, S. *et al.* The Loop Position of shRNAs and Pre-miRNAs Is Critical for the Accuracy of Dicer Processing In Vivo. *Cell* **151**, 900-911 (2012).

183 Ayuso, E. *et al.* High AAV vector purity results in serotype- and tissue-independent enhancement of transduction efficiency. *Gene Ther* **17**, 503-510 (2010).

184 Matsushita, T. *et al.* Adeno-associated virus vectors can be efficiently produced without helper virus. *Gene Ther* **5**, 938-945, doi:10.1038/sj.gt.3300680 (1998).

185 McClure, C., Cole, K. L., Wulff, P., Klugmann, M. & Murray, A. J. Production and titering of recombinant adeno-associated viral vectors. *J Vis Exp* **e3348** (2011).

186 Blaesse, P. *et al.* Oligomerization of KCC2 correlates with development of inhibitory neurotransmission. *J Neurosci* **26**, 10407-10419, doi:10.1523/JNEUROSCI.3257-06.2006 (2006).

187 Sagne, C., Isambert, M. F., Henry, J. P. & Gasnier, B. SDS-resistant aggregation of membrane proteins: application to the purification of the vesicular monoamine transporter. *Biochem J* **316 (Pt 3)**, 825-831 (1996).

188 Verkman, A. S., Sellers, M. C., Chao, A. C., Leung, T. & Ketcham, R. Synthesis and characterization of improved chloride-sensitive fluorescent indicators for biological applications. *Anal Biochem* **178**, 355-361 (1989).

189 Colombi, I., Mahajani, S., Frega, M., Gasparini, L. & Chiappalone, M. Effects of antiepileptic drugs on hippocampal neurons coupled to micro-electrode arrays. *Frontiers in neuroengineering* **6**, 10, doi:10.3389/fneng.2013.00010 (2013).

190 Frega, M. *et al.* Cortical cultures coupled to micro-electrode arrays: a novel approach to perform in vitro excitotoxicity testing. *Neurotoxicology and teratology* **34**, 116-127, doi:10.1016/j.ntt.2011.08.001 (2012).

191 El Merhie, A. *et al.* Single layer graphene functionalized MEA for enhanced detection of neuronal network development. *Sensors and Actuators B: Chemical* **277**, 224-233 (2018).

192 Chiappalone, M. *et al.* Burst detection algorithms for the analysis of spatio-temporal patterns in cortical networks of neurons. *Neurocomputing* **65**, 653-662 (2005).

193 Turnbull, L., Dian, E. & Gross, G. The string method of burst identification in neuronal spike trains. *Journal of neuroscience methods* **145**, 23-35 (2005).

194 Bologna, L. L. *et al.* Investigating neuronal activity by SPYCODE multi-channel data analyzer. *Neural networks : the official journal of the International Neural Network Society* **23**, 685-697, doi:10.1016/j.neunet.2010.05.002 (2010).

195 Maccione, A. *et al.* A novel algorithm for precise identification of spikes in extracellularly recorded neuronal signals. *J Neurosci Methods* **177**, 241-249, doi:10.1016/j.jneumeth.2008.09.026 (2009).

196 Slomowitz, E. *et al.* Interplay between population firing stability and single neuron dynamics in hippocampal networks. *Elife* **4**, doi:10.7554/eLife.04378 (2015).

197 Duchon, A. *et al.* Identification of the translocation breakpoints in the Ts65Dn and Ts1Cje mouse lines: relevance for modeling down syndrome. *Mamm Genome* **22**, 674-684, doi:DOI 10.1007/s00335-011-9356-0 (2011).

198 Kaila, K., Price, T. J., Payne, J. A., Puskarjov, M. & Voipio, J. Cation-chloride cotransporters in neuronal development, plasticity and disease. *Nat Rev Neurosci* **15**, 637-654, doi:10.1038/nrn3819 (2014).

199 Agarwal, V., Bell, W. B., Nam, J. W. & Bartel, D. P. Predicting effective mocroRNA target sites in mammalian mRNAs. *Elife* **4**, e05005 (2015).

200 Gu, S. *et al.* The loop position of shRNAs and pre-miRNAs is critical for the accuracy of dicer processing in vivo. *Cell* **151**, 900-911, doi:10.1016/j.cell.2012.09.042 (2012).

201 Seitz, H. Redefining microRNA targets. *Curr Biol* **19**, 870-873, doi:10.1016/j.cub.2009.03.059 (2009).

202 Salmena, L., Poliseno, L., Tay, Y., Kats, L. & Pandolfi, P. P. A ceRNA hypothesis: the Rosetta Stone of a hidden RNA language? *Cell* **146**, 353-358, doi:10.1016/j.cell.2011.07.014 (2011).

203 Contestabile, A. *et al.* Lithium rescues synaptic plasticity and memory in Down syndrome mice. *J Clin Invest* **123**, 348-361 (2013).

204 Costa, C. S. A., Scott-McKean, J. J. & Stasko, M. R. Acute Injections of the NMDA Receptor Antagonist Memantine Rescue Performance Deficits of the Ts65Dn Mouse Model of Down Syndrome on a Fear Conditioning Test. *Neuropsychopharmacology* **33**, 1624-1632 (2007).

205 Salehi, A. *et al.* Restoration of norepinephrine-modulated contextual memory in a mouse model of Down syndrome. *Science translational medicine* **1**, 7ra17 (2009).

206 Belichenko, P. V. *et al.* An Anti-beta-Amyloid Vaccine for Treating Cognitive Deficits in a Mouse Model of Down Syndrome. *PLoS One* **11**, e0152471, doi:10.1371/journal.pone.0152471 (2016).

207 Salehi, A. *et al.* Increased App expression in a mouse model of Down's syndrome disrupts NGF transport and causes cholinergic neuron degeneration. *Neuron* **51**, 29-42, doi:10.1016/j.neuron.2006.05.022 (2006).

208 Kleschevnikov, A. M. *et al.* Deficits in cognition and synaptic plasticity in a mouse model of Down syndrome ameliorated by GABAB receptor antagonists. *J Neurosci* **32**, 9217-9227 (2012).

209 Kleschevnikov, A. M. *et al.* Evidence that increased Kcnj6 gene dose is necessary for deficits in behavior and dentate gyrus synaptic plasticity in the Ts65Dn mouse model of Down syndrome. *Neurobiol Dis* **103**, 1-10, doi:10.1016/j.nbd.2017.03.009 (2017).

210 Garcia-Cerro, S. *et al.* Overexpression of Dyrk1A is implicated in several cognitive, electrophysiological and neuromorphological alterations found in a mouse model of Down syndrome. *PLoS One* **9**, e106572, doi:10.1371/journal.pone.0106572 (2014).

211 Neumann, F. *et al.* DYRK1A inhibition and cognitive rescue in a Down syndrome mouse model are induced by new fluoro-DANDY derivatives. *Scientific reports* **8**, 2859, doi:10.1038/s41598-018-20984-z (2018).

212 Altafaj, X. *et al.* Normalization of Dyrk1A expression by AAV2/1-shDyrk1A attenuates hippocampal-dependent defects in the Ts65Dn mouse model of Down syndrome. *Neurobiol Dis* **52**, 117-127, doi:10.1016/j.nbd.2012.11.017 (2013).

213 Voronov, S. V. *et al.* Synaptojanin 1-linked phosphoinositide dyshomeostasis and cognitive deficits in mouse models of Down's syndrome. *Proc Natl Acad Sci U S A* **105**, 9415-9420, doi:10.1073/pnas.0803756105 (2008).

214 Chrast, R. *et al.* The mouse brain transcriptome by SAGE: differences in gene expression between P30 brains of the partial trisomy 16 mouse model of Down syndrome (Ts65Dn) and normals. *Genome Res* **10**, 2006-2021 (2000).

215 Ben-Ari, Y. Excitatory actions of gaba during development: the nature of the nurture. *Nature reviews. Neuroscience* **3**, 728-739 (2002).

216 Ben-Ari, Y. NKCC1 Chloride Importer Antagonists Attenuate Many Neurological and Psychiatric Disorders. *Trends Neurosci* **40**, 536-554 (2017).

217 Rivera, C. *et al.* The K^+/Cl^- co-transporter KCC2 renders GABA Hyperpolarizing during neuronal maturation. *Nature* **397**, 251-255 (1999).

218 Yamada, J. *et al.* Cl^- uptake promoting depolarizing GABA action in immature rat neocortical neurons is mediated by NKCC1. *Journal of Physiology* **557**, 839-841 (2004).

219 Lozovaya, N. *et al.* GABAergic inhibition in dual-transmission cholinergic and GABAergic striatal interneurons is abolished in Parkinson disease. *Nature communications* **9**, 1422, doi:10.1038/s41467-018-03802-y (2018).

220 Palma, E. *et al.* Anomalous levels of Cl- transporters in the hippocampal subiculum from temporal lobe epilepsy patients make GABA excitatory. *Proc Natl Acad Sci U S A* **103**, 8465-8468 (2006).

221 Eftekhari, S. *et al.* Bumetanide reduces seizure frequency in patients with temporal lobe epilepsy. *Epilepsia* **54**, e9-12 (2013).

222 Kahle, K. T. *et al.* Modulation of neuronal activity by phosphorylation of the K-Cl cotransporter KCC2. *Trends Neurosci* **36**, 726-737, doi:10.1016/j.tins.2013.08.006 (2013).

223 Puskarjov, M., Ahmad, F., Kaila, K. & Blaesse, P. Activity-dependent cleavage of the K-Cl cotransporter KCC2 mediated by calcium-activated protease calpain. *J Neurosci* **32**, 11356-11364, doi:10.1523/jneurosci.6265-11.2012 (2012).

224 Rivera, C. *et al.* Mechanism of activity-dependent downregulation of the neuron-specific K-Cl cotransporter KCC2. *J Neurosci* **24**, 4683-4691, doi:10.1523/jneurosci.5265-03.2004 (2004).

225 Doshina, A. *et al.* Cortical cells reveal APP as a new player in the regulation of GABAergic neurotransmission. *Scientific reports* **7**, 370, doi:10.1038/s41598-017-00325-2 (2017).

226 Fuchs Wightman, F., Giono, L. E., Fededa, J. P. & de la Mata, M. Target RNAs Strike Back on MicroRNAs. *Frontiers in genetics* **9**, 435-435, doi:10.3389/fgene.2018.00435 (2018).

227 de la Mata, M. *et al.* Potent degradation of neuronal miRNAs induced by highly complementary targets. *EMBO reports* **16**, 500-511, doi:10.15252/embr.201540078 (2015).

228 Li, X. *et al.* Long-term expressional changes of Na+ -K+ -Cl- co-transporter 1 (NKCC1) and K+ -Cl- co-transporter 2 (KCC2) in CA1 region of hippocampus following lithium-pilocarpine

induced status epilepticus (PISE). *Brain Res* **1221**, 141-146, doi:10.1016/j.brainres.2008.04.047 (2008).

229 Di Cristo, G., Awad, P. N., Hamidi, S. & Avoli, M. KCC2, epileptiform synchronization, and epileptic disorders. *Prog Neurobiol* **162**, 1-16, doi:10.1016/j.pneurobio.2017.11.002 (2018).

230 Sen, A. *et al.* Increased NKCC1 expression in refractory human epilepsy. *Epilepsy Res* **74**, 220-227, doi:10.1016/j.eplepsyres.2007.01.004 (2007).

231 Palma, E. *et al.* Anomalous levels of Cl- transporters in the hippocampal subiculum from temporal lobe epilepsy patients make GABA excitatory. *Proc Natl Acad Sci U S A* **103**, 8465-8468, doi:10.1073/pnas.0602979103 (2006).

232 He, Q., Nomura, T., Xu, J. & Contractor, A. The developmental switch in GABA polarity is delayed in fragile X mice. *J Neurosci* **34**, 446-450 (2014).

233 Merner, N. D. *et al.* Regulatory domain or CpG site variation in SLC12A5, encoding the chloride transporter KCC2, in human autism and schizophrenia. *Front Cell Neurosci* **9**, 386, doi:10.3389/fncel.2015.00386 (2015).

234 Merner, N. D. *et al.* Gain-of-function missense variant in SLC12A2, encoding the bumetanide-sensitive NKCC1 cotransporter, identified in human schizophrenia. *J Psychiatr Res* **77**, 22-26, doi:10.1016/j.jpsychires.2016.02.016 (2016).

235 Duarte, S. T. *et al.* Abnormal expression of cerebrospinal fluid cation chloride cotransporters in patients with Rett syndrome. *PLoS One* **8**, e68851, doi:10.1371/journal.pone.0068851 (2013).

236 Navarro-Romero, A. *et al.* Cannabinoid type-1 receptor blockade restores neurological phenotypes in two models for Down syndrome. *Neurobiol Dis* **125**, 92-106, doi:10.1016/j.nbd.2019.01.014 (2019).

237 Li, Q. *et al.* Timing specific requirement of microRNA function is essential for embryonic and postnatal hippocampal development. *PLoS One* **6**, e26000, doi:10.1371/journal.pone.0026000 (2011).

238 Caudy, A. A., Myers, M., Hannon, G. J. & Hammond, S. M. Fragile X-related protein and VIG associate with the RNA interference machinery. *Genes Dev* **16**, 2491-2496, doi:10.1101/gad.1025202 (2002).

239 Jimenez-Mateos, E. M. *et al.* miRNA Expression profile after status epilepticus and hippocampal neuroprotection by targeting miR-132. *Am J Pathol* **179**, 2519-2532, doi:10.1016/j.ajpath.2011.07.036 (2011).

240 Li, M. M. *et al.* Genome-wide microRNA expression profiles in hippocampus of rats with chronic temporal lobe epilepsy. *Sci Rep* **4**, 4734, doi:10.1038/srep04734 (2014).

241 Xu, Y. *et al.* Analysis of microRNA expression profile by small RNA sequencing in Down syndrome fetuses. *Int J Mol Med* **32**, 1115-1125, doi:10.3892/ijmm.2013.1499 (2013).

242 Lippi, G. *et al.* MicroRNA-101 Regulates Multiple Developmental Programs to Constrain Excitation in Adult Neural Networks. *Neuron* **92**, 1337-1351, doi:10.1016/j.neuron.2016.11.017 (2016).

243 Friedman, L. M. *et al.* MicroRNAs are essential for development and function of inner ear hair cells in vertebrates. *Proc Natl Acad Sci U S A* **106**, 7915-7920, doi:10.1073/pnas.0812446106 (2009).

244 Chi, S. W., Zang, J. B., Mele, A. & Darnell, R. B. Argonaute HITS-CLIP decodes microRNA-mRNA interaction maps. *Nature* **460**, 479-486, doi:10.1038/nature08170 (2009).

245 Chaves, J. C. S., Machado, F. T., Almeida, M. F., Bacovsky, T. B. & Ferrari, M. F. R. microRNAs expression correlate with levels of APP, DYRK1A, hyperphosphorylated Tau and BDNF in the hippocampus of a mouse model for Down syndrome during ageing. *Neurosci Lett*, 134541, doi:10.1016/j.neulet.2019.134541 (2019).

246 Xu, J. *et al.* Extensive ceRNA-ceRNA interaction networks mediated by miRNAs regulate development in multiple rhesus tissues. *Nucleic Acids Res* **44**, 9438-9451, doi:10.1093/nar/gkw587 (2016).

247 Poliseno, L. *et al.* A coding-independent function of gene and pseudogene mRNAs regulates tumour biology. *Nature* **465**, 1033-1038, doi:10.1038/nature09144 (2010).

248 Hansen, T. B. *et al.* Natural RNA circles function as efficient microRNA sponges. *Nature* **495**, 384-388, doi:10.1038/nature11993 (2013).

249 Memczak, S. *et al.* Circular RNAs are a large class of animal RNAs with regulatory potency. *Nature* **495**, 333-338, doi:10.1038/nature11928 (2013).

250 Zhao, Y., Alexandrov, P. N., Jaber, V. & Lukiw, W. J. Deficiency in the Ubiquitin Conjugating Enzyme UBE2A in Alzheimer's Disease (AD) is Linked to Deficits in a Natural Circular miRNA-7 Sponge (circRNA; ciRS-7). *Genes (Basel)* **7**, doi:10.3390/genes7120116 (2016).

251 Junn, E. *et al.* Repression of alpha-synuclein expression and toxicity by microRNA-7. *Proc Natl Acad Sci U S A* **106**, 13052-13057, doi:10.1073/pnas.0906277106 (2009).

252 Cai, Y. & Wan, J. Competing Endogenous RNA Regulations in Neurodegenerative Disorders: Current Challenges and Emerging Insights. *Front Mol Neurosci* **11**, 370, doi:10.3389/fnmol.2018.00370 (2018).

253 Valluy, J. *et al.* A coding-independent function of an alternative Ube3a transcript during neuronal development. *Nat Neurosci* **18**, 666-673, doi:10.1038/nn.3996 (2015).

254 Zhang, W. *et al.* Amyloid precursor protein regulates neurogenesis by antagonizing miR-574-5p in the developing cerebral cortex. *Nat Commun* **5**, 3330, doi:10.1038/ncomms4330 (2014).